CHARACTERIZATION AND ANALYSIS OF SEISMOCARDIOGRAM FOR ESTIMATION OF HEMODYNAMIC PARAMETERS

by

Kouhyar Tavakolian
Master of Science, University of Northern British Columbia 2005
Master of Science, University of Tehran, 2003
Bachelor of Science, Tehran Polytechnics 2000

DISSERTATION SUBMITTED IN PARTIAL FULFILLMENT OF THE REQUIREMENTS FOR THE DEGREE OF

DOCTOR OF PHILOSOPHY

In the
Engineering Science Department

SIMON FRASER UNIVERSITY

Fall 2010

APPROVAL

Name: **Kouhyar Tavakolian**

Degree: **Doctor of Philosophy**

Title of Thesis: **CHARACTERIZATION AND ANALYSIS OF SEISMOCARDIOGRAM FOR ESTIMATION OF HEMODYNAMIC PARAMETERS**

Examining Committee:

Chair: **Name**
Dr. Carlo Menon

_____

Name
Senior Supervisor
Dr. Bozena Kaminska

_____

Name
Supervisor

Dr. Andrew Blaber

_____

Name
Supervisor

Dr. William New

_____

Name
Internal Examiner

Dr. Andrew Rawicz

_____

Name
External Examiner
Dr. Kevin Shoemaker
University of Western Ontario

Date Defended/Approved: December 13th 2010

Partial Copyright Licence

Ethics Statement

The author, whose name appears on the title page of this work, has obtained, for the research described in this work, either:

a. human research ethics approval from the Simon Fraser University Office of Research Ethics,

or

b. advance approval of the animal care protocol from the University Animal Care Committee of Simon Fraser University;

or has conducted the research

c. as a co-investigator, collaborator or research assistant in a research project approved in advance,

or

d. as a member of a course approved in advance for minimal risk human research, by the Office of Research Ethics.

A copy of the approval letter has been filed at the Theses Office of the University Library at the time of submission of this thesis or project.

The original application for approval and letter of approval are filed with the relevant offices. Inquiries may be directed to those authorities.

Simon Fraser University Library
Burnaby, British Columbia, Canada

update Spring 2010

ABSTRACT

In this research work, systolic time intervals and stroke volume were extracted through the processing of recorded mechanical cardiac vibrations from the sternum, seismocardiogram (SCG). These hemodynamic parameters were extracted based on the physiological characterization of SCG with different modalities including echocardiography, ballistocardiography, Doppler ultrasound, and finite element modelling. For the first time, an extensive evaluation of the SCG estimation of systolic time intervals compared to those from Doppler ultrasound and impedance cardiogram was performed (n=25). It was shown that SCG can estimate pre-ejection period (p-value=0.16), left ventricular ejection time (p-value=0.93), and QS2 (p-value=0.91).

In a novel approach, the effects of respiration on SCG was studied on 45 participants. As the results of this study it was found that there is a difference between SCG cycles during inspiration and the ones during expiration (p-value<0.01). It was also shown that expiration cycles are more similar to each other compared to inspiration cycles. Based on this finding, a new averaging algorithm for SCG was proposed based on the consideration of the respiration effect on SCG.

The previously defined IC point, isotonic contraction, on SCG was redefined to correspond to the point of maximum acceleration of blood in the

aorta. This finding was confirmed using Doppler ultrasound (n=23, r=0.85) and ultra low frequency ballistocardiography (n=5, p-value=0.95).

Keywords: seismocardiography; mechanical heart performance; systolic time intervals; stroke volume; electrocardiography; ballistocardiography; echocardiography; Doppler ultrasound; 3D final element electromechanical heart model; impedance cardiography; infrasonic cardiac signals; phonocardiography; multiple linear regression, neural networks.

EXECUTIVE SUMMARY

This thesis represents an integrative, multidisciplinary approach to the improvement of seismocardiography and development of a better understanding of the genesis of the SCG waves.

The project presented in this thesis is not simply another biomedical engineering project that aims to develop new tools or techniques for the acquisition or processing of biological signals. The thesis includes the development of new engineering techniques and seeks to answer fundamental questions about the relation of the acquired biological signals to the physiological phenomenon creating them. Apart from the engineering developments, I have also engaged myself with the science behind signal formation and the very reasons, motivating us to carry on such a research.

The thesis outlines a five-year project to extract hemodynamic parameters from beat to beat vibration signals on the surface of the chest. In particular, the recording, processing and characterization of seismocadiogram (SCG), obtained from accelerometers placed on the sternum, has been investigated. The following conclusions were made:

1. The systolic time intervals, (PEP, LVET and QS2) were estimated using SCG and compared to the same measurements using, Doppler ultrasound and

impedance cardiogram on 25 participants. It was demonstrated that SCG was able to reliably determine these important hemodynamic indexes.

2. For the very first time, the SCG signal morphology was studied from the point of view of the respiration effect on it. Statistical analysis revealed that respiration affects the SCG morphology differently and that expiration cycles are more similar to each other compared to inspiration cycles, thus, a better candidate to be chosen for averaging of SCG.

3. The physiological interpretations of SCG waves were addressed and different methodologies were used to discover the cardiovascular events underlying the morphology of SCG. This lead to a new interpretation for isotonic contraction (IC) point on SCG. Previous groups gave the assignment of isotonic contraction, which was not based on experimental studies. Our study, as presented in this thesis, redefined the meaning of this point and corresponded it to the point of maximum acceleration of blood in the aorta, or MA.

4. SCG acquisition methods were implemented with a new multilayer sensor technology. Two non-contact methods based on microwave radar and laser were proposed for SCG recording as well. These touch-less methodologies may provide possibilities for SCG monitoring where direct sensor application is not feasible. The new proposed SCG acquistion technologies were compared to existing reference methodologies and it was shown that they can provide the same accuracy of signal acquisition.

5. A novel modelling approach was developed, in collaboration with Johns Hopkins University, which incorporated a 3D electromechanical finite element model of the heart to simulate SCG morphology. This model could reliably reproduce the isovolumic contraction period of SCG and was also used to interpret the SCG waves and their cause, at the cellular myocardial level. This unique approach to SCG will provide a powerful tool to analyze the effects of different cardiac malfunctions on SCG morphology.

6. Our results on the estimation of stroke volume from SCG suggests that SCG is capable of providing a surrogate measure of stroke volume. This study was done on signals recorded on different days and it was shown that the SCG signal recorded on one day can be used to develop an estimator that can be used on another day for estimation of stroke volume.

7. This thesis was not limited to study of vibration signal recorded from the sternum or SCG. For the first time a broader investigation in the more general field of infrasonic cardiac signals, that SCG belongs to, was conducted. This broader approach has contributed in the following ways:

    - The results of this broader approach can assist other investigators, to properly locate and compare their research within the frame of infrasonic cardiac signals. A division of infrasonic cardiac signals into two separate fields of the centre of mass recordings and precordial measurements was proposed to help remove some of the ambiguity which was created by the use of similar terminology in different areas of infrasonic cardiac signals.

- The comparison with ballistocardiography helped translate some of the knowledge accumulated in this very old non-invasive cardiology technique, to the SCG field. This comparison helped to develop a new interpretation of one of the SCG points that corresponds to maximum acceleration of blood in aorta and the “I” point on ballistocardiogram.
- The comparison with other techniques such as Emfit and weight scale BCG can provide reference points to further understand the underlying physiology behind the morphology of these signals.

The current advances in sensor technology and digital signal processing have provided new opportunities for older technologies such as SCG to be studied again. There are still many challenges to bring these techniques to common clinical medicine and preventive care. Apart from technological development, which is essential, one needs to persuade the clinicians of the physiological values embedded in the vibration signals created by the heart. In other words, a more thorough and integrative approach is required to bring these signals to real use, rather than just remaining an investigative apparatus. This thesis, through a multi-disciplinary approach, has tried to address all these challenges and has provided the foundation for renewed use of these techniques in clinical practice.

To Shamsi and Reza

ACKNOWLEDGEMENTS

I am heartily thankful to my supervisor, Dr. Bozena Kaminska, whose leadership and support provided me with the opportunity to conduct this project.

I would not have been able to conclude this thesis without Dr. Andrew Blaber's support during the two final years of this project.

It is an honour for me that I have had the consultation and inspirations of two giants of non-invasive cardiology in the past few years, Dr. William New and Dr. Abraham Noordergraaf, from whom I have learnt a lot.

Special thanks to Brandon Ngai as he made available his support in a number of different ways to this research during the past few years.

This thesis would not have been possible in such a scale unless I could receive a valuable help from Dr. Alireza Akhbardeh, Dr. Ali Vaseghi, Holly Kennedy Symonds and Dr. Viatcheslav Gurev. I am also indebted to my colleagues at SFU and Ciber lab for supporting me: Dr. Fartash Vasefi, Dr. Marcin Marzencki, Yindar Chuo, Brent Carmichael, TJ Snider, Michelle Bruner, Amanmeet Garg, Victor Gusev, Parastoo Dehkordi and Mohammad Izadi.

I would like to show my gratitude to those scientists that have contributed to this work in their email communications or personal meetings: Dr. Roman Baevsky, Dr. William Mckay, Dr. Roy Kerckhoffs, Dr. Natalia Trayanova and Dr. Peter Pretorius.

Lastly, I offer my regards and blessings to all of those who supported me in any respect during the completion of the project: Dr. Wilson Lee, Lisa Fear, Dr Karim Arabi, Peter Matino, Niloufar Tamadondoost, Amireza Tamadondoost, Kaveh Naziripour, Ian Bercovitz, Angela Dublanko, Joan Dublanko, Dr. Azam Mohammadi, Kamyar Tavakolian and Pantea Tavakolian.

TABLE OF CONTENTS

LIST OF FIGURES

LIST OF TABLES

GLOSSARY

AC	Aortic valve closure
AO	Aortic valve opening
ACG	Apexcardiography
BCG	Ballistocardiography
CHF	Congestive heart failure
CMA	Cardiac micro-acceleration
ECG	Electrocardiography
EMFiT	Electromechanical film transducers
HF-BCG	High frequency BCG
IC	Isotonic contraction
ICG	Impedance cardiogram
KCG	Kinetocardiography
LVET	Left ventricular ejection time
LPC	Left parasternal cardiogram
MA	Maximum acceleration
MC	Mitral valve closure
MO	Mitral valve opening
MCG	Mechanocardiography
MEMS	Micro-electromechanical systems
PCG	Phonocardiography
PEP	Pre-ejection period
QS2	Total electromechanical systole
Q-BCG	Quantitative BCG
Q-SCG	Quantitative SCG
R-SC	Radar SCG
SAB	Sternal acceleration BCG
SCG	Seismocardiography
SCSB	Static-charge-sensitive bed
ULF-BCG	Ultra low frequency BCG
VCG	Vibrocardiography

1: INTRODUCTION

"Exercitatio Anatomica de Motu Cordis et Sanguinis"

On the Motion of the Heart and Blood, William Harvey 1628

The pulsatile phenomena of the body's surface with every heart beat has attracted the attention of physicians since the beginning of medicine (Weissler, Harris and Schoenfeld 1968). Precordial examination or cardiac examination is performed as part of the regular physical examination for the purpose of the detection of cardiovascular pathologies. These tests include palpation and auscultation. With palpation, the pulsations of the heart and great arteries that are transmitted to the chest wall are qualitatively assessed through tactile observations. The main context of this thesis is the study of one of the many methods that quantifies these pulsations and records the acceleration, velocity, or displacement of specific points on the chest caused by these pulsations (Braunwald and Perloff 2001). These low frequency signals have been shown to have correspondences to contractility and mechanical performance of the heart as a pump, and can be used as tools in non-invasive cardiology (Smith 1974).

William Harvey's book, quoted above, on the motion of the heart and blood is the source from which most fundamental ideas concerning the human

circulatory system were derived, and is the context of this thesis. Although there have been huge developments in our tools and techniques for the assessment and treatment of cardiovascular diseases (heart disease, disease of blood vessels and stroke) since William Harvey's book, at the end of the 20th century, cardiovascular disease accounted for half of the deaths in the developed world, while this was less than 10 percent in the beginning of the century (Gaziano 2001).

In Canada, based on 2005 data, every seven minutes someone dies from cardiovascular disease and this is the leading cause of death in this country. The leading cause of hospitalization in Canada is circulatory disease (heart disease and stroke) which costs the Canadian economy $22.2 billion annually. It is estimated that 400,000 Canadians live with congestive heart failure (CHF), and up to 50% of CHF patients die within five years of diagnosis (Canada 2005). Early diagnosis of CHF can significantly increase the rate of survival while monitoring diagnosed CHF patients can reduce the costs of hospitalization.

On the technology side, seamless, continuous monitoring has become feasible with the advent of ubiquitous, worldwide cellular communications coverage, and the inexorable progress of Moore's Law that has driven wireless microelectronics to ever-higher performance at ever-lower cost. Chip-level solutions are available and cost-effective to measure a variety of vital signs non-invasively: electrical and mechanical cardiac performance, blood oxygenation, body temperature, body activity and position, blood pressure tracking, and

patient location and movements, all of which are of high clinical value for CHF patients. From all these signals, the focus of this thesis is on the cardiac mechanical signals, in particular, seismocardiography (SCG). SCG is the recording of the acceleration of the sternum caused by the beating heart. SCG opens a window to the mechanical performance of the heart and compliments electrocardiogram (ECG) information on the electrical functioning of the heart.

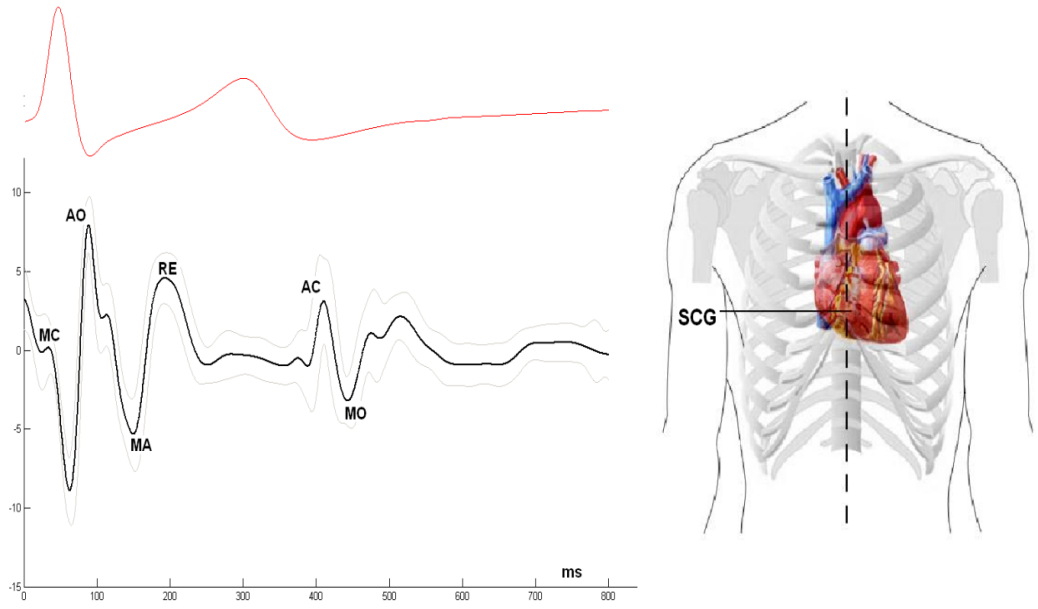

Figure 1. ***Left:*** **The ensemble average of 601 cycles of SCG (bottom) and ECG (top) for a healthy participant (31 years old, 78 Kg and 182 cm). The vertical line is acceleration in milli-g and horizontal line is time in ms. The thin lines are 95 percent intervals of the mean and SCG is annotated based on the results of this thesis and previous works. MC: mitral valve closure, AO: aortic valve opening, MA: maximum acceleration of blood in aorta, RE: rapid systolic ejection, AC: aortic valve closure and MO: mitral valve opening.** ***Right:*** **The anatomical place where SCG is recorded from. The right ventricle faces the sternum and the point where SCG is recorded from.**

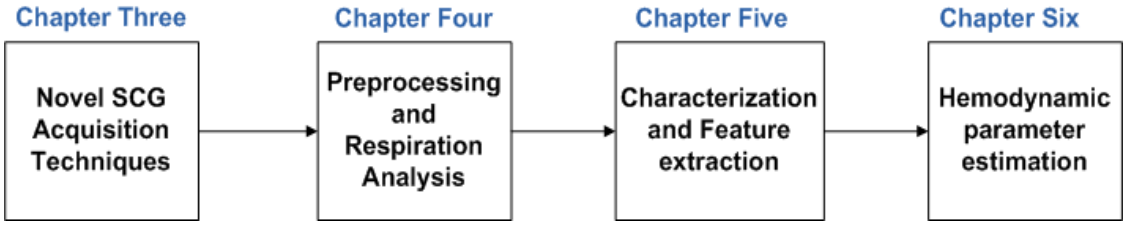

Figure 2. Block diagram of a system for extraction of hemodynamic parameters and the flow of this thesis from chapter three to chapter six

SCG was recorded from the sternum as demonstrated in Figure 1, and is annotated based on previous research and the results acquired from this thesis. In order to extract useful hemodynamic information from SCG, a system as in Figure 2 is required. The acceleration of the sternum needs to be picked up and properly processed. Proper features needed to be extracted from the processed data to obtain estimates of hemodynamic parameters such as systolic time intervals and stroke volume.

Synopsis

Chapter two of this thesis provides background information on seismocardiography. The sequence of chapters 3-6 is illustrated in Figure 2. Chapter seven details the results of all previous chapters with an emphasize on the specific contributions of the author. Each chapter begins with pertinent background information required to obtain a better understanding.

In chapter three, different methodologies for the acquisition of SCG, including a new multi-sensor recording and two novel contactless methods, are

explained. The performance of the new, integrated, multilayer sensor for the extraction of vibration signals from the chest is evaluated. In the same context, the two novel methods of microwave radar and laser are proposed for contactless recording of SCG. On the microwave radar, the possibility of detection of heart rate and respiration rate from the signal is also evaluated.

Recordings of the movement from the chest can contain movement artefacts and alterations caused by respiration. For the first time in this research, the effects of respiration on the morphology of SCG was studied on 45 participants. It was shown that the expiration cycles of the SCG were more similar to each other compared to the inspiration cycles. Based on this respiration study, in chapter four, a new averaging technique is proposed which was based on the separation of inspiration and expiration cycles.

Apart from the sequence of chapters, Figure 2 also roughly demonstrates the time development of the project. In the beginning of this study, the main concern was to obtain better acquisition and processing of the recorded vibration signals. After the first year of the project, the focus shifted toward understanding the physiological mechanisms behind the peaks and valleys observed on the SCG morphology. Other groups had previously published papers on the interpretation of SCG waves; however, the technology used in their research was outdated and, at times, conflicted with new observations (Crow, et al. 1994). Thus, a series of research studies was introduced to better understand the

mechanisms behind the formation of SCG morphology. These studies are detailed in chapter five.

Echocardiography was chosen as the first method to determine the genesis of SCG waves as it is the golden standard in cardiology. Because of limitations in M-mode echocardiography, reproduction of another very well studied, non-invasive cardiology method, ballistocardiography (BCG), was considered as a mechanical reference for peaks on SCG. Doppler ultrasound was used to further confirm the findings of ballistocardiogram.

The findings from these two methods helped identify a new point on SCG that had not previously been noted, the point of maximum acceleration (MA) of blood in the aorta. The statistical analysis on twenty-three participants showed that the maximum acceleration of blood in the aorta is followed by a nadir on SCG. The comparison of the same point on SCG with the “I” point on BCG on five participants further confirmed the findings of the ultrasound.

In the same line of research, and in a novel approach, efforts were made to model the seismocardiogram signal using a 3D finite element electromechanical model in collaboration with Johns Hopkins University. Further development of such a model can provide insight into the physiological events behind the peaks and valleys on SCG morphology, and provide a unique tool to study the effects of different cardiac abnormalities on the SCG signal. Simulation results of the model conclude the fifth chapter of the thesis.

Finally, SCG has been used in this study to extract hemodynamic parameters such as systolic time intervals and stroke volume; the results have been compared to conventional techniques in the field such as Doppler ultrasound and impedance cardiogram. In an analysis of 25 participants, three main systolic intervals of pre-ejection period (PEP), systolic ejection time, and total electromechanical systole were measured with SCG, impedance cardiogram, and Doppler ultrasound.

The statistical results proved the accuracy of the hemodynamic measurements obtained through SCG. Additionally, estimates of stroke volume derived from SCG may provide validation for future studies in this field. These results, and the details of the respective statistical analyses, are presented in chapter six.

Chapter 7 concludes the thesis with an emphasis on the specific contributions of the author of the thesis. There were studies that could not be accomplished during the course of this thesis because of time limitation or limitations in the resources while these works are essential research that needs to be done in order to bring seismocardiography closer to actual clinical use. A brief explanation of such research works is also presented in the last chapter of the thesis.

2: INFRASONIC CARDIAC SIGNALS

"That the heart is erected, and rises upwards to a point, so that at this time it strikes against the breast and the pulse is felt externally" William Harvey 1628

Infrasonic cardiac signals have their main components in the frequency range of 0 to 20 Hz and represent displacement, velocity, or acceleration of the body in response to the heart beating. These signals can provide information regarding the mechanical functioning of the heart as a pump, by quantifying the pulses appearing on the body with every heartbeat. The methods used for the recording of these pulses require minimal effort of the subjects except that they lie, sit or stand still and, during certain records, hold their breath. The act of recording is non-invasive and causes neither danger nor pain and little skill is required of the operator (Starr and Noordergraaf 1967).

Over the past century, extensive research has been conducted on interpretation of these signals in terms of their relationship to cardiovascular dynamics and their possible use in diagnostic cardiology. Today, new microelectronics and signal processing technologies have provided unprecedented opportunities to reintroduce some of these relatively old techniques as useful cardiac diagnostic and monitoring tools.

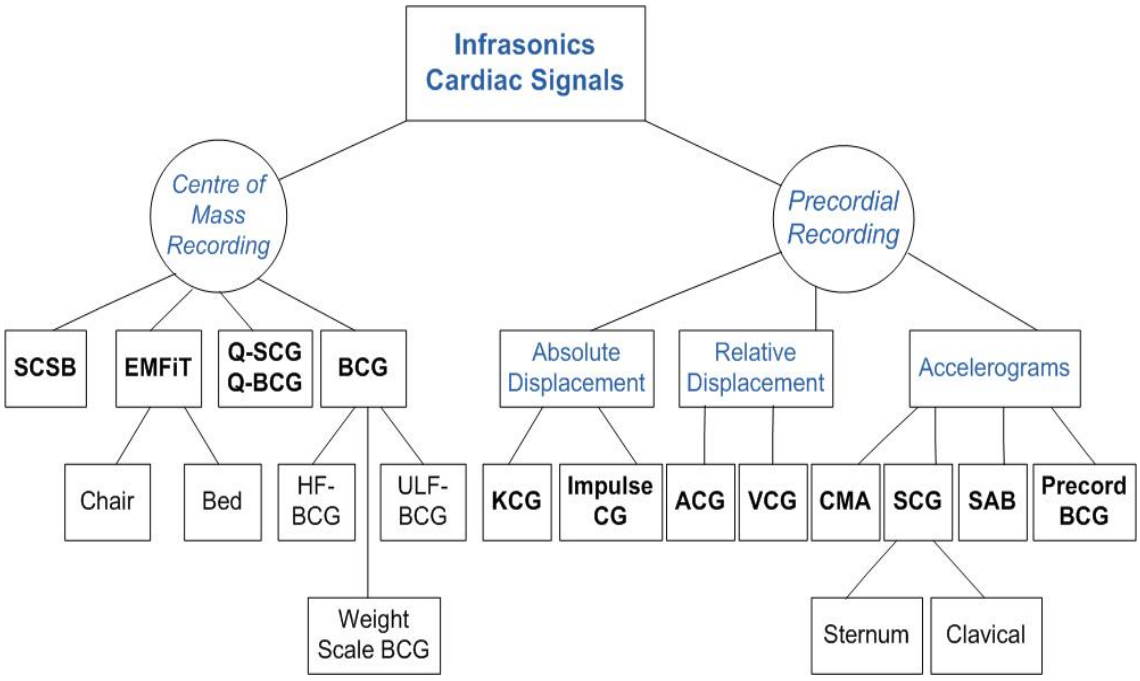

Figure 3. Different infrasonic cardiac signals categorised in two categories of signal created by the circulation of blood (left) and signals created by precordial vibration (right)

A comparative review of these methods is useful to give a thorough view of the whole area of infrasonic cardiac signals. Therefore, in this chapter, a selected number of the infrasonic cardiac signals are introduced and compared.

There are two distinct categories of infrasonic cardiac signals (Figure 3). In the first category the signal is created by changes of the centre of gravity of the whole or upper part of the body as the result of blood circulation. These centre of mass recordings include signals such as: ballistocardiogram (BCG), dynamocardiogram, quantitative seismocardiography (Q-SCG), quantitative ballistocardiogram (Q-BCG) and EMFit. Normally, these signals are recorded by

setting up a recording platform on which the subject can lie, sit or stand, and both subject and the platform are free to move with every heartbeat.

The second category contains surface measurements made from regions localized near the heart where pulsations over the heart (precordium) are recorded. Seismocardiogram (SCG), apexcardiogram (ACG), sternal acceleration ballistocardiography (SAB), kinetocardiogram (KCG), mechanocardiogram (MCG), left parasternal cardiogram (LPC), precordial ballistocardiogram and vibrocardiogram belong to this category. Signals of the second category can extend higher than infrasonic in their frequency range (up to 30Hz) but still have their main component in the infrasound range.

Precordial vibrations are recorded from sensors attached to specific points on the thorax and are hypothesized to be caused by myocardial contraction, rather than blood circulation that is associated with the centre of mass recording. This chapter provides a review and analysis of both categories in the same context as:

- Both categories signal the same cardiovascular events non-invasively in the same frequency range and both are utilized to extract similar hemodynamic parameters such as systolic time intervals or cardiac output.
- Both categories share the similar terminology that can create confusion over the cause of the observed signals. This is illustrated

in Figure 3 where SCG belongs to the precordial recordings while Q-SCG belongs to the centre of mass group. Similarly, BCG belongs to the centre of mass group while precordial BCG belongs to the precordial recording group. The same conventional annotations introduced in BCG, have been widely used in annotation of precordial recordings without consideration for the background behind these annotations and their physiological interpretations.

- The same tools such as echocardiography, ECG, impedance cardiography, Doppler ultrasound and phonocardiography have been used to study and characterize both signals in terms of their relations to cardiac events and their usefulness in estimation of hemodynamic parameters.

The proposed division of infrasonic cardiac signals into two categories clarifies some ambiguities in the field and will assist new researchers to better comprehend the scientific literature by developing a common terminology on infrasonic cardiac signals and to better locate their research within this range. In this chapter, all the major methodologies in the infrasonic cardiac range are introduced in chronological order as they appeared in clinical medicine. A comparative study of some of these signals is presented during and at the end of this chapter.

2.1 Background physiology

The heart is the muscular organ in human body responsible for pumping blood throughout the circulatory system by rhythmic contractions. A seismocardiogram is a record of the mechanical vibration resulting from these contractions. A brief review of heart's function is presented with an emphasis on the electrical and mechanical coupling in the heart that is the basis of a 3D finite element electromechanical model of the heart, used to simulate SCG (see chapter 5).

2.1.1 Electromechanical interactions

Cardiac muscle has typical myofibrils that contain actin and myosin filaments, which lie side by side, and slide along each other during contraction. In the process an increase of calcium ions creates more cross-bridges between myosin and actin and a stronger contraction of cardiac muscle occurs (Guyton and Hall 2006). The same coupling of electrical and mechanical components is used in the 3D finite element electromechanical model of the heart (chapter 5).

On a larger scale, the heart is divided into two separate pumps by a septum. A right heart that pumps blood through the lungs and a left heart that pumps blood through the rest of the body. Each of these pumps is composed of two chambers; an atrium and a ventricle. The atrium helps to move blood into the ventricle and in turn, the ventricle provides the required force for the blood to flow out of the heart.

Just as the heart is mechanically divided into two pairs of chambers, there is a division into two pairs for the electrical system that provides the trigger for the mechanical contraction. The atria and ventricle electrical systems are isolated by a fibrous tissue through which potentials are not conducted. This division allows the atria to contract a short time ahead of ventricular contraction (Noordergraaf 1978).

There are specialized cells in the wall of the right atrium that are capable of spontaneous periodic impulse generation, also known as sino-auricular (SA) node. The electrical impulses generated in this node propagate rapidly through both atria and then through atrioventricular, A-V, bundle into the ventricles. Because of this special electrical arrangement the atria contracts about 100 ms before the ventricles thus the blood gets a chance to be pumped from atria into ventricles before the ventricular contraction ejects the blood.

2.1.2 The cardiac cycle

On average, the human heart beats 72 times per minute leading to about 2.3 billions of cardiac cycles over a span of 60 years. Every cardiac cycle, in itself, is composed of different phases. A summary of the events of the cardiac cycle described by Wiggers gives important information on the temporal sequences of events and provides us with an insight into the seismocardiogram's morphology, which is created by these events (Guyton and Hall 2006).

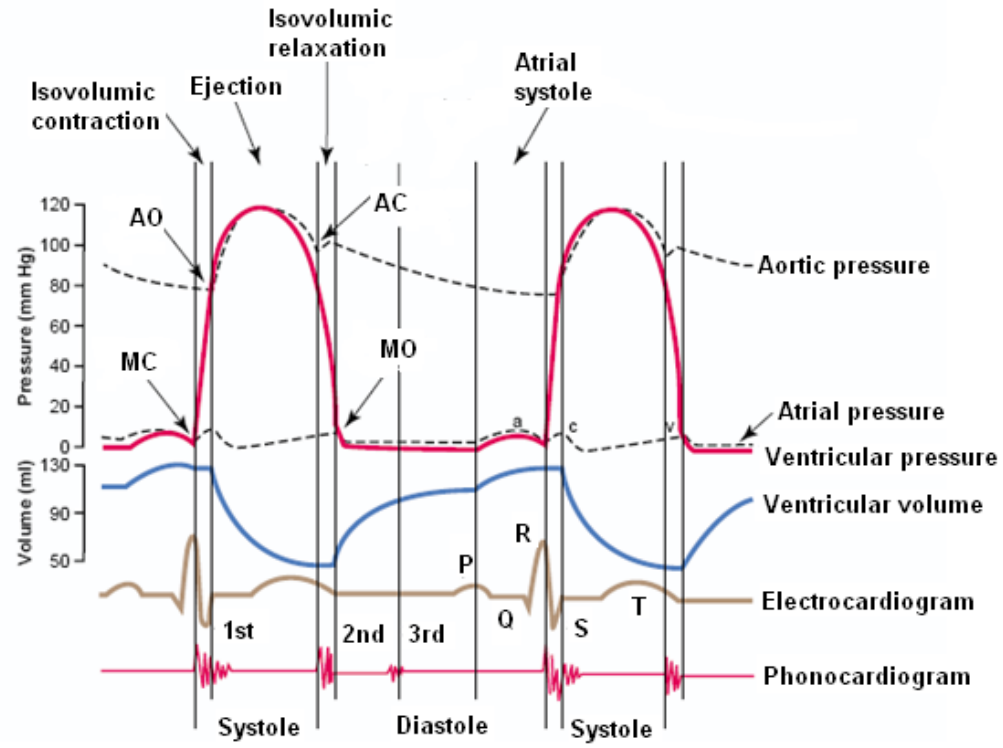

Figure 4. Wiggers diagram: set of events in cardiac cycle for left ventricle. (Guyton and Hall 2006) . AO: aortic valve open, AC: aortic valve close MC: mitral valve close MO: mitral valve open. Reproduced with written permission from Elsevier.

The pressure in left ventricle increases as the arrival of calcium ions starts to trigger actin-myosin interactions at the contractile proteins. The progression of the wave of depolarization is represented by the R wave of the ECG. As the pressure in the left ventricle exceeds the pressure in the left atrium the mitral valve closes shortly after 20 ms initiating the first heart sound S1 (Opie 2001). The pressure in the left ventricle continues to build very rapidly after mitral valve closure as more myofilaments get involved in the contraction. As soon as the pressure in left ventricle exceeds the pressure in aorta, the aortic valve is pushed open. The period when both mitral and aortic valves are closed is called

isovolumic contraction, as there is no flow of blood into or out of the heart. The opening of aorta is followed by a period of rapid ejection of blood.

As the calcium ions decline at the contractile sites more myofibers enter the state of relaxation and the rate of ejection of blood reduces in aorta as a result, and this period is the phase of reduced ejection. In this phase, the pressure in left ventricle decreases until it reaches the aortic pressure and the aortic valve closes. This is the first component of the second heart sound (S2). The closure of the aortic valve starts the period of isovolumic relaxation until the mitral valve opens when the pressure in the left ventricle falls below the pressure in left atrium.

The opening of the mitral valve creates the phase of rapid filling followed by a period of diastasis where the filling almost stops. This is followed by the atrial systole phase where atrial contraction further fills the ventricle. All these timings and cardiac events can be observed in Wiggers diagram (Figure 4).

2.2 Infrasonic cardiac signals: centre of mass measurements

In this category of infrasonic cardiac signals, the circulation of blood in the main arteries changes the centre of mass of the body on the measuring platform, which manifests itself in displacement, velocity and accelerations that can be detected by different methodologies. The basic physiology behind these signals is as follows: with each heart beat, blood rushes upward in the ascending aorta and pulmonary artery which pushes back the platform upon which the body lies.

On the other hand, when the blood rushes down the descending aorta the platform moves forward to keep the centre of mass of the system, including body and platform, in place.

Ballistocardiography is the most studied signal of the centre of mass movement category. Up until 1964, more than 1500 papers had been published on the topic. This is one of the oldest methods of non-invasive cardiology. Dynamocardiography (DCG) is also an obsolete technique of this category, where subjects rested on a sturdy table. Part of the table on which the thorax was located was separated from the rest of the table and supported by four stiff springs that allowed vertical movements (Starr and Noordergraaf 1967) (Komarov 1957).

A historic prospective on Ballistocardiography

The initial observations of BCG were made by people who noticed the movement of weight scale pointers in time with the heartbeat. Parry, in 1786, detected oscillations of the trunk synchronous with the heartbeat (Smith 1974). The first documented recording was from 1877 when, J.W. Gordon, recorded the movement from a bed suspended from the ceiling, (Figure 5) Gordon came up with the following interpretation of it:

> "When the heart is contracting it propels blood in all directions; but the greatest column is propelled downward, along the aorta, almost in the direction of the axis of the body which therefore must give rise to a

recoil in the opposite direction. Indeed, *the case is precisely analogous to that of a ball propelled from a gun*" (Gordon 1877)

Later, in 1905, Yandel Henderson, an American physiologist, constructed a suspended bed with the resonance frequency of 0.2 Hz and recorded the displacements on a smoked drum with 100 times mechanical magnification (Henderson 1905). He simultaneously recorded carotid pulse and divided the obtained wave from the bed into four sections, D_s, D_f, D_h and D_d (Figure 5c). He assigned D_f, the rapid and considerable feetward movement to the rush of the blood headward into the arch of aorta:

"If therefore during systole 100 grams of blood were moved 7cm headward, the reminder of the body of a man weighing 70,100 grams would be moved 0.01 cm in the feetward direction" (Henderson 1905)

With the same reasoning, he assigned the D_h to the moment where the pulse wave passes the arch of aorta and starts feetward. The structure used by Henderson to secure BCG recordings and the original recordings of Gordon are reproduced in Figure 5.

Thirty years later Isaac Starr, a cardiologist at University of Pennsylvania, reproduced the same instrument as Henderson's but with more accurate optical magnification and recording. He was the person who coined the name "Ballistocardiography". Starr soon gave up on Henderson's method as it required subjects to suspend their respiration, since the respiration effect was about ten

times bigger than the cardiac effect (Smith 1974). The required breathing technique worked well on trained subjects but not patients, making it difficult to use in clinics.

Starr moved from BCG beds with frequencies less than heart rate, such as Henderson's BCG, to ones with higher than heart rate, later known as high frequency beds (HF-BCG). With HF-BCG there was no need for patients to hold their breath. They designed the HF-BCG with stiff springs and this began the high-frequency era in BCG that lasted for 15 years. Different research groups started using the HF-BCG and patients were monitored for long periods.

In many clinical cases, cardiac abnormalities could be identified even when the ECG and other clinical tests were negative. Nevertheless, further research indicated a weakness of body-table coupling that could create an appreciable distortion in HF-BCG tracings (Starr and Noordergraaf 1967).

In 1949, a new method of direct-body ballistocardiogram was introduced by Dock where the velocity of vibration was recorded from the subject's shins (Dock, Mandelbaum and Mandelbaum 1953). Because of the ease of recording, this new technique attracted many researchers but these recordings were highly sensitive to subject-platform coupling; even more than HF-BCG. In these recordings, the properties of body tissues warped the recordings, and these properties differed from person to person (Smith 1974).

At the end of the BCG era, the original methods of Gordon and Henderson were reintroduced where subjects were suspended and almost free to move longitudinally. BCG beds were constructed with a resonant frequency of less than the heart rate and were known as ultra low frequency ballistocardiograms, ULF-BCG. This was the method of choice after 1950s and was mostly emphasized by biophysicists. Noordergraaf developed equations for ballistoardiograms and with these equations they could predict the shape and size of one type of BCG recording from the other one and explain the differences between different methodologies (Starr and Noordergraaf 1967).

A single, outstanding book on the topic of BCG that Starr and Noordergraaf (1967) wrote in 1967 contained a general overview of all the prior BCG methods. They showed that the genesis of the BCG is thoroughly understood and is solely caused by movements of the body's centre of gravity. Through mathematical models, experiments on cadavers, hydraulic models, and electrical models, they related the BCG waves to the physiological events that caused them. They reproduced many of the abnormalities commonly encountered in clinical medicine using these models, and established a solid foundation of the genesis of both normal and abnormal records and these were the inspiration for the similar studies on SCG as presented in chapter 5.

Because of the growing interest in the BCG field, researchers gathered under a committee in the American Heart Association (AHA) and came up with

standards for different BCG systems. The standard axis directions agreed upon are shown in Figure 5e and they defined different waves of the BCG.

The ideal BCG waveform (Figure 6) consists of seven waveform peaks labelled H through N (Scarborough & Talbot 1956). H is the first upward deflection after the electrocardiograph (ECG) R-wave on the acceleration BCG when recorded simultaneously. The letter I is the downward wave immediately after H, and, lastly, the letter J is the upward wave after I. The L, M and N waves correspond to the diastolic phase of the cardiac cycle.

Nevertheless, there has been a decline in publication in the BCG field since the 1970s. The instruments recording BCG were quite bulky, and new, non-invasive technologies appeared, such as echocardiography, that distracted the clinicians from the potential values of ballistocardiography. It also appears that researchers were unable to persuade clinicians of the values of ballistocardiogram recordings despite the vast number of papers published in the area. In the next section, ULF-BCG is explained in more detail as the method of choice at the end of classical BCG studies in the 1960s.

Currently, there are new approaches where the BCG signals are acquired when the subject is resting on a bed (Lindqvist, et al. 1996), seated on a chair (Junnila, Akhbardeh and Varri 2009), or standing on weight scale (Inan, Etemadi and Wiard, et al. 2009), and all these methods will be reviewed in more detail in the coming sections.

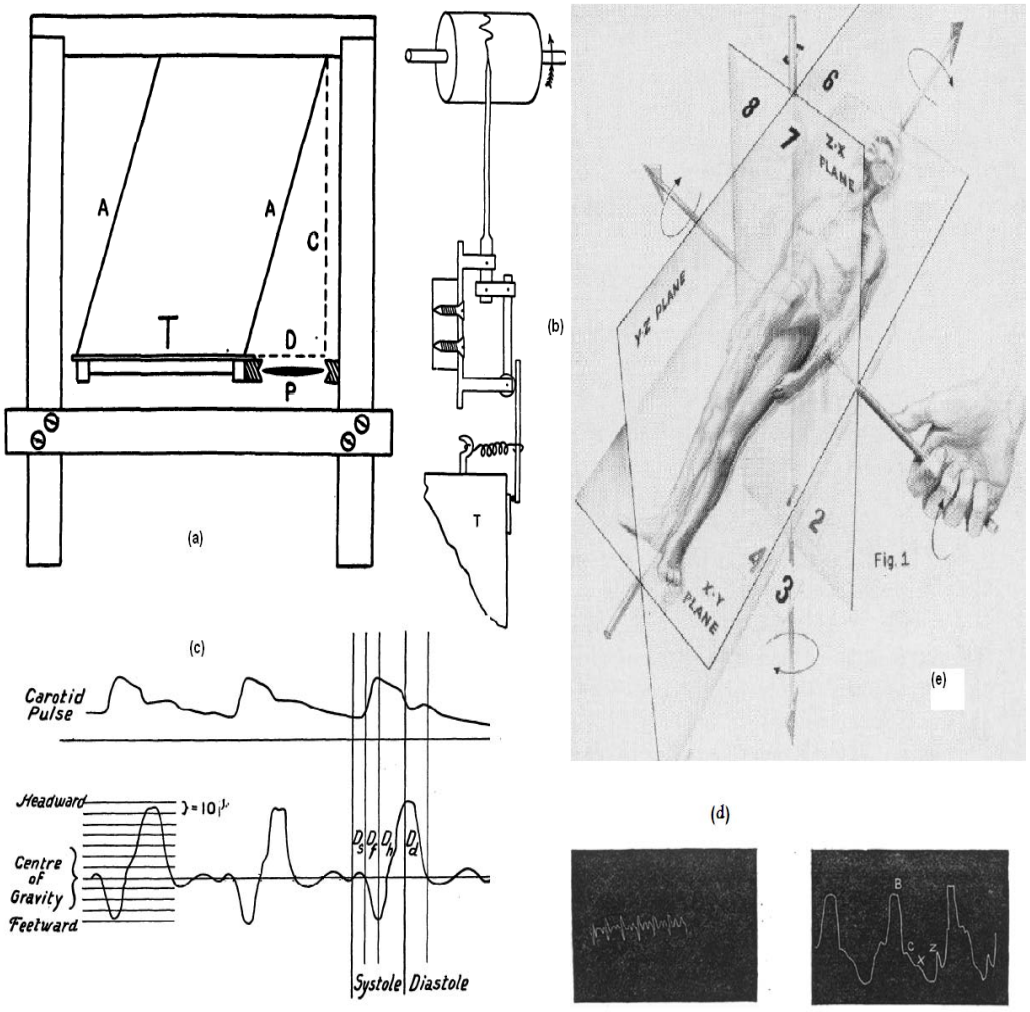

Figure 5. (a) The bed structure constructed by Henderson was 2 x 1.8 x 0.8 meters. The recording was performed in direction perpendicular to the drawing. The table itself was a thing plank 50 cm wide and 1.2 cm thick and weighted 9 kilos. The movement of the table was limited to the longitudinal direction. (b) The arrangement of the recording lever attached to the open corner of the table, T. This lever gives an amplification of 100 to every displacement. (c) The recordings obtained from the bed together with Carotid pulse while the subject was asked to hold their breath (Henderson 1905). (d) the initial Ballistocardiogram recording in 1877. On the left side the tracing for a subject standing on weight scale and on the rights a subject lying on a platform suspended by four ropes (Gordon 1877). (e) The BCG spatial axes and the arrows point the point to the positive direction (Scarborough, et al. 1956) (reproduced with a written permission from Wolters Kluwer Health)

2.2.1 Ultra low frequency ballistocardiogram (ULF-BCG)

Most types of classical BCGs, except for direct body BCG, involve a platform upon which a subject lies supine. BCG systems were categorized by their natural frequency with respect to the heart‘s natural frequency of approximately 1 Hz. BCG apparatuses with higher natural frequencies of 10 Hz to 15 Hz are deemed high frequency BCG (HF-BCG). Those with natural frequencies of approximately 1 Hz are low frequency (LF-BCG), and those lower than 1 Hz are ultra-low frequency (ULF-BCG).

Binding and dampening of the BCG apparatus can be thought of as filtering the resultant signal such that frequencies below its natural frequency are removed. Thus, HF-BCG removes more of the low frequency spectrum and reflects forces, whereas ULF-BCG measures displacement. The physical basis of these BCG apparatuses is examined in elegant detail by Noordergraaf (Starr & Noordergraaf, 1967), but the equations for ULF-BCG are explained in appendix 1 as this type of ballistocardiography has been reproduced in the research presented in this thesis. A sample of ULF-BCG tracing, together with ECG and phonocardiogram, is illustrated in Figure 6.

In BCG, a number of events act simultaneously. A wave tip means that the sum of several events are maximal or minimal and, unlike ECG, cannot be attributed to a single physiological event although one event may be the main contributor (Starr and Noordergraaf 1967). The ULF-BCG waves can be assigned to three categories of pre-ejection (FGH), ejection (IJK), and diastolic

(LMN) waves. The H wave on BCG happens about 10 msec before left ventricular ejection, and the tip of the I wave happens at the same time with the maximal acceleration of blood in the aorta. The J wave is the acceleration of blood in the descending aorta and the initial deceleration of blood in the ascending aorta (Smith 1974).

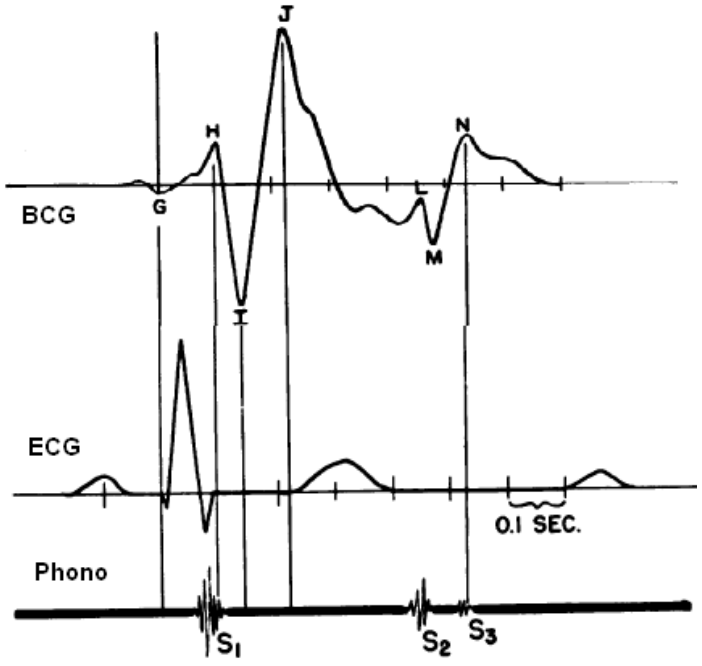

Figure 6. Simultaneous ULF-BCG, ECG and Phonocardiograph signals (Scarborough & Talbot 1956). (Reproduced with a written permission from Wolters Kluwer Health)

2.2.2 Static-charge-sensitive bed (SCSB)

The static-charge sensitive mattress was used to measure BCG on regular beds. The morphology of the signal was compared to the ULF-BCG recordings, and it was demonstrated that the systolic component of the SCSB-BCG has a delay compared to the same component on ULF-BCG. This type of

recording can also be used for the simultaneous measurement of the respiration signal, and to monitor patients while sleeping on their bed (Alihanka, Vaahtoranta and Saarikivi 1981). An algorithm was proposed to separate the BCG and respiration from the signal recorded from SCSB setup (Jensen, Larsen and Shankar 1991).

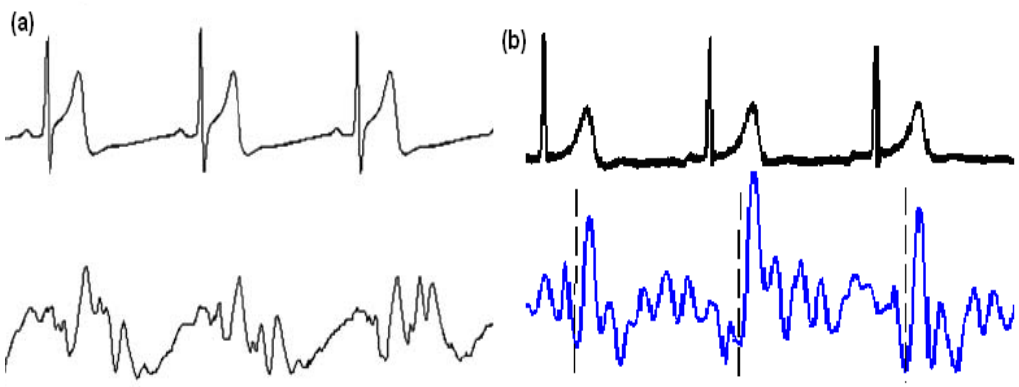

Figure 7. ***(a)*** **Simultaneous record of EMFi chair BCG signal recorded from the seat (Junnila, Akhbardeh and Varri 2009). Reproduced by a written permission of Springer.** ***(b)*** **Q-SCG signal recorded from the seat (Stork and Trefny 2010). The peak of signal in both recordings happen around the same position from ECG T wave.**

2.2.3 Quantitative BCG and EMFiT recordings

Quantitative BCG and SCG were recorded from subjects seated on special, calibrated chairs, and could manifest the force of the cardiovascular system on the chair. The clear advantage of Q-BCG to the previous methods was the fact that there was a linear relationship between the displacement and the amount of force exerted by the circulation, and the fact that the system could be calibrated and show the actual values of these cardiovascular forces. The

same nomenclature as classical BCG has been used in Q-BCG and Q-SCG research, and as the displacement in these types of BCG is linearly related to the force of cardiovascular origin, the system can be categorized in the HF-BCG systems.

In a new study, electromechanical film sensors (EMFi), manufactured by Emfit Ltd, were used to record infrasonic cardiac signals from the back and seat of chairs. The flexibility characteristic of EMFi sensors made them suitable for such purposes as they were easy to install on chairs and beds. In the most recent research from this group, the chair was implemented using wireless technology; a sample record of a subject is seen in Figure 7 (Junnila, Akhbardeh and Varri 2008).

The recordings of Q-SCG as in Strok and Terfny (2010) work look very similar to the same recording from the EMFiT system, as seen in Figure 7 (Junnila, Akhbardeh and Varri 2008). This is not far from expectations as they both record forces of the cardiovascular system from the same point on the body (seat). Most of the published research on EMFiT-based recordings has been on the development of sensor and hardware systems and advance signal processing techniques for improved signal processing.

In a study on the signal recorded from the back of the chair, it was shown that the pre-ejection period (PEP) could be extracted and compared to the same parameter measured with impedance cardiography (Lim, et al. 2006). It is known

that the hemodynamic state of the body changes between sitting and lying supine. In a study performed on seven healthy participants, it was shown that the timing of the EMFiT recording changed between sitting and lying supine (Alamestsa, et al. 2008).

2.2.4 Weight-scale BCG

As discussed in the review of the classical BCG, the original observations that lead to the invention of BCG was made by physicians who observed fluctuations of the weight scale pointer in time with heart beat. Extensive studies on the acquisition of vertical BCGs dates back to Starr's earlier works (Starr and Rawson 1941).

In a novel approach to vertical BCGs, weight scales were modified to record BCGs in research conducted at Stanford university, and were used to record quite stable BCG signals from twenty one healthy adults (Inan, Etemadi and Wiard, et al. 2009). Later, the hardware was improved to lower noise. (O. T. Inan, M. Etemadi, et al. 2010).

In the effort to extract hemodynamic parameters from their vertical BCG system, the weight scale BCG was recorded, together with Doppler echocardiogram, from nine healthy participants. It was demonstrated that the percent change in root-mean square power of the BCG were strongly correlated with the percent change in cardiac output measured by Doppler echocardiography (O. T. Inan, M. Etemadi, et al. 2009).

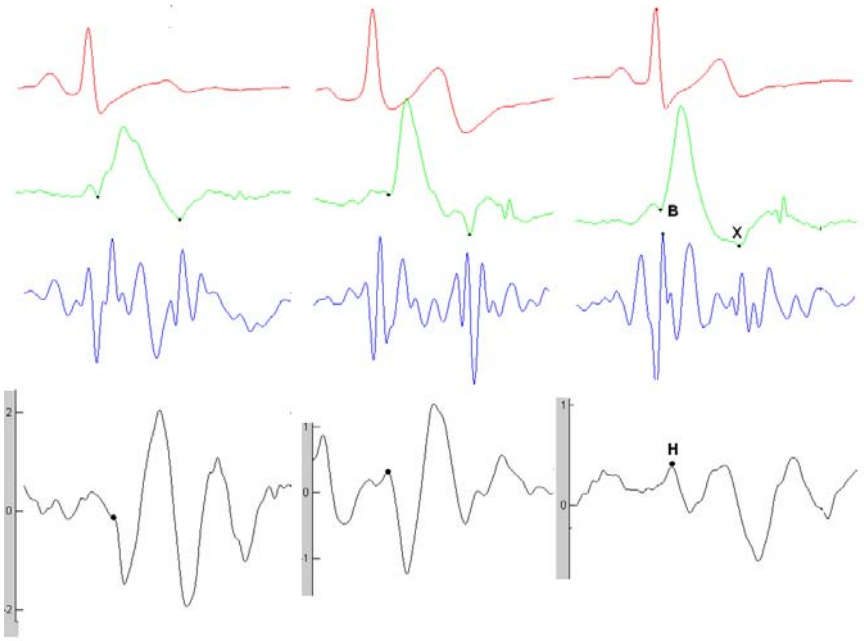

Figure 8. Left to right: Standing, sitting and lying on force plate. Bottom to top: simultaneous recording of force in foot to head direction, SCG, ICG and ECG. The horizontal axes is time and the vertical line is in Newton. The B and X points on ICG and the H point on BCG is annotated.

A different group in Korea, inspired by the research in Stanford, recorded the weight scale BCG, together with blood pressure using Finapress (FMS 2007) instrument, showed that the delay between the R wave of ECG and the global peak on the BCG signal is correlated, r=0.76, with systolic blood pressure (Shin, Lee and Park 2009). Prior to this study, the same group conducted separate research on the estimation of blood pressure from sensors on the toilet sink (Kim, et al. 2006).

Using a force plate, the force of cardiovascular origin was recorded in a foot-to-head direction, in addition to SCG, ICG and ECG as demonstrated in Figure 8. The standing position produced a signal morphology very similar to the reported weight-scale BCG (Inan, Etemadi and Wiard, et al. 2009), and the

seated position produced a morphology resembling the Q-SCG (Stork and Trefny 2010). Standing position BCG corresponded to almost a two-fold amplitude compared to the recordings obtained while the participants were seated, and approximately thrice that of lying supine (Figure 8). The upright position could also provide a more stable beat to beat morphology compared to the other two methods.

2.3 Infrasonic cardiac signals: Precordial recordings

Precordial or cardiac examination is performed as part of the routine physical examination to detect the presence of cardiovascular pathologies. These tests include the examination of palpation and auscultation. In the palpation examination, the pulsations of the heart and great arteries that are transmitted to the chest wall are appreciated qualitatively, with tactile sense, while in auscultation exam, the sounds of the heart are obtained through phonocardiography (Braunwald and Perloff 2001). The amplitude of the signals are different depending on the point on the chest were recordings are picked up from, and can be from 3.6 mm in the left parasternal region up to about 1 cm on the point of maximum impulse (Droitcour 2006).

The precordial palpation examination dates back to the beginning of medicine, and there are records that indicate it was performed more than six hundred years ago. William Harvey has also mentioned the apical pulse in his famous book on circulation (Harvey 1628).

A number of different terms have been employed by physicians to describe these pulsations such as “lift”, “heave,” or “bulge”. The techniques reviewed in this section are methods that quantify such pulsations, and record the acceleration or displacement of specific points on the chest caused by these pulsations. Figure 9 shows different classical precordial recordings as far back as the 1970s (Stapleton and Groves 1971). This area of research is ambiguous as many different apparatuses have been used for precordial recordings and there is a lack of a common standard method of recording.

With every heartbeat, shape and positional changes of the heart and intracardiac events vibrate the pericardium. These vibrations are divided into two different frequency ranges: high frequencies (20-2000 Hz, or auditory range) and low frequencies (0-30 Hz, which also includes the infrasonic range). The first group, high frequencies, are those produced by intracardiac events such as the opening and closure of the heart valves, ejection, and murmurs and are studies in phonocardiography.

Shape changes and movements of the heart cause the second group, low frequencies, during ejection and filling, which is the focus of this study. These two categories of signals overlap at times in the way they relate to intracardiac events, but the low-frequency range provides us with a different spectrum of clinical information from that of the phonocardiogram (Eddleman 1974).

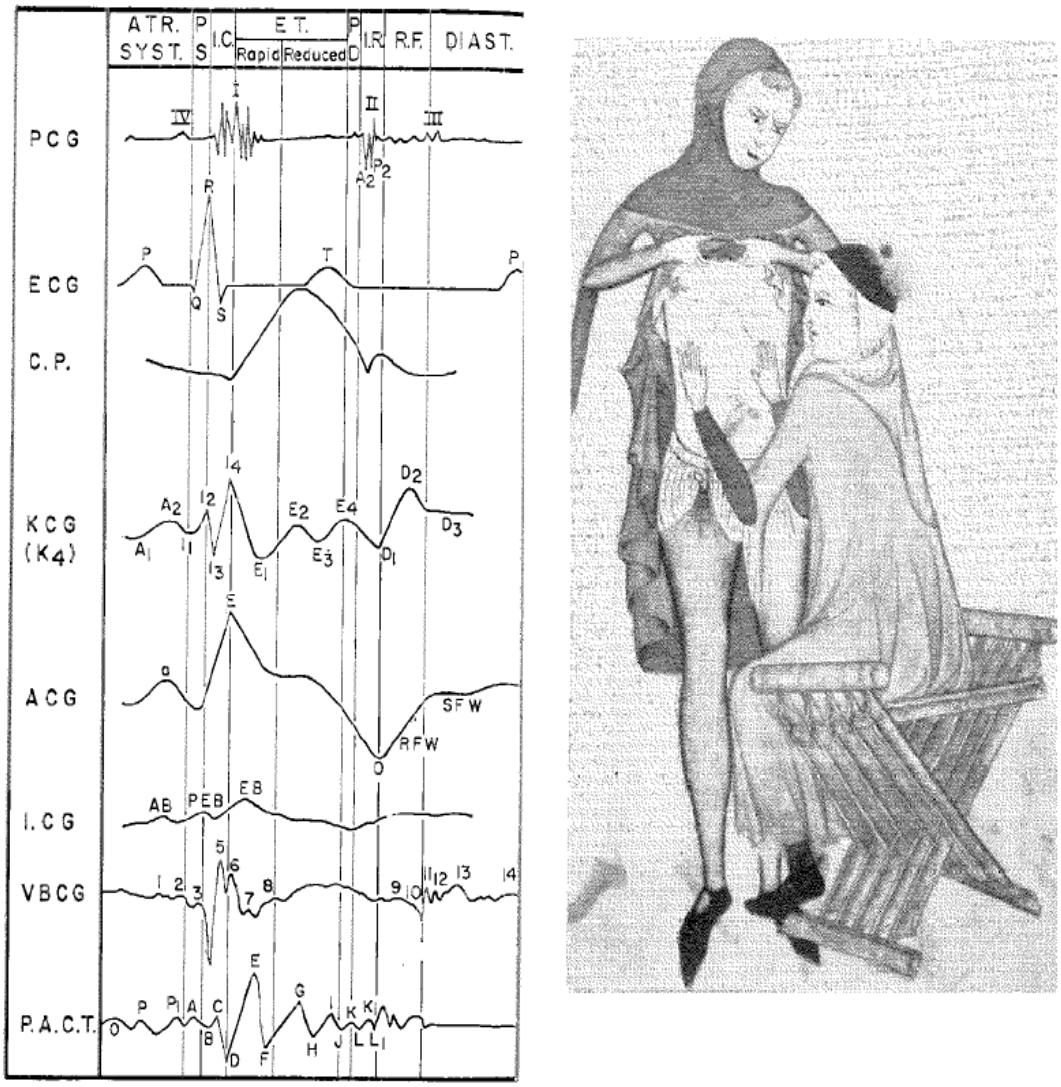

Figure 9. On the right: shows a fourteenth century physician palpating his patient. On the left: Older methods of quantifying precordial palpations. CP: carotid pulse, VBCG: vibrocardiogram, PACT: precordial accelerogram (Stapleton and Groves 1971). Reproduce by written permission from Elsevier.

As BCG was the most studied signal in this wide area of research, there has been a tendency, on occasion, to use the same terminology as used in BCG to look into this category of precordial cardiac signals (Mounsey 1957) (Mckay, et al. 1999). On the other hand, one needs to distinguish the fact that BCG is solely

created by the movements of the centre of mass of the body while the signals of the category studied in this section are created by local vibrations of the chest.

The interest in precordial recordings dates back to 1885 when Marey studied the movements of the pericardium with the use of a capsule; however, systematic study started after the work of Dressler on pulsations of the chest wall (Dressler 1937). As mentioned before, there has always been difficulty in the interpretation of different precordial recordings because of a variety of names and apparatuses used for recording these signals. In the past, precordial recordings were extensively studied in two categories of relative displacement records such as apexcardiography, and absolute displacement records such as kinetocardiography. In the first category, the frame of reference is locally on the chest, and in the second is a point outside the body (Schweizer, Bertrab and Reist 1965).

Kinetocardiogram and impulse cardiogram are basically the same systems, and the frame of reference for both is outside the body; in apexcardiogam (ACG), mechanocardiogram (MCG), and vibrocardiogram (VCG) the reference is on the chest (Eddleman 1974). Another distinct group of precordial recordings were those directly measuring precordial accelerations. Seismocardiogram, which is the main context of this research, belongs to this later group of precordial recordings, and was first recorded in 1964 by Baevski who borrowed the technology and concepts from seismology and recorded precordial accelerations deemed seismocardiograms. These three categories of

precordial recordings are explained in detail in the coming sections, but first, a brief physiological back ground underlying these pulses is presented.

2.3.1 Chest pulsations during cardiac cycle

The changes in the volume and shape of the heart during different phases of the cardiac cycle move the ribs and tissues near the heart, and cause pulsations in the chest with every heart beat. These pulsations are recorded from different points of the chest, take different clinical names, and are mainly in the infrasonic cardiac range, as mentioned earlier in this chapter.

The human heart is located in the middle of the thorax, between and partially overlapped by the lungs. Almost two thirds of the heart is to the left of the midline. The sternum, where SCG is recorded from, covers the front of the heart, as do the third, fourth, and fifth ribs. The heart sits on the diaphragm and is directed forward and to the left so the heart apex is the most anterior point. The pulsation created by the apex of the heart can be felt at the fourth or fifth intercostal space where ACG is recorded (Droitcour 2006).

The left ventricle in particular has the dominant effect in the creation of these pulses. During the isovolumic contraction phase, the heart rotates counter-clockwise, facing the subject, and the lower anterior part of the left ventricle strikes the anterior chest wall which causes a short, outward motion. This is followed by medial retraction of the adjacent chest wall during ejection. The peak

of the left ventricular impulse occurs simultaneously with or immediately after the aortic valve opens, then the apex moves inward (Braunwald and Perloff 2001).

There is a belief that two processes have simultaneously opposing effects on the thoracic wall (Dressler 1937). The change in shape (i.e. the increase in curvature) and, in particular, the rise of the apical portion during systole forces the thoracic wall outward, whereas the reduction in ventricular volume tends to draw the thoracic wall inward. When the left ventricle shortens longitudinally, its shape becomes more spherical, and this increases the diameter and pushes the chest wall outward.

Recordings of the left parasternal impulse has shown that in the beginning of systole, the chest is pushed outward by the ventricle, while later in systole, inward movement occurs (Gillam, Deliyannis and Mounsey 1964). This is in accordance with Braunwald and Perloff (2001) as they also reported an outward movement of the apex during diastolic filling.

2.3.2 Relative displacement recordings

In this section, a category of precordial recordings, in which the movement is measured relative to a point on the chest, are briefly introduced. The most important recording in this category is apexcardiography (ACG).

2.3.2.1 Apexcardiogram

Apexcardiogram is a signal recorded from the point of maximum impulse (PMI) where the apical pulse is the strongest. This point is normally located in the fifth intercostal space of the thorax, left of the midclavicular line. A valuable observation on ACG is the lack of delay between the cardiovascular events and the ACG peaks (Tavel, et al. 1965). A trace of normal ACG is in Figure 9.

Tavel has introduced ACG as a reference for phonocardiogram. In his experiments, Tavel showed that the peak of the A wave in ACG occurs at the same time as the fourth heart sound, S4. The beginning of the abrupt rise after the A wave on ACG occurs in conjunction with the initial vibrations of the first heart sound; the E point is synchronous with the third component of the first heart sound, S1. The sharp downward slope near the end of systole occurs close to the A2 component of the second heart sound, S2; the O point coincides with the mitral valve opening. The peak of rapid filling is approximately at the third heart sound (M. E. Tavel 1967).

Apart from being a reference to phonocardiography, it is demonstrated that ACG shows characteristic changes in certain cardiac diseases. Benchimol and Dimond (1962) showed that the A wave is larger in ischemic heart patients. A detailed relation of ACG to cardiac abnormalities can be found in M.E. Tavel's (1967) extensive research on the topic.

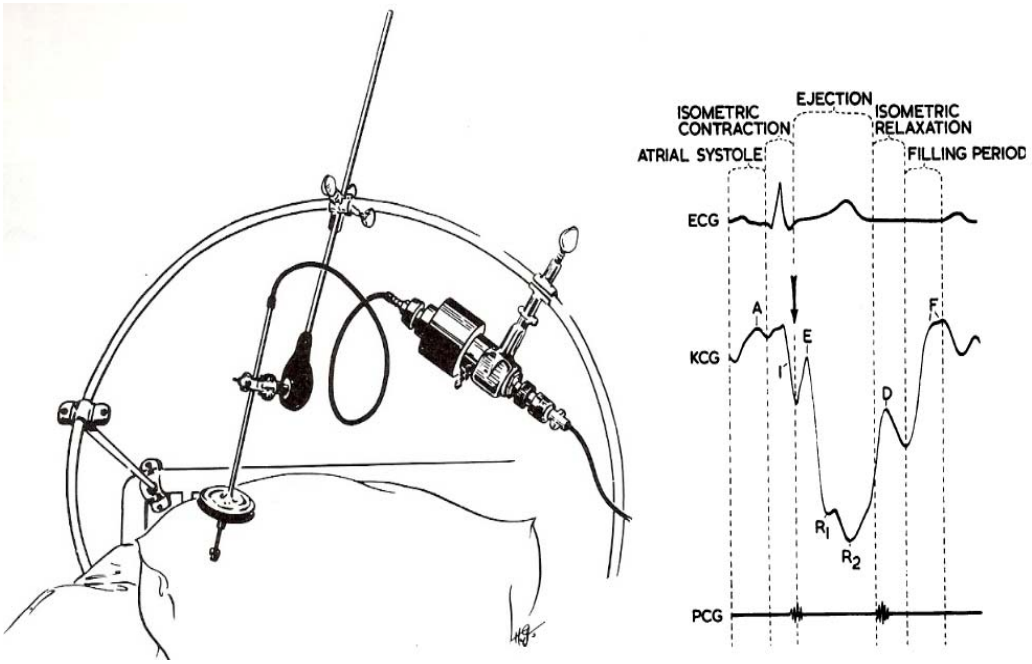

Figure 10. On the left a device for recording of KCG (Bancroft and Eddleman 1967)with written permission from Elsevier. On the right KCG signal recorded with ECG and PCG. (Schweizer, Bertrab and Reist 1965) with written permission from BMJ publishing group Ltd

2.3.3 Absolute displacement recordings

As mentioned previously in this category of recordings, the reference point for the measurement of displacement is outside the body.

2.3.3.1 Kinetocardiography (KCG)

An apparatus for measurement of KCG is seen in Figure 10, together with a recording of KCG at the K4 lead. The KCG points of recording are the same as ECG ventral leads after the “V” has been replaced with K. Thus, K4 lead in KCG indicates the position of the recording probe on the fourth left interspace at the

sternal edge; K4 is the same apical impulse as recorded in ACG (Stapleton and Groves 1971).

2.3.3.2 Left Parasternal Cardiogram (LPC)

Left parasternal cardiogram impulse was recorded from the left side of the sternum at the third or fourth intercostal space (Gillam, Deliyannis and Mounsey 1964). It was observed that in most normal participants, the left parasternal region moved outward during early systole followed by a retraction in late systole, while patients with right ventricular hypertrophy had an abnormal signal contour. It was shown later that the left parasternal cardiogram can be used to obtain a non-invasive assessment of the severity of mitral regurgitation (Basta, et al. 1973).

2.3.4 Precordial accelerograms

Precordial accelerograms were direct measurements of acceleration from the chest obtained through a different recording technique known as precordial ballistocardiography (Mounsey 1957).

2.3.4.1 Seismocardiography (SCG)

A German geophysicist, Angenheister, in 1928 was the first to borrow the technology used in seismology to record infrasonic cardiac signals (centre of mass category). He did this by placing a seismograph on a rigid table and recorded signals similar to BCG (Starr and Noordergraaf 1967).

The first use of the word seismocardiogram was traced back to two separate Russian research works by Roman Baevski (1964) and Bozhenko (1961). These groups were inspired by the technology used in seismology for the measurement of acceleration, and used it to measure precordial accelerations. Baevski's intent was to measure the fluctuations caused by heart, similar to a seismologist registering underground vibrations to predict earthquakes. A sample of some original SCGs are depicted in Figure 11, and in all the recordings, the systolic and diastolic complexes can be visually distinguished from each other.

Bozhenko recorded signals from 4 Hz to 40 Hz by placing the accelerometer on the chest between the ribs. He recorded signals from abnormal hearts, such as mitral valve problems, and compared their morphology to normal SCGs as in Figure 11. The basis of Baevski's accelerometer was a magnetic mass connected to a spring that could mechanically oscillate between two induction coils; the current induced in the induction coils was proportional to acceleration. In a study on 20 participants, Baevski calculated the mean values of the time intervals from the ECG's Q wave to systolic and diastolic components of SCG.

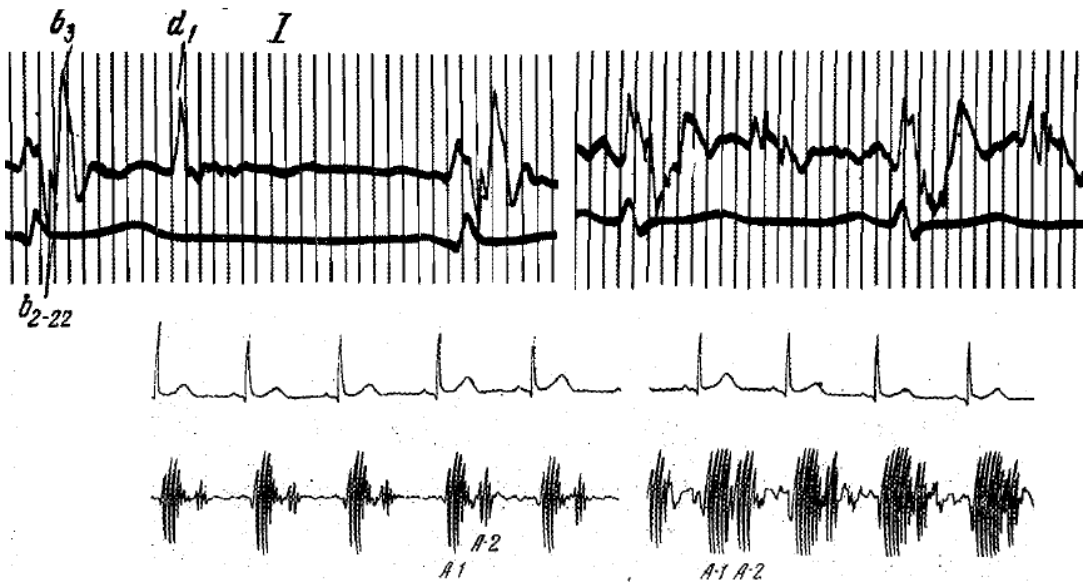

Figure 11. The first recordings of SCG. Top: SCG recording together with ECG as in Bozhenko's work (Bozhenko 1961) on the left a healthy heart and on the right a heart with mitral stenosis. Bottom: Simultaneous SCG and ECG before (left) and after (right) exercise as in Baevski's work (Baevski and Egerov 1964). The bottom figure is reproduced with a written permission from Roman Baevski.

In the beginning, SCG was mainly used in aerospace program in Russia. The first SCG in microgravity was recorded in a dog onboard of the third Russian sputnik in 1960. The first SCG in cosmonauts during space flight has been recorded onboard of Vostok 5-6 from 1962 to 1964. SCG was used for crew health monitoring onboard the spacecraft "Sojus" in the early seventies and is used onboard the ISS since March 2007 as part of the Pneumocard and Sonocard experiments.

Twenty five years later, seismocardiography was first introduced into clinical medicine and commercialized by J. Zanetti (earthquake seismologist) and D. Salerno (cardiologist) in USA. Unlike Baevski, who recorded SCG from different points on the torso, they recorded acceleration in the supine position

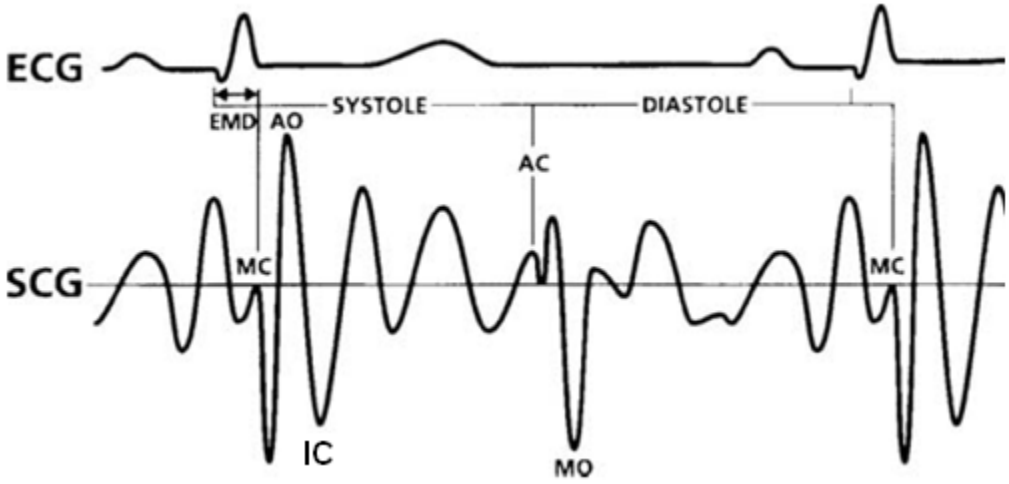

Figure 12. SCG signal annotated based on the cardiac events by Zanetti (Salerno and Zanetti 1991). MC and MO are for mitral valve closure and opening respectively, AC and AO are for aortic valve closure and opening respectively, EMD is the electromechanical delay. IC is the isotonic contraction time which is renamed to maximum acceleration (MA) as the results of the research conducted for this thesis. The figure is reproduced with a written permission from John Wiley and Sons.

from a fixed point on the sternum in the dorso-ventral direction or in the negative z-direction of the conventional axes of Figure 5e. This is the same recording setup that has been used in this thesis work; a sample of recorded SCG signal in this research was shown in Figure 1 and a sample of signal recorded by Salerno and Zanetti(1991) is in Figure 12.

Through the simultaneous study of SCG and ECG, Salerno and Zanetti claimed that changes in SCG after exercise were more sensitive for the detection of moderate coronary artery stenosis than ECG (Salerno and Zanetti 1991). Later, the claim that the qualitative seismocardiography was more accurate, both in sensitivity and specificity than electrocardiography for the detection of coronary artery stenosis was further investigated on more patients (n=505). SCG was

able to accurately detect the presence of moderate or severe multi-vessel disease, in addition to the presence or absence of myocardial infarction (Salerno, Zanetti and Crow 1992) .

Seismocardiogram is comprised of two different subgroups of signals. In the first group, which is utilized in the majority of the papers, the signal is recorded by positioning an accelerometer on the sternum, In the second group, the accelerometer is placed at other locations on the torso, such as left clavicle (Castiglioni et al. 2007). In one research work the signal is recorded from the seat and it is called Q-SCG (Stork and Trefny 2010). Q-SCG belongs to the centre of mass measurement category not the precordial recordings as also seen in Figure 3.

The first commercial SCG instrument was a failure and this was to some extent because of the heavy and bulky seismology sensor on the sternum, which was cumbersome to tolerate for a long period. New sensor technologies have provided new possibilities for portable and wireless sensors that can be worn under clothing to record the SCG signal during daily activities. A new line of research has emerged aiming to re-introduce SCG as a clinical instrument that can be used to non-invasively, and inexpensively, diagnose cardiac abnormalities (Castiglioni et al. 2007;Tavakolian et al. 2008b).

The analysis of SCG provides new information on the mechanical aspects of the cardiovascular system. In a study conducted by Salerno, the SCG signal

was simultaneously recorded with echocardiograph images for 39 participants; it was shown that aortic and mitral valve opening and closures could correspond to peaks and valleys on the SCG signal. Nevertheless, this study was done using M-mode echocardiography with an old echocardiograph machine back in 1991 that limited the accuracy of the measurements due to its time resolution (Crow, et al. 1994).

An example of SCG trace recorded and annotated by the Salerno group is shown in Figure 12. After the P wave on ECG, and during the QRS complex, there is a local maximum corresponding to the mitral valve closure (MC). The interval between this point and the next maximum (the aortic valve opening) is the iso-volumic contraction interval. Rapid systolic ejection point (RE) is the next maximum after that. At the end of the systole the aorta closes (AC) followed by the opening of the mitral valve (MO).

The minimum point after the AO point was named isotonic contraction (IC) by Salerno and Zanetti (1991) but this claim was not fortified by experimental evidence for it. The results presented in chapter 5 of this thesis provides evidence for this point to have been created by maximum acceleration of blood in the aorta rather than isotonic contraction time.

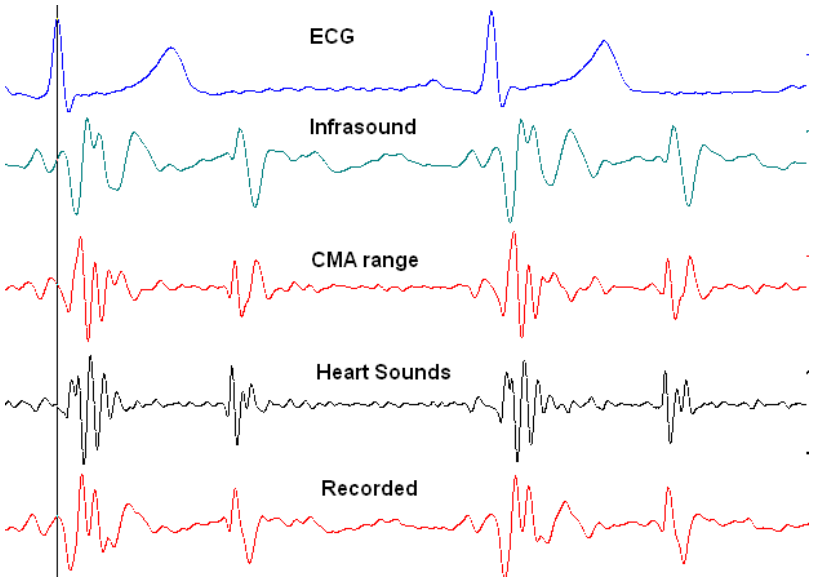

Figure 13. The signal recorded from the sternum, the bottom trace, filtered in different bandpass frequency ranges from bottom to top; unfiltered original signal, phonocardiogram range (50-1000Hz), CMA range (15-100Hz) and Infrasound range (SCG).

2.3.4.2 Triaxial Recordings

Using tri-axial accelerometers to record precordial vibrations is a new trend motivated by the development of accurate MEMS sensors (Shell, Peters and Russell 2007). The novelty also offered by the new technique is the simultaneous extraction of auscultation information, or phonocardiogram, that belongs to higher frequencies, and infrasonic information from the same accelerometer (Castiglioni, et al. 2007). The accuracy of MEMS accelerometers in the extraction of low frequency vibration signals has also been investigated (Chuo, Tavakolian and Kaminska 2009).

2.3.4.3 Sternal Acceleration Ballistocardiography (SAB)

The precordial recording from sternum was also recorded by another group in Canada, and although being aware of seismocardiography, they chose the name sternal ballistocardiography as the recordings were in the same axis as most classic ballistocardiograms (foot to head direction) (W. P. Mckay, et al. 1999). Nevertheless, the actual direction of recording in SAB research was opposite to the traditional foot to head drection as in BCG. An effort was made by this group to estimate stroke volume and cardiac output from the SAB signal, in conjunction with the arterial pressure signal.

The SAB recording setup was reproduced for this research, and signals were recorded, together with ULF-BCG and ECG, that are plotted in Figure 13 for one participant. The signal in the reverse direction is also plotted.

2.3.4.4 Cardiac micro acceleration (CMA)

Cardiac resynchronization therapy, CRT, or biventricular pacing, is a form of therapy for specific types of congestive heart failure in which the ventricles are asynchronous, and specialized pacemakers are used to restore synchrony to the ventricles. The delay between atrial and ventricular activation must be optimized in order to gain the optimum mechanical performance of the heart. In a study by the Sorin medical group, a micro-accelerometer was placed close to the electrode which served to pace the ventricles (Giorgis L 2008).

Using this accelerometer, a signal was obtained which was generated by the left myocardium during the isovolumic contraction period. It was proven that the amplitude of this signal was related to the optimal atrioventricular delay. What brings this research close to the context of the research presented in this thesis is the fact that in a separate study, the same group recorded vibrations from sternum based on the external version of the same accelerometers (used to record the endocardial accelerations), and called these non-invasively recorded vibrations cardiac micro-acceleration or CMA. For these non-invasively recorded signals, CMA, the timings of cardiac intervals was compared with that of Doppler echocardiography.

The CMA signal was analogically band-pass filtered between 15-100 Hz which puts it outside the infrasonic range. Using Doppler ultrasound it was shown that, the aortic and mitral valve closure times could be estimated with high accuracy from the features extracted from the CMA signal. The results on the valve opening times were not as successful for the CMA signal compared to results for closing times.

In order to assess the similarities and differences of the morphology between different frequency ranges, signals were recorded using the same accelerometer with a wide recording band, then filtered in different frequency ranges as phonocardiogram, CMA and SCG, and the results can be seen in Figure 13.

2.4 Non-Contact Methods

Non-contact monitoring of human cardiac and respiration activities through clothing can provide us with a unique tool in home monitoring and sleep analysis studies. On the other hand, a common problem with surface recordings is that when the recording sensors contact the surface of the chest (to record vibrations created by the heartbeat), they induce loading effects on the mechanical system based on their size and weight. Determination of the effects of loading the chest with a microphone has been studied in the past, and such studies need to be expanded in order to more accurately assess the underlying signals that could have been recorded if the loading effect was absent(Vermarien and Vollenhoven 1984).

Non-contact techniques, such as laser or microwave radar recordings, can relieve us from such tedious modelling. On the contrary, non-contact methods can provide new possibilities for monitoring the cardiovascular state that might not be feasible in contact recording schemes, such as the usability in monitoring sudden infant death syndrome. Different non-contact methods such as laser and radar have been used in the past for recording infrasonic cardiac signals and precordial recordings.

2.4.1 Laser

Laser Doppler vibrometry is a method in which laser beams are directed at the surface of interest, and the movement of the surface is detected via

measurement of the Doppler shifts in the returning beam. This method is used in the biomedical field because of its high accuracy, high resolution (8 nm), and the non-contact nature of the recording (Morbiducci, et al. 2006).

Laser displacement has been used to measure precordial movements (Aubert, et al. 1984), and has been compared with conventional apexcardiography (Ronaszeki, Aubert and Geest 1990). In a study by Morbiducci, et al (2006), the vibrations of the chest were simultaneously recorded with ECG. The capability of the signal for heart rate variability studies were investigated compared to ECG, but the exact point on the chest where the recordings were taken from was not specified. Laser was used to record SCG in this research work and is described at the end of chapter 3.

2.4.2 Microwave radar

Although laboratory demonstrations of the use of Doppler radar for cardiovascular and respiratory measurements date back to the late 1970's and early 1980's (Lin 1975) (Lin, Kiernicki, et al. 1979), cost-efficient, wearable body signal monitoring devices have not been reported until recently; the implementation of low-cost, low-power, battery-operated devices is more feasible than ever by virtue of the availability and advances in high-integration technologies, signal processing techniques, and high-speed communication networks (Droitcour 2006).

Depending on the application, microwave Doppler radar systems may use a continuous-wave or a time-gated radar signal. Continuous-wave Doppler radar has been shown to be comparable with impedance cardiography methods to measure the mechanical activity of the heart. In fact, the derivative of the radar signal shows correlations with the impedance cardiogram signal (ICG) (Thijs, et al. 2005).

The only effort in the past to compare microwave radar recordings to other methods of precordial recording was reported by Geisheimer and Grenker (1999). The radarcardiogram signal was compared to the tri-axial accelerometer recordings, and there was a clear morphological difference between the two recordings. An extensive review of radar use for the acquisition of vital signals is presented in the next chapter and also in appendices.

2.5 Comparative analysis of infrasonic cardiac signals

As mentioned before, the BCG signal is the most studied signal in the field of infrasonic cardiac signals, and has been around for about a century. BCG is different compared to SCG as it reflects the movement of the centre of gravity of the whole body and its support, while SCG reflects the mechanical vibration of the upper part of the body as recorded from its surface. Figure 14 shows the acquisition setup and sensors that were used for the simultaneous acquisition of infrasonic cardiac signals in this research.

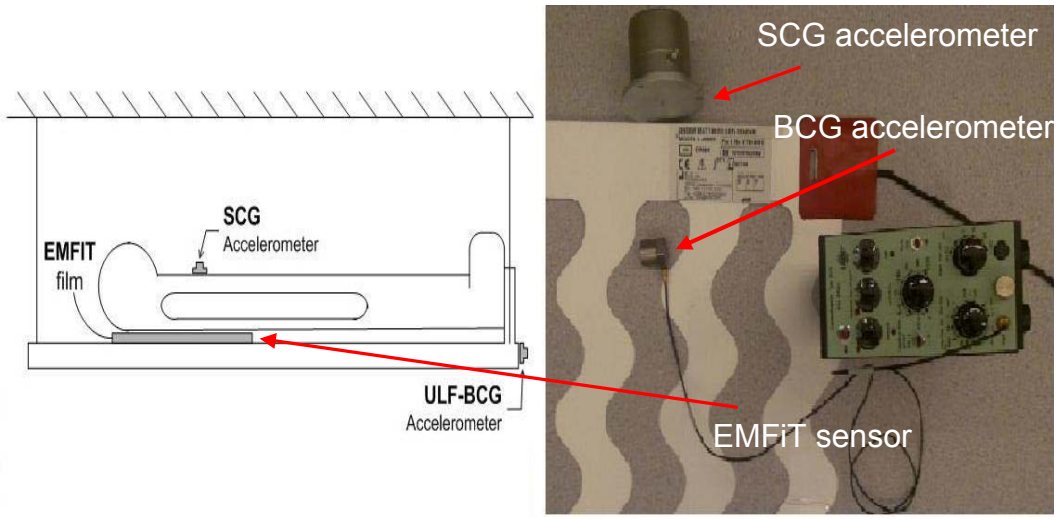

Figure 14. Left: Data acquisition setup for simultaneous acquisition of SCG, ULF-BCG and EMFiT. Right: The sensors used for recording of these signals.

As SCGs are recorded from positions closer to the heart, there is less mechanical damping of the cardiac vibration compared to classical BCG, in which the heart moves the whole body and the recording system (bed, chair, and weight scale). This is important because precordial recordings are taken close to the heart and are, therefore, able to trace valvular activities which would get dampened out by centre of mass recordings such as ULF-BCG beds. Thus, in terms of the evaluation of the timing of valvular events, precordial recordings such as SCG are a better candidates compared to BCG.

On the other hand, as BCG is a record of the sum of all the cardiovascular forces exerted on the body, its amplitude is a more faithful representation of the force of the cardiac system compared to precordial recordings, such as SCG, which reflect a portion of this force that affects the upper body. thus, BCG is a better candidate to estimate stroke volume and cardiac output (Starr and

Noordergraaf 1967). The old BCG instruments were quite bulky and required patients to lie down on beds suspended from the ceiling, while SCG facilitates signal recording, and, thus, provides alternative possibilities that BCG was inherently unable to provide.

A comparative analysis of SCG (a representative of the precordial recording category), with ULF-BCG and EMFiT recordings (representatives of the centre of mass recording category), was performed in this research (Tavakolian, et al. 2009). Data from one cycle of simultaneous recording of SCG and ULF-BCG for four young (less than 30 years old), healthy male participants are shown in Figure 15. A quantitative comparison of SCG and ULF-BCG is presented in chapter five. These comparisons clarified that the “I” point on ULF-BCG occurs at the same time as the MA point on SCG, as also observed in Figure 15.

The well-tested commercial sensor technology by EMFIT was also used to observe the mechanical activities of the heart (EMFiT Ltd 2010). Model L-4060, which is approximately 40cm by 60cm, was used for data acquistion (Figure 14). The sensor was located on the suspended ULF-BCG bed which allowed participants to lay supine on top of it supinely (Figure 14). The obtained recordings were not similar to the original reported records as in Junnila et al (2008) thus, the recordings depicted in the right side of Figure 15 were taken from a sturdy bed instead, and not the hanging bed as in Figure 14.

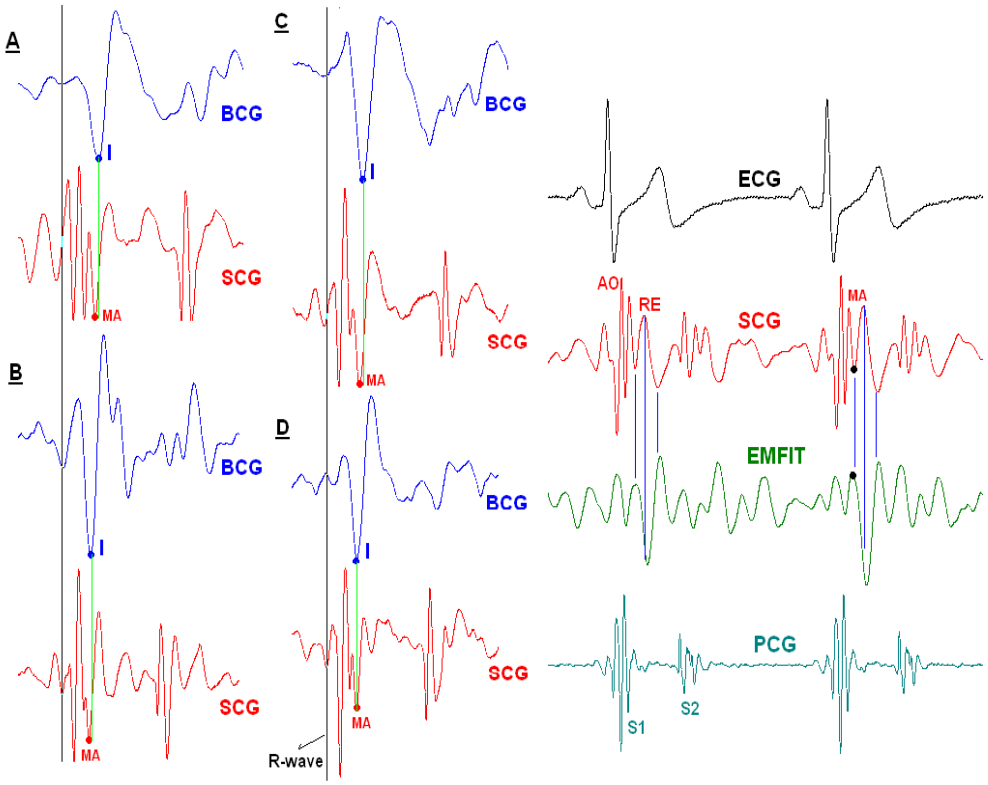

Figure 15. Left: One cycle of simultaneous recording of SCG and ULF–BCG for four participants (A,B,C and D). The black vertical line shows the ECG R wave and the I wave on BCG is connected by a green vertical line to the maximum aortic blood acceleration point (MA) on SCG. Right: two cycles of simultaneous recording of ECG, SCG, EMFiT and PCG. The MA point on SCG is connected by a line to its corresponding point on EMFiT recording.

The EMFIT sensor is a permanently charged elastic film. If a force is induced to the film, a change in charge is generated which can be detected at the sensor output with a simple charge amplifier. For instance, if a pressure of 100 kPa is induced, the EMFIT sensitivity will be above 100 pC/N (Junnila, Akhbardeh and Varri 2008). A slightly modified version of this charge amplifier, suggested by EMFIT, was implemented in this work to convert the change in charge to voltage (EMFiT Ltd 2010).

As it is observed from the right side of Figure 15, the RE wave on the SCG corresponds to a reverse replica of itself on the EMFIT recording. A change in polarity was expected between the EMFiT and SCG, considering that they record the same cardiovascular force from opposite points of view (SCG from the front and EMFiT from the back). The categorization of EMFiT into the centre of mass group makes more sense because the EMFiT recording's main component, occurs after the opening of the aorta when blood flows out of the heart, similar to ULF-BCG.

3: SEISMOCARDIOGRAM RECORDING

"The heart, consequently, is the beginning of life; the sun of the microcosm, even as the sun in his turn might well be designated the heart of the world; for it is the heart by whose virtue and pulse the blood is moved" William Harvey 1628

The equipment currently available to the medical community for recording precordial vibrations is either large and bulky or difficult to synchronize. In this chapter, novel technologies for the acquisition of seismocardiogram are proposed and explained. Section one describes a new, integrated sensor system that was developed to record cardiac vibration and cardiac potential simultaneously and synchronously from a single, compact site on the chest. This sensor system is lightweight, small in size, and suitable for mounting on ambulatory patients. The sensor was evaluated for its adequacy in measuring cardiac vibrations and potentials. In this evaluation, 45 independent signal recordings were studied from 15 volunteers. The morphology of the recorded signals was analyzed qualitatively (by visual inspection) and quantitatively (by computational methods) against larger devices used in established cardiac vibration studies (reference devices).

It was found that the cardiac vibration signals acquired by the integrated sensor had 92% and 82% identifiable systolic and diastolic cardiac complexes, respectively, when compared to the cardiac vibration signals recorded from the reference device. Further, the cardiac potential signals acquired by the integrated sensor showed a high correlation coefficient (r= 0.89) and a high estimated signal-to-noise-ratio of 22.00 dB when compared to the reference electrocardiogram acquired through a common clinical machine.

Sections 3.2 and 3.3 describe the non-contact methods of ultrasound and laser as proposed methods for the acquisition of SCG. The radar acquisition of SCG is explained in more detail. These three methods have been compared to a previous method of precordial recordings used by McKay, et al (1999); they used a B&K, high sensitivity accelerometer for SCG recording (Brüel & Kjær 2006). For this chapter, the sensor used by Salerno and Zanetti (1991) was not used as it was too large (1 Kg) to be used while standing or sitting.

3.1 Multisensor recordings

In all cases of cardiac vibration studies, interpretation of the vibration signals is difficult without a reference cardiac potential (electrocardiography, ECG) recorded synchronously. In most embodiments of infrasonic cardiac signals the ECG is an integral requirement of the point pick process of the vibration signal as it provides a fiducial reference to permit averaging of the mechanical waveforms.

Off-the-shelf instruments for digitization of multiple channel analogue signals were often used for this purpose (e.g. BIOPAC and NI DAQ). Some advanced, portable instruments may be used; however, their size and weight limits the system to a table-top setup, at best. Furthermore, wiring between sensors and the digitizer makes its use in ambulatory clinical settings impractical. To address these concerns, a new sensor platform was developed to support multiple sensors for the recording of multiple physiological parameters simultaneously and synchronously from a single site (Chuo and Kaminska 2009).

The sensor system was small, light-weight, easily-applied, and mechanically flexible for tight coupling with the body surface. The system consisted of multiple, stacked layers across which the processing electronics and sensors were distributed. The layer closest to the body's contact surface was configured to carry both the vibration and biopotential sensors. An overview of the architecture of the integrated sensor system is presented in the appendices, and more details of the integrated sensor system design and implementation are presented in two published papers (Chuo, Tavakolian and Kaminska 2009) (Chuo and Kaminska 2009).

3.1.1 Participants and data-acquisition

Forty five independent sessions were recorded from 15 different participants. The integrated multisensor and reference sensors were placed on each participant, and the cardiac vibration and cardiac potential signals were

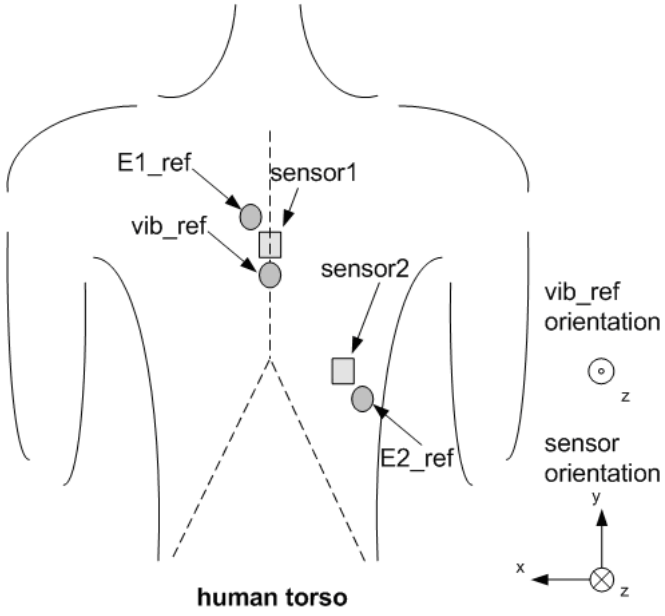

Figure 16. Sensor placements for acquiring signals for comparison between novel integrated sensor devices and reference sensors: sensor1 placed at mid-length of the sternum, while the reference high-precision vibration sensor immediately lower on the sternum; sensor2 is placed at approximately 2-in. from the xiphoid process about the sixth rib on the left-side of the torso; reference electrodes E1_ref and E2_ref are placed immediate beside sensor1 and sensor2 respectively (Chuo, Tavakolian and Kaminska 2009) Reproduced with written permission from Springer.

recorded over three separate trials of 15-s duration. Of all three trials, each of the participants were instructed to hold their breath in one, breathe deeply in one, and breath normally (lightly) in one. The variation in breathing pattern provided a means to verify that the novel sensor was suitable for recording cardiac vibration signals without drastic failures in a few (but critical) commonly encountered situations during real-life clinical recordings.

The participants ranged in age from 20 to 57 years old, and included both males and females. The participants ranged in height from 152 to 187 cm, weighed between 41 to 86 kg. Most participants had little to no hair in the torso

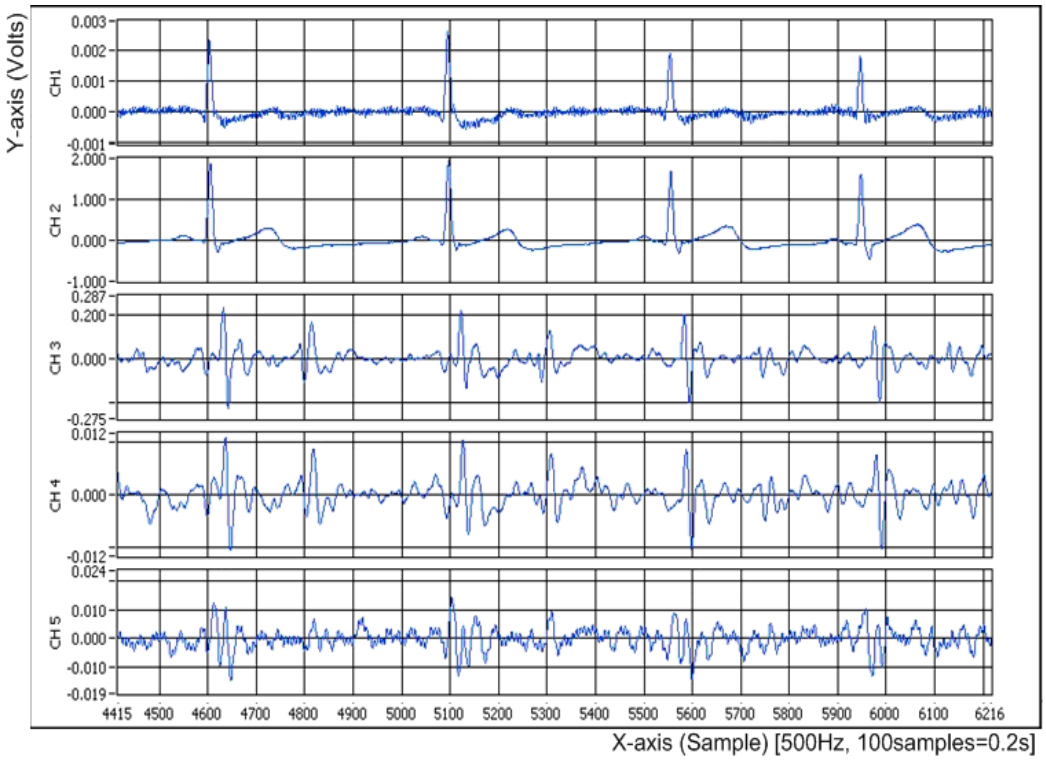

Figure 17. A section of waveforms from Session-1 as a representative example of most signal traces. Post-processing filters applied. CH1— cardiac biopotential from sensor1 and sensor2; CH2—reference ECG.

region which allowed for secure attachment and signal coupling. The small demographic sample was considered sufficient for the preliminary evaluation of the integrated multisensors against the reference sensors to verify its ability to output waveforms of similar morphology, and sufficiently adequate for identification of key cardiac phases.

The placement of the integrated multisensors and reference sensors on the participant torso are shown in Figure 16. Integrated multisensors, sensor1, was placed at mid-length of the sternum, while another, sensor2, was placed at

approximately 5 cm lateral from the xiphoid process near the sixth-rib on the left side of the participant's torso.

The reference vibration sensor was placed immediately below sensor1 on the sternum. The placement of sensor1 and the reference vibration sensor on the sternum followed that of previous studies (Salerno and Zanetti 1990). The placement of sensor2 provided additional insight on cardiac vibration closer to the apex of the heart for exploratory comparison.

Two standard disposable ECG electrodes were placed immediately beside sensor1 and sensor2 at the 10-o'clock and 4-o'clock positions, respectively. The disposable ECG electrodes were connected to the standard ECG machine. The potential difference between sensor1 and sensor2 formed a non-standard ECG lead, while the potential difference between the disposable reference ECG electrodes also form the same (or as close as possible) non-standard bipolar ECG output. The reference ECG signal formed by the setup of disposable electrodes was connected to a standard ECG machine, thus only differed from the dual-multisensor setup by the contact coupling and signal conditioning effects.

As discussed in the previous subsection, the use of ECG signals simultaneously and synchronously with infrasonic cardiac signals assists in the interpretation of the cardiac vibration signals. The QRS-complex of the ECG is often used as a fiducial reference to identify consecutive cardiac vibration signal

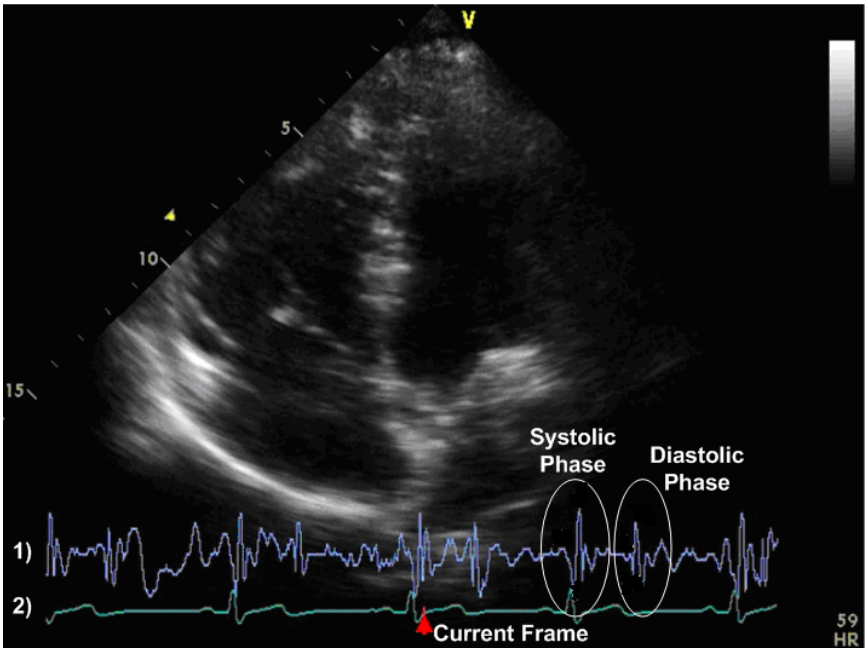

Figure 18. Snapshot of the M-mode echocardiograph video showing signals SCG(1) and ECG(2) recorded synchronously. Both systolic and diastolic phase of the cardiac cycle are seen on the SCG

and to permit averaging of the mechanical waveforms. Although as part of the research leading to this thesis, an alternative embodiment on SCG was evaluated for cardiac events without reference to the ECG (Tavakolian, Vaseghi and Kaminska 2008). Nevertheless, existence of simultaneous ECG can also provide the possibility of calculation of electromechanical delay and systolic time intervals of the heart that provides clinical information as explained in detail in chapter 6.

As a result, for the purpose of assisting cardiac vibration analysis, the ECG signal can be recorded from non-standard ECG leads (i.e. different electrode locations on the human torso than standard lead-I, II, III) as long as the

R-peak of the ECG signal is captured with sufficient resolution for (computer - aided) identification of cardiac cycles.

A digital acquisition module (NI-DAQ 9205) was configured to synchronously sample and save data from the multisensors and reference sensors. Each channel was sampled at 500 Hz with a conversion time of 4 μs. The sampling rate was well above the Nyquist requirements for ECG or SCG signals; the short conversion time was negligible compared to the time resolution of ECG or SCG events.

A total of five channels were recorded. The first channel recorded a bipolar cardiac potential signal from the pair of multisensors (sensor1 and sensor2); the second channel recorded bipolar ECG signal from the pair of reference electrodes. The third channel recorded the reference cardiac vibration signal (with axis of orientation normal to the frontal plane of the body). A fourth and fifth channel recorded the cardiac vibration signals (also in the axis of orientation normal to the frontal plane of the body) of sensor1 and sensor2, respectively.

3.1.2 Analysis of multisensor performance

A total of 45 sessions from 15 participants were recorded as described. A portion of the recording from Session-1 is shown in Figure 17 as an example representing the typical quality of the waveforms after post-processing. The signal-charts and filtering were generated in a custom LabView program. Post-

processing filtering, as described in the methods section, has been applied to both the reference and integrated multisensor signals. It can be seen from Figure 17 that the cardiac biopotential signal produced by the difference of sensor1 and sensor2 (CH1) is quite similar to that of the reference ECG signal (CH2).

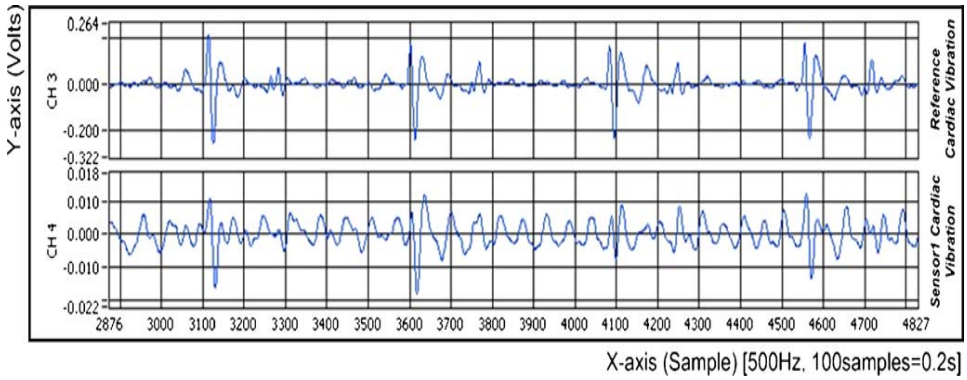

Figure 19. A section of the waveforms from Session-5 showing a by noise in the same frequency range as the signal. Post-processing example of noisy cardiac vibration signal from sensor1 where systolic filters applied. CH3—reference cardiac vibration; CH4—sensor1 complexes are identifiable while the diastolic complexes are masked cardiac vibration.

By visual inspection, the R-to-R peaks of CH1 seem to correspond exactly to that of CH2 (more precise analysis is presented later). The distinct T-waves of an ECG seen on CH2 can also be seen in some cycles of CH1. This example qualitatively shows that the cardiac biopotential signal produced by the integrated multisensors are similar to that of the reference ECG, and is adequate for assisting in the interpretation of SCG or other similar cardiac vibration signals.

It can also be seen from Figure 17 that the cardiac vibration signals acquired through the integrated multisensors (CH4 and CH5) are very similar in morphology to the reference SCG cardiac vibration signal (CH3). The vibration signal in CH4 corresponds to sensor1, which is located close to the reference

sensor, as shown in Figure 16. Meanwhile, the vibration signal in CH5 corresponds to sensor2, which is located farther from the reference sensor. As expected, the vibration signals recorded from sensor1 follow much more closely to the reference vibration signal than the signal from sensor2.

Since senor1 and sensor2 are identical hardware units, the difference in the waveform obtained can be primarily attributed to the difference in the location of the sensors on the torso. This is an intuitive observation and confirms that the cardiac vibration signals sensed from the chest surface vary in morphology as the location varies. On the other hand, when two sensors are placed close together, the resulting signals can be expected to be quite similar. The signal acquired from sensor1 mirrors the reference vibration sensor, and shows distinct systolic and diastolic phases of the cardiac cycle as in a classical SCG.

The three different respiration patterns performed by the participants resulted in cardiac vibration signal recordings that were very similar in morphology in all cases. The acceleration of the chest due to breathing was superimposed on the SCG signals; however, no significant morphological differences could be observed across different trials. As stated previously, although the intent of this study was not to characterize SCG signals in relation to various breathing patterns, rather, trials included various basic respiration patterns which provided a means to verify that the novel sensor was suitable for general recording of SCG signals, regardless of breathing behaviour.

Table 1. Summary of systolic and diastolic complexes correctly identifiable in the signals measured by the integrated multisensor compared to the reference vibration sensor.

Session	Participant	Age Sex (M/F)	Height (cm), Weight (kg),	Trial	SCG Systole	SCG Diastole
1	**1**	27	170, 66	Deep Breath	15/15	15/15
2		M		Hold Breath	17/17	17/17
3				Light Breath	-	-
4	**2**	25	175, 68	Deep Breath	14/14	13/14
5		M		Hold Breath	11/16	3/16
6				Light Breath	14/15	12/15
7	**3**	25	165, 68	Deep Breath	14/15	15/15
8		M		Hold Breath	9/13	11/13
9				Light Breath	14/14	13/14
10	**4**	22	162, 52	Deep Breath	8/10	8/10
11		M		Hold Breath	-	-
12				Light Breath	-	-
13	**5**	25	162, 61	Deep Breath	10/12	6/13
14		M		Hold Breath	11/13	6/13
15				Light Breath	13/13	8/13
16	**6**	26	168, 77	Deep Breath	14/15	13/15
17		M		Hold Breath	17/17	16/17
18				Light Breath	15/15	15/15
19	**7**	24	176, 64	Deep Breath	16/17	13/17
20		M		Hold Breath	13/13	13/13
21				Light Breath	13/13	13/13
22	**8**	29	187, 74	Deep Breath	12/12	9/12
23		M		Hold Breath	13/13	13/13
24				Light Breath	9/9	9/9
25	**9**	54	173, 86	Deep Breath	15/15	13/15
26		M		Hold Breath	16/17	13/17
27				Light Breath	14/14	13/14
28	**10**	56	168, 67	Deep Breath	-	-
29		M		Hold Breath	10/11	10/11
30				Light Breath	11/11	11/11
31	**11**	20	165, 66	Deep Breath	9/11	7/11
32		F		Hold Breath	8/9	8/9
33				Light Breath	9/10	9/10
34	**12**	27	152, 41	Deep Breath	20/21	13/18
35		F		Hold Breath	18/20	13/20
36				Light Breath	19/19	14/19
37	**13**	23	159, 52	Deep Breath	13/14	13/14
38		F		Hold Breath	12/12	12/12
39				Light Breath	12/12	12/12
40	**14**	39	153, 45	Deep Breath	14/14	10/14
41		F		Hold Breath	14/14	14/14
42				Light Breath	15/15	14/15
43	**15**	57	160, 62	Deep Breath	14/14	11/14
44		F		Hold Breath	12/13	9/12
45				Light Breath	13/14	11/14
Total Avg					*0.92379*	*0.81769*

The cardiac vibration signals from the reference and integrated multisensor (sensor1) were further compared quantitatively for all 45 sessions. The systolic and diastolic complexes (as indicated in Figure 18) were identified in both the reference and sensor1 for each independent recording. The number of correct identifications of the complex against the reference is reported in Table 1. For example, in Session 6, 14 out of 15 systolic cycles were identified in the integrated multisensor signal, while for diastolic complexes, 12 out of 15 were correctly identified.

A descriptive statistical summary of the results is presented in calculated to be 0.89±0.10;this high average suggested high resemblance between the two signals compared in each session. In one participant (10), excess chest hair resulted in poor electrode contact, which compromised the ECG signal; therefore, the ECG comparison analysis was disregarded.

It was found that the cardiac vibration signals acquired by the integrated sensor had 92% and 82% identifiable systolic and diastolic cardiac complexes, respectively, when compared to the cardiac vibration signals recorded from the reference device. Further, the cardiac potential signals acquired by the integrated sensor showed a high correlation coefficient (r= 0.89) and a high estimated signal-to-noise-ratio of 22.00 dB when compared to the reference electrocardiogram acquired through a common clinical machine.

Table 2. Descriptive statistical summary on accuracy of correctly identifiable cardiac signal complexes.

Category	Statistical Value	SCG Systole	SCG Diastole
Total	**Sample Size**	41	41
	Average (Mean)	0.92379	0.81769
	Median	1.00000	0.88889
	Standard Deviation	0.08155	0.17931
	Range	0.68750 – 1.0000	0.18750 – 1.0000
Male	**Sample Size**	26	26
	Average (Mean)	0.94041	0.83926
Female	**Sample Size**	15	15
	Average (Mean)	0.94931	0.82880
Under 30	**Sample Size**	30	30
	Average (Mean)	0.93295	0.82716
Over 30	**Sample Size**	11	11
	Average (Mean)	0.97290	0.85801

It was also noticed that there was no significant difference in the percentage of correctly identified cardiac cycles between male and female subsets of the data sample, nor between subsets under and over the age of 30. In four sessions (3, 11, 12, and 28), due to poor sensor attachment, some of the cardiac vibration signals were distorted, therefore, the total sample size considered in the statistical summary included 41 of the 45 sessions.

A portion of the recording from Session 5 is provided in Figure 19, which shows an example of a noisy portion of the cardiac vibration signal compared to the reference signal. In Session 5, 11 of 16 systolic complexes were correctly identified while only 3 of 16 diastolic complexes were correctly identified.

As can be seen in the portion shown in Figure 19, most of the systolic complexes are clearly identifiable, while none of the diastolic complexes are identifiable when examined independently without any reference signals. This

example demonstrates a case of noisy signal trace even after basic signal conditioning (fourth order B-BPF 0.5–25 Hz) is applied.

The noisy recording is likely due to poor sensor-to-body coupling, attachment, or unaccounted external vibration factors. The same noise is not present in the trace from the reference sensor because the heavier industrial transducer improves contact and coupling. Such pitfalls can be avoided with more careful attachment, novel sensors, or improvements to the body-to-sensor adhesion mechanism in future prototypes.

To further examine the similarities between the reference ECG and the integrated multisensor cardiac biopotential signal, two factors were calculated from both signals: the correlation coefficients of all corresponding cardiac cycles and the differences of the ECG's R–R intervals. In order to do this, the R-waves of the ECG signals were detected using a well-known, high accuracy algorithm (Afonso, et al. 1999).

The correlation coefficients of each corresponding cycle on the reference ECG signal, and the integrated multisensor cardiac biopotential signal, were calculated and averaged over all cycles to yield the values presented in Table 3. The resulting average (mean) correlation coefficient over all sessions was calculated to be 0.89±0.10;this high average suggested high resemblance between the two signals compared in each session. In one participant (10),

excess chest hair resulted in poor electrode contact, which compromised the ECG signal; therefore, the ECG comparison analysis was disregarded.

Using the same correlation coefficient, the signal-to noise (SNR) ratio of the ECG waveform was estimated for each session using a well accepted method (Bershad and Rockmore 1974). In this method, the correlation coefficients of corresponding cycles were calculated and applied to the formulas below:

$$SNR = A\frac{r}{1-r} + B$$

$$A = \exp\left(\frac{-2}{N-3}\right)$$

$$B = -\frac{1}{2}\left(1 - \exp\left(\frac{-2}{N-3}\right)\right)$$

The SNR was estimated where r is the calculated correlation coefficient, and N is the length of the cycle under study. The SNR was averaged over all cycles to give the total estimated SNR for every session in decibels (shown in Table 3). The total averaged, SNR over all participants was 22.00 dB with a standard deviation of 8.32 dB. Lastly, the difference of corresponding R–R intervals on both signals were calculated for every individual cycle, and averaged over all cycles (Table 3). The resulting averaged (mean) R–R interval difference is approximately 1.34 ms with a standard deviation of 1.38 ms, which are very small values relative to the time resolution of cardiac events.

Table 3. Summary of quantitative measures in similarity between reference ECG and biopotential signals from the integrated multisensor pair: results of the averaged correlation coefficients of are shown in the forth column; the estimated SNR comparing the signal from the multisensor to the reference is shown in the fifth column; the averaged R-R intervals are shown in the sixth column.

Session	Participant	Trial	Averaged-corrcoef ECG	ECG SNRdB (Ps/Pn)	R-R (ms)
1	**1**	Deep Breath	0.9434	25.8014	0.8571
2		Hold Breath	0.9508	25.8225	0.6667
3		Light Breath	0.9266	22.3396	1.0667
4	**2**	Deep Breath	0.9485	26.3144	1.8462
5		Hold Breath	0.9645	29.5236	3.0000
6		Light Breath	0.9464	25.4006	2.0000
7	**3**	Deep Breath	0.9498	26.2234	0.8571
8		Hold Breath	0.9400	23.9186	0.9231
9		Light Breath	0.9428	24.4102	0.7692
10	**4**	Deep Breath	0.7362	10.0658	1.8750
11		Hold Breath	0.6675	6.2871	3.4545
12		Light Breath	0.7315	8.7164	1.2847
13	**5**	Deep Breath	0.6440	5.0355	2.8800
14		Hold Breath	0.7813	11.1090	1.7143
15		Light Breath	0.5842	4.6719	8.1538
16	**6**	Deep Breath	0.9745	32.1806	0.5714
17		Hold Breath	0.8645	16.0711	1.0667
18		Light Breath	0.9634	28.5051	0.0000
19	**7**	Deep Breath	0.8416	14.8006	1.8750
20		Hold Breath	0.9841	35.9521	1.0000
21		Light Breath	0.8620	15.9800	0.6154
22	**8**	Deep Breath	0.9590	28.0667	1.0000
23		Hold Breath	0.9407	25.3804	0.7692
24		Light Breath	0.7378	13.4391	0.8000
25	**9**	Deep Breath	0.8384	17.3459	3.7333
26		Hold Breath	0.9580	27.1792	0.5000
27		Light Breath	0.8677	16.4230	0.2857
28	**10**	Deep Breath	-	-	-
29		Hold Breath	-	-	-
30		Light Breath	-	-	-
31	**11**	Deep Breath	0.9688	29.9673	0.8333
32		Hold Breath	0.9710	30.6437	1.2727
33		Light Breath	0.9649	28.8498	0.4444
34	**12**	Deep Breath	0.9721	30.9814	0.2857
35		Hold Breath	0.9758	32.1304	0.2105
36		Light Breath	0.9700	30.4160	0.0000
37	**13**	Deep Breath	0.8812	17.5196	1.0000
38		Hold Breath	0.8986	18.9626	1.4545
39		Light Breath	0.7636	10.9037	1.8333
40	**14**	Deep Breath	0.9129	20.5512	1.0667
41		Hold Breath	0.9208	21.4326	0.7143
42		Light Breath	0.8972	18.9531	1.5385
43	**15**	Deep Breath	0.9619	28.2337	0.7692
44		Hold Breath	0.9766	32.4916	0.3333
45		Light Breath	0.9457	25.1106	0.7692
Total Avg		*Mean*	*0.8912*	*22.0026*	*1.3355*

3.2 Radar SCG

A continuous microwave Doppler radar based system was developed at the Centre for Integrative Bio-engineering Research (CiBER lab) of Simon Fraser University (Tavakolian, et al. 2008). The developed device was completely implemented on board and is the first reported device that can be used independently as a stand-alone system or connected to a PC. This device was tested to measure the heart and respiration rate of human participants, and demonstrated a noticeable accuracy of 91.35% for respiration rate, and 92.9% for heart rate. More importantly, this system was used to extract radar SCG (R-SCG) signal discussed in the next subsections. The only similar reported approach for the acquisition of precordial vibration such as SCG, was published by Geisheimer (1999) but the reported morphology between of the SCG and the signal recorded from the radar were clearly different.

In this section, the basics of microwave Doppler radar systems are investigated as a cost-efficient, non-invasive, ubiquitous solution for continuous monitoring of in-vivo body signals; in particular, non-invasive sensing of cardiac, respiratory, and arterial movements. Microwave Doppler radar can detect motions and velocity based on the Doppler effect; therefore, a variety of body signals, including the mechanical motions of the chest because of the heart beat (the radar seismocardiogram, R-SCG) and blood flow velocity in major blood vessels, can be monitored. Hemodynamic parameters such as heart-rate, blood flow velocity and respiration rate can be estimated using these devices.

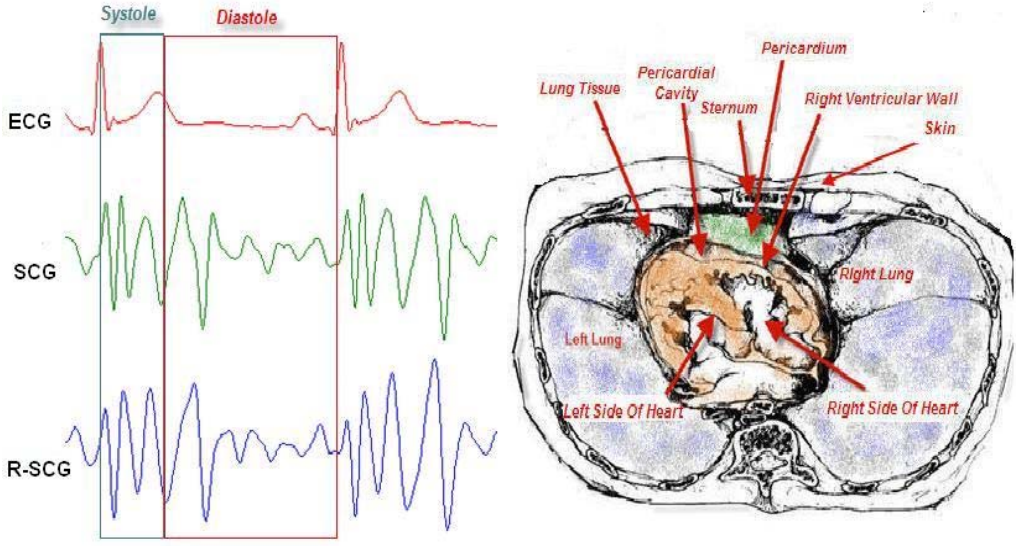

Figure 20. Right: Positioning of different layers of tissues that the radar signal will go through. Left: two cycles of the R-SCG, SCG and ECG signals (Tavakolian, et al. 2008) .

Microwave Doppler radar systems do not require direct contact with the body, and can function through blankets or clothing. A detailed overview of the use of radar in biomedical applications is presented in the appendices.

Depending on the application, microwave Doppler radar systems may use a continuous-wave or a time-gated radar signal. Continuous-wave Doppler radar has been shown to be comparable to, and even exceed, the conventional impedance cardiography methods for measuring the mechanical activity of the heart and heart-rate variability (HRV) (Staderini 2002). In fact, the derivative of the radar signal showed better correlations with the impedance cardiogram signal (ICG) (Thijs, et al. 2005). Some signals have been confirmed to be clearer on the captured radar signal than on the ICG, for example, the opening of the aortic and

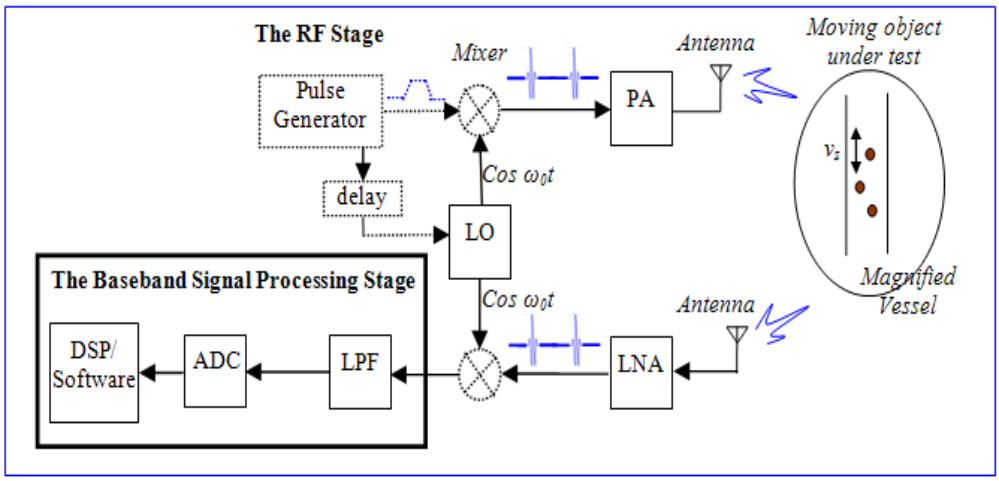

Figure 21. The Microwave Doppler Radar-based system block diagram (Mazlouman, et al. 2010)

mitral valves (Thijs, et al. 2005). Radar seismocardiogram (R-SCG), also known as radar mechanocardiogram (Tavakolian et al., 2008a) (Mazlouman, et al. 2010), reflects the mechanical dynamics of the heart recorded by contactless methods.

While monitoring the heart away from the chest, the signal passes through only a few layers of different tissues between the sternum and the heart which can be seen in Figure 20. The tissue layers between the sensor and heart muscle include skin, sternum, lung and pleural tissue, pericardium, and pericardial space. From the sternum, these tissue layers are thinner compared to the other positions. Therefore, the best position to record the heart's R-SCG signal is from the sternum. R-SCG signal has a close relationship to the SCG signal as can be seen in Figure 20. In other words, proper processing of the radar signal reflected from the chest will enable us to extract a signal (R-SCG)

which is very similar in morphology to SCG, thus, it can be used for the extraction of the same parameters as SCG which is discussed in detail in chapter 6.

3.2.1 The UWB radar for biomedical applications

In 2002, the Federal Communications Commission (FCC) allocated the 3.1 GHz to 10.6GHz band to ultra-wideband (UWB) communication systems in which the systems have a bandwidth greater than 500MHz and a maximum equivalent isotropic radiated power (EIRP) spectral density of −41.3dBm/MHz (FCC, 2002). This broad definition has encouraged a variety of UWB variants for different applications including UWB Doppler radar for vital signal monitoring (Staderini 2002). UWB power levels are very low, and therefore, reduce the risk of molecular ionization (Jauchem, et al. 1998). In addition, advances in modern silicon integration technologies with high cutoff frequencies allow for small, low-power implementation of UWB sensors. Time-gating of short radar UWB pulses allows for additional power efficiency; however, as explained in section 3.2., new design challenges on the control of sampling at the receiver is introduced.

Doppler radar-based systems for cardiovascular and respiratory measurements date back to the late 1970's and early 1980's for the X-band, around 10GHz (Lin, Kiernicki, et al. 1979) (Lin 1975) (Chen, et al. 1986). In mid-1980s, a frequency-modulated-continuous wave (FM-CW) system was developed to detect the vital signs of a wounded soldier in live fire situations at distances up to 100 meters (Greneker 1997). Despite its severe limitations, such

as sensitivity to surrounding objects, this device was the first of the many later developed radar vital sign monitor (RVSM) devices (Thansandote, Stuchly and A.M. 1983).

RVSM devices are capable of detecting human heart and respiration rates in a contact-less manner by transmitting a radio frequency signal to the participant, and measuring the phase shift in the reflected signal based on the Doppler Effect. During the 1996 Olympics, a variant of the RVSM, developed by Georgia Tech Research Institute (GTRI) (Greneker 1997) was developed to assess the performance of athletes in the archery and rifle competitions. Human heart beat and respiration signals were measured at ranges exceeding 10 meters using this RVSM that was mounted onto a 0.6m parabolic dish antenna, and transmitted an output power of 30mW at 24.1 GHz. Other suggested applications for these devices include home telemedicine monitoring systems and security applications. Major problems with these devices include environmental sensitivity due to weak signal processing, and their high cost due to bulkiness.

The use of a microwave Doppler radar system was reported by Thansondote, et al, (1983) for the continuous monitoring of time-varying biological impedances. The radar compared the phase of the signal scattered from the biological tissue with that of the transmitted signal. The phase variations of the scattered signal indicated the net impedance changes in the test region due to physiological processes, e.g. movements of blood vessels during the cardiac cycle. The system operation at both frequencies of 3GHz and 10.5GHz

was tested with healthy human participants. The 3GHz operation frequency for the Doppler radar system was shown to have significantly greater penetration in tissues, but was less sensitive to changes in biological impedance than the 10.5GHz system.

A simple add-on module was reported by (Lubecke, Boric-Lubecke and Beck 2002) that allows Doppler radar based detection of human respiration and heart activity using a 2.4 GHz cordless telephone system without requiring modifications in the existing telephone infrastructure. This module includes an inverted F-type antenna combined with a Schottky diode as the mixing element.

A digital signal processor was described by (Lohman, et al. 2002) for the determination of respiration and heart rates in Doppler radar measurements in remote monitoring. The processor can reliably calculate both rates for a participant at distances up to 2m. Several enhancement techniques, such as autocorrelation and center clipping, are used. The calculated heart rates agree for over 88% of the cases within a 2% margin for all datasets.

The first single-chip radios for the remote sensing of vital signs using direct-conversion radars integrated in low-cost silicon technologies were implemented by (Droitcour 2006). Two Doppler radar systems operating at 1.6GHz were fabricated using CMOS/BiCMOS technologies with more than 83% agreement with references. Despite the high phase noise of the integrated

oscillators, heart and respiration rates were detected remotely using phase noise reduction through range correlation.

The data obtained from a commercially available continuous-wave Doppler radar sensor (KMY24) (Thijs, et al. 2005) was compared to an ICG device using a cardiac cutput monitor (Medis Niccomo). The obtained data were shown to be clearer on the captured radar signal than on the ICG, for example, the opening of the aortic and mitral valves. An infant vital sign monitor device is reported by (Li, et al. 2009). This device operates at 5.8 GHz, and monitors the existence of the infant's heart and respiration rate. Therefore, the signal processing required for this device is simplified.

Several UWB microwave Doppler radar based implementations have also been reported in the literature based on work by McEwan (1994). A bread-board UWB prototype was implemented by Michahelles and Wicki (2004) that determined the heart-rate at a distance up to 15cm with a relative error of 5% compared to oximeter measurements. Another UWB prototype developed by Stadernini (2002) used a dipole antenna that emited 2ns pulses with a mean pulse repetition frequency (PRF) of 2MHz.

This prototype was used to measure the HRV signal. Fast Fourier transform (FFT) was used to compare the spectral content of the radar captured signal to an ECG-derived HRV signal; good correlations were confirmed. UWB radar systems have also been reported to detect human beings behind walls

(Meyerhoff 2007), as lie detectors (Staderini 2002), or as human activity monitoring, e.g., detection of walking, running, sleeping, etc., (Dutta and Arora 2006) (Such 2006) using the body signals.

3.2.2 The microwave Doppler-based radar system specifications

A block diagram depicting the main blocks of the microwave Doppler-based radar system is shown in Figure 22, and is explained in detail in Appendix 4. These devices are generally composed of two main stages: the RF stage and the baseband signal processing stage. The RF stage includes an RF/UWB transceiver block to transmit the radar wave and receive the reflected wave. The received wave includes the frequency shift due to the motion/velocity of the target (e.g. thorax, blood flow).

The received signal is down-converted and low-pass filtered to extract the baseband shifting data. This baseband signal is further amplified, digitized, and processed in the baseband stage. Digital signal processing techniques can be implemented in hardware or software. In the appendix, the Doppler based radar system was analyzed based on the main stages as shown in Figure 21, and some major reported ideas for on-board and CMOS integrated implementation of these blocks are discussed.

3.2.3 R-SCG

The principal design of the radar-based R-SCG device is shown in the block diagram of Figure 22. The antenna mounted on the device is HFMD24 by

Siemens, and contains a transmitter and a receiver in the same housing and the operating frequency is 2.45GHz. The transmitter transmits continuous wave radio frequency energy towards participant body. The output signal from the receiver is filtered and amplified (signal conditioning block). The cut-off frequencies for the band-pass filter are 1Hz and 100Hz, and the gain of the amplifier is around 800Hz. After filtering and amplifying, the R-SCG signal was sent to the A/D unit, then to the ATMEL CPU for further processing. The CPU was connected to a thin-film transistor (TFT) display via the SPI (Serial Peripheral Interface) port. The R-SCG device was powered by two AA batteries (2.45V) (Tavakolian, et al. 2008).

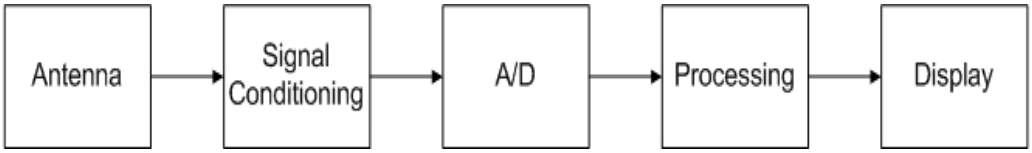

Figure 22. Block diagram of the R-SCG device

Because the R-SCG device has its own CPU and monitor, it can be used as a standalone device to acquire and process the R-SCG signal. Additionally, The data may be sent to a personal computer for more advanced processing of it with Matlab. To have this option on the device, the digitized R-SCG signal was transformed to packets and sent through UART to the USB, and finally, to the host personal computer for possible further processing.

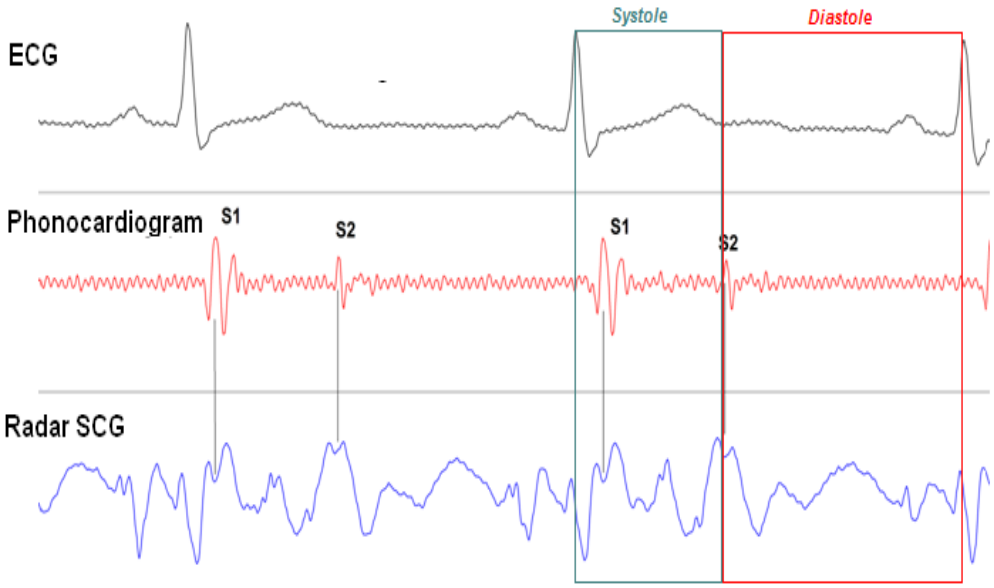

Figure 23. Two cycles of synchronous radar displacement SCG, Phonocardiograph and ECG signal showing the correlation of cardiac cycle events to radar SCG signal. Systolic and diastolic complexes can be identified in the radar MCG signal corresponding to S1 and S2 of heart's sounds.

The R-SCG signal was acquired by the sensor 10cm away from the participant's chest. The data acquisition also involved the measurement of ECG and respiration signals. The RF signal with a carrier frequency of 2.45 GHz was transmitted toward the participant's chest, and the reflected signal was band-passed filtered between 0.5 to 25 Hz. The filtered signal was differentiated, then band-pass filtered again between 4 Hz to 20 Hz. The comparison of the processed R-SCG signal to the SCG signal recorded simultaneously from the sternum can be seen in Figure 23 together with the synchronized ECG signal.

It was observed that there was a close correlation between the signal acquired from the radar-based R-SCG device and the simultaneous signal

recorded from the SCG sensor attached to the sternum. The systolic and diastolic phases of the cardiac cycle were shown to identify the correlations of these mechanical signals with heart function. As explained prior, due to the close resemblance of the signal to SCG, it is possible to transfer the knowledge about the genesis of waves in the SCG field to R-SCG analysis as discussed in chapter 5.

The phonocardiograph signal reflects the heart sounds that can be heard using a stethoscope. Heart sound S1 corresponds to the systolic phase of the heart cycle, and S2 corresponds to the diastolic phase. For comparison purposes, the R-SCG signal was acquired simultaneously with the phonocardiogram signal; it was observed that S1 and S2 sounds of the phonocardiograph signal corresponded to similar complexes on the R-SCG displacement signal (Figure 23).

For the heart rate measurement, the experimental setup included the acquisition of the R-SCG signal and two leads of ECG as a reference. For the respiration rate measurement, the setup included the acquisition of R-SCG signal together with the respiration signal as the reference. Eight participants took part in the respiration measurement tests, and six of these participants took part in the heart rate measurement tests. Breathing rate measurement experiments were 60 seconds long, while heart rate measurement experiments were 15 seconds long.

Table 4. The heart rate and respiration rate measurements using the SCG device for eight participants. The numbers represent the percentage of correctly detected heart beats or breathing cycles to the total number of heart beats or breathing cycles.

Participants	Heart rate	Respiration rate
1	93	90
2	-	94.2
3	84	90
4	91	90
5	100	87.1
6	89.4	92
7	100	100
8	-	87.5
Averages	**92.9**	**91.35**

To detect the respiratory rate, the radar signal was low pass filtered under 0.4Hz, and the peaks were counted and compared to the results acquired from a strain gauge transducer that measured changes in thoracic circumference using a belt fastened to the participant's thorax. The accuracy of the respiration rate measurement was 91.35% over all eight participants. Heart rate was measured using a radar-based R-SCG device, and was compared to the heart rate calculated from the simultaneous ECG signal for six participants. The average heart rate accuracy on these participants was calculated to be 92.9 percent. The results for the eight participants and both heart and respirations rates are listed in Table 4.

3.2.4 Future R-SCG improvements

Vital signs are measures of various physiological statistics in order to monitor basic body functions. There are four standard vital signs: heart rate, respiratory rate, blood pressure, and body temperature. Using R-SCG, heart and respiratory rates can be estimated as explained in the previous sections. Besides, these R-SCG measurements could be used for measurement of systolic time intervals in the same manner as SCG is proposed for this in chapter 6.

In order to standardize and commercialize the developed device, the radar sensor's SAR (specific absorption rate) should be determined. SAR measurements are often used assess the thermal effect of cellphone handsets on human body tissue due to cellphone radiation. It is also a measure of the amount of energy absorbed by the human body. The SAR value for similar sensors is lower than a standard cellphone handset (Thijs, et al. 2005).

Microwave Doppler radar-based systems can be used to monitor vital signs such as heart and respiratory rates, and to extract radar seismocardiogram, by which several other cardiac dynamic parameters can be potentially estimated. Thus, in this chapter, a brief review of reported devices using continuous-time and ultra-wideband microwave Doppler radar were presented as the technical basis of the R-SCG device. Basic system design and implementation criteria were discussed and measurement results are shown as in Table 4.

Although there are a variety of applications for vital signals monitoring where movement is not an issue, such as avalanche victims, wireless monitoring of patients in a hospital, or the elderly overnight, future work should focus on methods to detect and classify body movements as also recommended by Michahelles and Wicki (2004).

For this purpose, more elaborate signal processing methods can be used to decrease the effects of the motion artefacts due to other body motions or movements of objects in the environment (Morgan and Zierdt 2009). For example, multiple antenna methods are recommended by Li, et al (2009) to eliminate noise caused by random body movements and clutter. A more recently used parametric and cyclic optimization algorithm, referred to as RELAX algorithm, is suggested by Li and Stoica (1996) for spectral analysis of captured signals.

3.3 Laser SCG

As mentioned in chapter 2 laser has been used in the past for the measurement of precordial vibrations. In an experiment LTS Twin Sensor laser, model 15/3, was used to record the displacement of the sternum together with ECG and SCG signal (recorded using the B&K sensor).

The acquisition setup is in Figure 24 and the doubly differentiated laser recording together with the synchronous SCG and ECG can be seen in Figure 25. Signals were recorded from five participants and as can be seen in Figure 25the laser derived SCG follows the classical SCG signal very closely. Nevertheless, because of the sensitivity of the sensor the system was highly sensitive to motion artifact and many of the cycles could not be used, thus, a quantification of this similarity was not considered in this research.

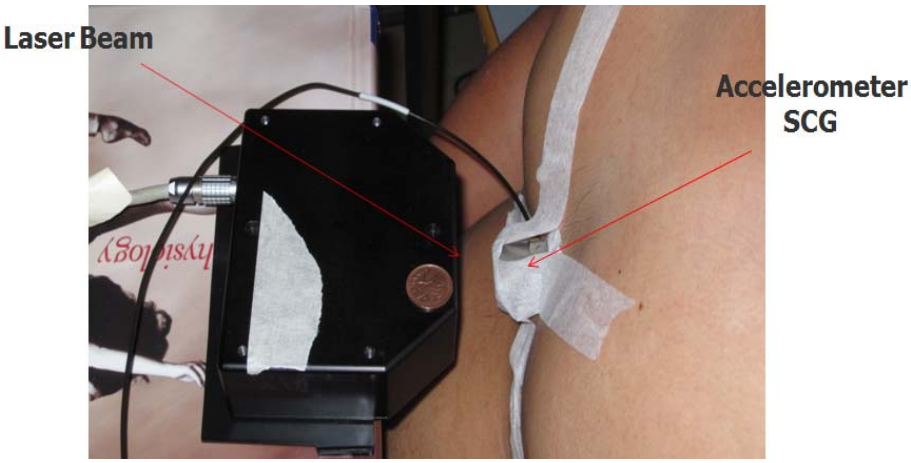

Figure 24. Simultaneous acquisition of laser and SCG signal using B&K sensor

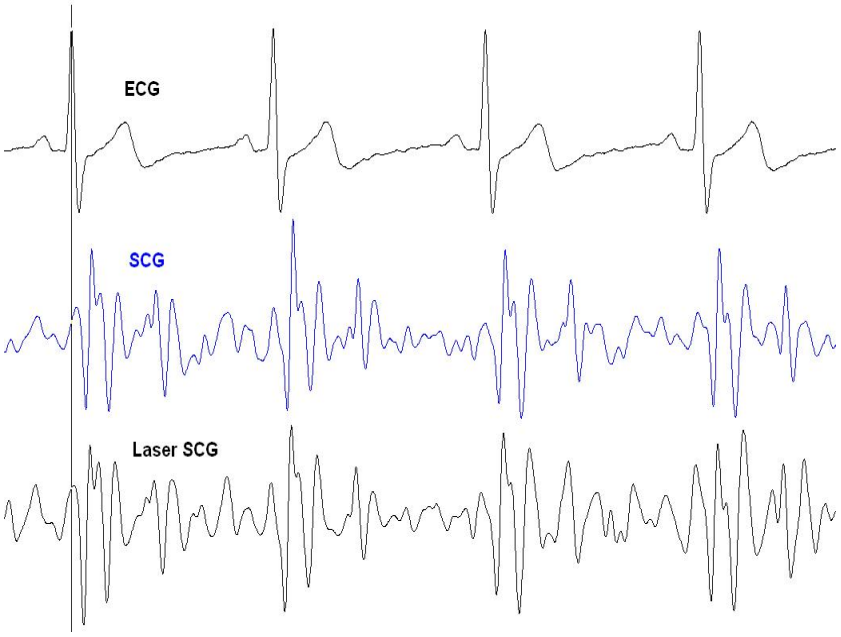

Figure 25. The laser SCG signal derived from double differentiation of the laser output

4: ARTIFACT REMOVAL AND RESPIRATION ANALYSIS

"And then the lungs, in respiration, are perpetually rising and falling: motions, the effect of which must needs be to open and shut the pores and vessels"

William Harvey 1628

Movement artefacts significantly affect recordings of precordial vibrations, such as SCG, and proper pre-processing of these signals is required to extract the useful hemodynamic parameters. Even while recording supine from a resting participant, normal respiration affects the morphology of the SCG. The easiest approach to resolve this problem is to treat the respiration signal like a regular motion artefact and remove it with a low-pass filter.

In fact, because of this research, we know that the morphology of SCG changes with different phases of respiration. The proposed method to process SCG, as in this chapter, is to use the respiration information to separate the cycles belonging to different phases of respiration before removing the respiration signal. This separation can provide a more statistically relevant averaging of the SCG signal.

Averaging a number of SCG beats provides a more statistically reliable template for further processing and interpretation of the data. A robust averaging for SCG signal similar to ECG (Egorouchkina, et al. 2005), EEG (Gupta 2002) and other physiological data, helps remove noise from the signal, and reduce the effect of possible transient changes in the signal.

It is shown in this research that SCG cycles corresponding to expiration phase of respiration are more closely related to each other when compared to cycles corresponding to inspiration and therefore, expiration cycles are better candidates to be selected for the calculation of the averaged SCG signal. The new SCG average calculated based on this methodology is then considered as the representative and a template of the SCG signal for further processing. This template can be considered as the output of a clinical SCG instrument with higher reliability and accuracy compared to the previous processing methods.

This chapter is organized as follows: in the next section, previous research on the cause of respiratory variation of the ballistocardiogram is reviewed. Section two of the paper explains the data acquisition setup and protocol, section three presents the methodology, which is followed in this research to process the SCG data and acquire the results, presented in section four. There is a statistical analysis in section five to support the assumption behind our proposed averaging algorithm. The last section presents different SCG classes considering the respiration effect.

4.1 Respiration studies in ballistocardiography

There has been no research work reported on the analysis of the effects of respiration on SCG and the only related research to us was the respiration analysis performed on BCG signal. Having similar effects on all infrasonic cardiac signals, these preliminary research works are summarized in this section.

From the early investigation of BCG signal, it was clear that respiration has significant effects on the morphology of the BCG signal (Starr and Friedland 1945). In particular, Starr noticed that in BCG signals recorded during normal breathing, identical BCG complexes were found, not in adjacent heartbeats, but in heartbeats occupying a corresponding position in other respiratory cycles (Starr and Noordergraaf 1967).

In the beginning of the new series of BCG research in the 1930's, respiration variation was attributed to the position of the diaphragm, which makes the BCG wave bigger when it is lowered during inspiration and smaller when it returns during expiration. One proposed mechanism was that the diaphragm rises during the expiration phase of respiration, and the cardiac apex moves to the left, rotating the heart's axis in counter-clockwise direction (Otis, Rahn and Mullins 1947).

However, few observations made the researchers doubtful of this explanation. One of the observations was that while the glottis was kept open when the breath was held after a deep inspiration, the BCG wave amplitudes remained large. Likewise, when the breath was held after a deep expiration, the

BCG amplitudes remained small until respiration was resumed. Thus, a series of experiments were conducted by Starr that illustrated that change of pressure, rather than the heart's position, causes the main respiratory variation seen in the normal BCG (Starr and Friedland 1945).

Considering this important respiration effect on BCG, the pre-processing approach that was taken by previous research works was simply the removal of respiration signal by high-pass filtering of respiration from the BCG signal. In some other research works breath holding was advised during the BCG recording to remove the respiration effect. Breath holding is uncomfortable for many patients and cannot be used for ambulatory monitoring purposes. On the other hand, it is observed that holding the breath changes the morphology of the BCG signal, depending on the position in the respiratory cycle in which the breath is held (Starr and Noordergraaf 1967).

In case of precordial recordings such as SCG, the local vibrations of the chest because of the respiration also distort the waveforms. In the simulation studies, which are presented in the next chapter, it is demonstrated that a change in the angle of the rib with respect to the myocardium can change the simulated SCG morphology. MRI videos show that the position and surface of contact between the right ventricle (which is the surface of the heart facing the interior part of the sternum) and the sternum clearly changes during different phases of respiration.

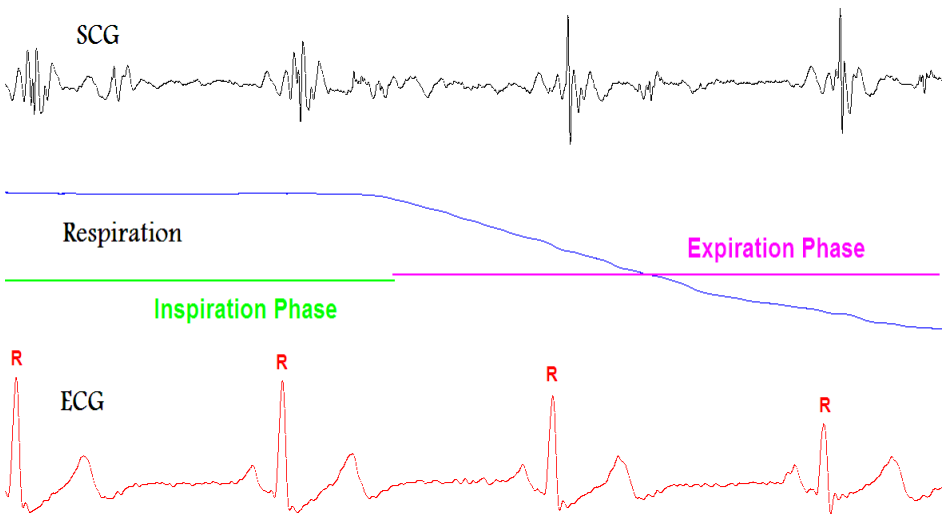

Figure 26. The signal at the top of the figure is the SCG signal of a patient who had myocardial infarction three years ago (participant 35). The signal in the middle is part of one respiration cycle in which the inspiration and expiration phases are separately shown. The difference of SCG signals corresponding to inspiration and expiration cycles can be observed from the morphology of the SCG waves. The signal in the bottom of the figure is the second lead of the ECG signal, from which the R wave is detected and used to segment SCG cycle.

For SCG case, this research proposes a different approach by using respiration information, before filtering and removal of the respiration effect, to improve the averaging of the SCG signal and thus, its overall processing and interpretation accuracy. This approach is based on the observation that SCG cycles corresponding to the expiration phase are more closely related to each other compared to inspiration SCG cycles and therefore, expiration cycles can statistically produce a better template for representation of the SCG cycles. Thus, based on our proposed method, the expiration cycles are selected to be averaged and presented as the output of the SCG instrument.

The above finding is also fortified by the early clinical studies conducted by Starr (1967) and Brown on BCG, stating that in many cardiac abnormalities

the expiration cycles get affected first. By the progress of the abnormality the inspiration cycles start getting affected too. Thus, in order to have an earlier diagnosis of the cardiac abnormality it is better to concentrate on the expiration cycles. This does not deny the fact that the inspiration cycles can also be used to extract information about the cardiac cycle but it suggests that if there is going to be one averaged beat presented to the users of SCG instrument as the output of the system, this average is better to be done over the expiration cycles

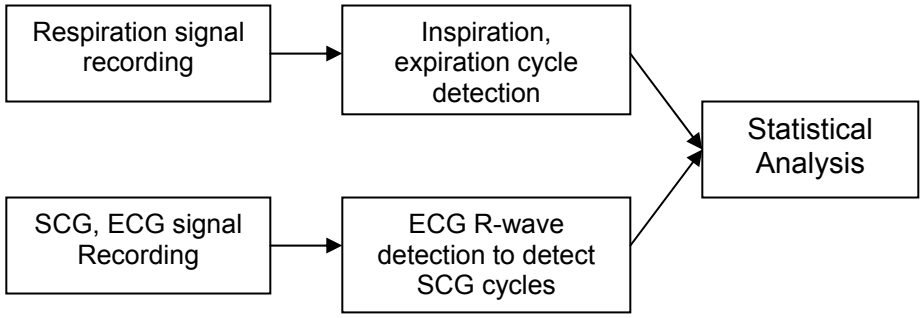

Figure 27. General SCG signal acquisition and processing as performed for the respiration analysis of the SCG signal.

4.2 SCG-Respiration signal acquisition and processing

The SCG dataset was acquired from participants with and without heart-related pathologies, most of whom were provided by Burnaby General Hospital. Out of the 45 participants taking part in our study, 19 were females and 26 were males. The participants were between 44 to 80 years old, with the average age of 66 years. The ethical approval for this data acquisition was granted by Simon Fraser University and the Fraser Health Authority of British Columbia (Fraser Health

2006). The data acquisition involved measurement of SCG, twelve lead ECG, pulse oximetry, respiration and heart sounds. All of the signals were acquired by a Biopac biological data acquisition system (Biopac 2006). All participants were tested before and after exercising on a treadmill.

The SCG signal was measured using a high sensitivity (1000millivolts/g) accelerometer, which was positioned on the sternum. The accelerometer sensor was factory calibrated, weighed 54grams, and was connected to a charge amplifier (Brüel & Kjær 2006). The ECG signal was measured in twelve leads and the R-wave of the second lead of the ECG signal was used to identify SCG cycles. The respiration was recorded using a strain gauge transducer that measures the changes in thoracic circumference, using a belt which is fastened to the participant's thorax. The participants were asked to pause and hold their breath on maximum inhalation and exhalation respectively for short periods of time.

The purpose of the pause and hold manoeuvre was to clearly differentiate the SCG cycles corresponding to inspiration from the expiration ones and to also maximize the respiration effect on SCG. A sample of the SCG and the respiration signals, together, is in Figure 26.

The general methodology which was followed in this research is outlined in Figure 27. To prove the usability of our proposed averaging method, which will be explained in details in the next section of the paper, we have calculated the

averages during the inspiration phase and expiration phase separately. In order to implement this averaging the following steps were followed:

- The points corresponding to the start of inspiration and expiration cycles were found from the respiration signal. The R wave peaks of the ECG signal, as the timing mark of individual BCG beats, were detected. The R wave detection was performed using the filter bank method (Afonso, et al. 1999).
- Those R-R intervals that were shorter than three quarter of averaged R-R interval length were removed to avoid very short beats and the shortest remaining beat was considered as the standard beat.
- The remaining beats were truncated to match the standard beat's length. A linear regression line was fitted to each cycle and the signal was subtracted from this line in order to remove the slight drift caused by respiration on the level of the SCG signal.
- The BCG beats corresponding to inspiration were averaged sample-by-sample to create the inspiration SCG average and by the same procedure the SCG beats corresponding to expiration were averaged to create the expiration SCG template, which can be seen in Figure 28.

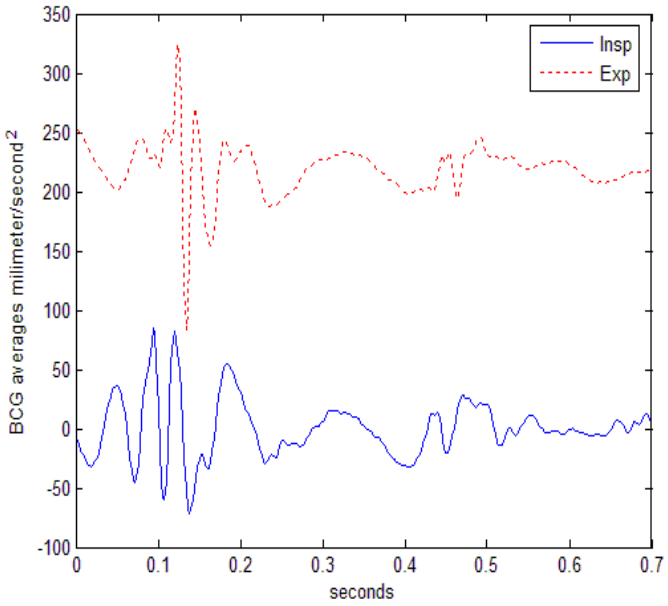

Figure 28. The average of SCG during inspiration (bottom) and expiration (top) is calculated for participant 35.

An approach based on piecewise linear approximation has been developed to remove the changes of the signal level which is created by respiration. This method is based on approximating the respiratory component of the signal by line segments of equal length and the residual signal, obtained after subtracting the piecewise linear approximation from the actual signal will not be affected by changes in the level of the signal because of the chest movement. The piecewise approximation is done by fitting a line to each SCG cycle using a least square method (Jensen, Larsen and Shankar 1991).

The averaging results for inspiration and expiration cycles of one of the patients are shown in Figure 28 where the average of expiration cycles is shown

on the top and the average of inspiration cycles on the bottom and there is a clear difference in the morphology of the two calculated averages.

For the proof of concept in this research, SCG, ECG and respiration signals were recorded independently as explained before. It should be noticed that in development of the SCG device one does not need to have a separate respiration sensor. The respiration signal can be estimated by low pass filtering of the signal acquired by the high precision accelerometer which is the fundamental component of a SCG device. The higher bound for this low pass filter can be set to 0.3 Hz.

At the same time the feasibility of detection of SCG cycles independent of ECG signal has been investigated in the past (Akhbardeh, Kaminska and Tavakolian 2007). Although the combined SCG-ECG sensor can give more diagnostic information compared to the accelerometer sensor alone, the accelerometer sensor is still able to differentiate between inspiration and expiration phases and average the SCG signal accordingly and independently.

4.3 Statistical analysis of SCG-derived respiration data

A sample of the SCG and respiration signals of one of the patients, participant number 35, can be observed in Figure 26. This patient had a myocardial infarction three years before the test. Following the heart attack she had angioplasty and had two fixed stents while being tested at the hospital. There is a clear difference in the morphology of her signal during inspiration and

expiration cycles, which can be observed both from her unprocessed signal in Figure 26 and her averaged SCG signal of Figure 28.

It is clearly observed from Figure 28 that her expiration average can be annotated, similar to standard SCG, while her inspiration average is very different in morphology and hard to annotate without considering other reference signals such as ECG. Such observations motivated this research and the goal of quantification of such differences.

As a measure of similarity for all the participants, all the inspiration cycles were cross correlated, and the average of all their correlation coefficients, compared to one another, was considered as the measure of similarity of the inspiration cycles for that individual participant. The same procedure was repeated for expiration cycles and for all the forty-five participants to produce the results of Table 5. All these calculations were performed in Matlab software (Mathworks 2006). For some of the participants the pre-exercise signal and for some of them the post-exercise signal was not available.

As an example, in participant four, and for his post exercise signal, fifteen inspiration cycles were selected and 15 multiplied by 14, or 210, correlation coefficients of cycles compared to each other were calculated and averaged, to compute the similarity index of 0.6558 for the inspiration cycles. The same procedure for participant four's expiration cycles resulted in the similarity index of 0.9409.

From the data provided from Table 5 a randomized incomplete block design analysis was used to compare average inspiration response variable between pre and post exercise data. The null hypothesis in this analysis was that the average of inspiration values for pre and post exercise sessions were the same and a p-value of 0.86 was achieved. This shows there is no evidence to reject the null hypothesis and it can be concluded that there is no difference in averages between pre and post exercises for inspiration values.

The same analysis was performed considering expiration as the response variable and a p-value of 0.83 was achieved that again confirmed that there is no difference between inspiration and expiration values. These results suggest that the SCG cycles before and after a mild exercise, for participants having normal sinus rhythm, will not change in both inspiration and expiration.

From Table 5 it is noticed that expiration cycles are 0.1272 more in the average similarity index, compared to inspiration cycles for pre exercise signal. In order to have a statistical analysis of the importance of this difference, a t-test was used to find out whether mean difference in a response variable, consisting the difference between expiration and inspiration values, was equal to zero for the pre exercise signal. The analysis showed a significant statistical difference (p-value<0.01) between the inspiration and expiration averages. The same analysis was performed for the post exercise signal and again a p-value less than 0.01 was obtained. The statistical analysis for this study was done using the JMP software (JMP 2010).

These results suggest a meaningful difference between the inspiration and expiration cycles and that the expiration cycles are statistically more closely related to each other compared to inspiration cycles. This can be attributed to the fact that expiration is a passive process in which muscles relax and the thorax moves more smoothly, while inspiration is an active process in which the muscles contract and add more movement artefacts to the SCG sensor that is placed on the sternum.

This statistical difference further proves that averaging the expiration cycles and excluding the inspiration cycles can result in a better statistical representation of SCG signal, which can be used in further processing of the signal, such as feature extraction, for diagnostic purposes.

Table 5. For each participant measures of similarity of inspiration and expiration cycles were calculated. The last two rows on the right show the average of the similarity indexes over all 45 participants, taking part in the study for pre and post exercise.

Subjects	Pre/ Post	Inspiration	Expiration	Subjects	Pre/Post	Inspiration	Expiration
1	Pre	-	-	**24**	Pre	0.4577	0.7482
	Post	0.5050	0.5013		Post	0.2167	0.3021
2	Pre	-	-	**25**	Pre	0.3277	0.6051
	Post	0.4681	0.5538		Post	-	-
3	Pre	-	-	**26**	Pre	0.5333	0.3788
	Post	0.6826	0.7233		Post	0.5606	0.3717
4	Pre	-	-	**27**	Pre	0.2453	0.3171
	Post	0.6558	0.9409		Post	-	-
5	Pre	-	-	**28**	Pre	0.6515	0.5417
	Post	0.7960	0.9078		Post	0.5293	0.6764
6	Pre	-	-	**29**	Pre	0.6669	0.7067
	Post	0.4260	0.5295		Post	0.7970	0.6747
7	Pre	-	-	**30**	Pre	0.3713	0.6244
	Post	0.3681	0.3533		Post	-	-
8	Pre	-	-	**31**	Pre	0.2643	0.4055
	Post	0.2040	0.4259		Post	0.2676	0.4018
9	Pre	-	-	**32**	Pre	0.3013	0.2351
	Post	0.5823	0.7370		Post	-	-
10	Pre	-	-	**33**	Pre	0.4875	0.7984
	Post	0.4191	0.6432		Post	0.4718	0.7205
11	Pre	0.1906	0.4544	**34**	Pre	0.1783	0.3970
	Post	0.1947	0.4617		Post	0.2466	0.4349
12	Pre	0.3093	0.5969	**35**	Pre	0.3942	0.3744
	Post	0.4196	0.5647		Post	0.3941	0.4232
13	Pre	0.1016	0.3972	**36**	Pre	0.7448	0.6585
	Post	0.1385	0.3184		Post	0.7441	0.6612
14	Pre	0.2488	0.5907	**37**	Pre	0.8426	0.8509
	Post	0.4424	0.5743		Post	-	-
15	Post	0.2747	0.2576	**38**	Pre	0.2206	0.5532
	Post	0.2591	0.2080		Post	0.3479	0.6625
16	Post	0.2341	0.5512	**39**	Pre	0.5494	0.3468
	Post	0.3841	0.4811		Post	0.3656	0.4827
17	Post	0.6911	0.7821	**40**	Pre	0.3964	0.5612
	Post	0.6666	0.7254		Post	-	-
18	Post	0.4005	0.7425	**41**	Pre	0.3779	0.5428
	Post	0.3394	0.5886		Post	0.2050	0.6232
19	Post	0.7363	0.6948	**42**	Pre	0.6015	0.5260
	Post	0.8002	0.7055		Post	0.4578	0.5392
20	Pre	0.2448	0.2702	**43**	Pre	0.6077	0.6598
	Post	0.3739	0.3703		Post	0.5245	0.5439
21	Pre	-	-	**44**	Pre	0.6031	0.7651
	Post	0.5381	0.7069		Post	0.3606	0.6808
22	Pre	0.2685	0.7127	**45**	Pre	0.3841	0.4758
	Post	0.2523	0.7605		Post	0.1552	0.5633
23	Pre	0.4168	0.5371	**Average**	**Pre**	**0.4404**	**0.5676**
	Post	0.5822	0.5811	**Average**	**Post**	**0.4364**	**0.5630**

4.4 SCG respiration classes

In terms of the effect of respiration on morphology of SCG signals three classes could be identified and in terms of the same effect on amplitude two classes could be detected. For morphology classes, class I was assigned to cases where both inspiration and expiration cycles are regular. Class II was assigned to cases where Inspiration was irregular and expiration was regular and class III was assigned to cases where both expiration and inspiration cycles were irregular in their morphology.

Samples of the three morphology classes for three different participants is as in Figure 29. The two classes based on the amplitude include class ‘a’ where the inspiration amplitude is bigger than expiration amplitude and class ‘b’ where expiration amplitude is more than the inspiration amplitude.

The results of manual classification of participants to different respiration categories can be seen in Table 6 for the same participants as the previous study. For this study we used 68 SCG signals recorded from 43 participants. The signals from two participants were discarded as they could not be used for classification purposes. It is observed that 78% of recordings the amplitude of SCG during inspiration is more than that of expiration, belonging to class ‘a’.

This observation has been also observed on BCG too and we do expect the inspiration effect to be generally amplifying the BCG signal’s amplitude (Starr and Noordergraaf 1967).

Table 6. The columns of this table indicates the morphological classes for the respiration effect on SCG and the rows indicate the amplitude classes and the rows indicate the two amplitude classes. Total of 68 SCG recordings were evaluated.

	I	II	III
a	35	11	7
b	8	6	1
Total	43	17	8

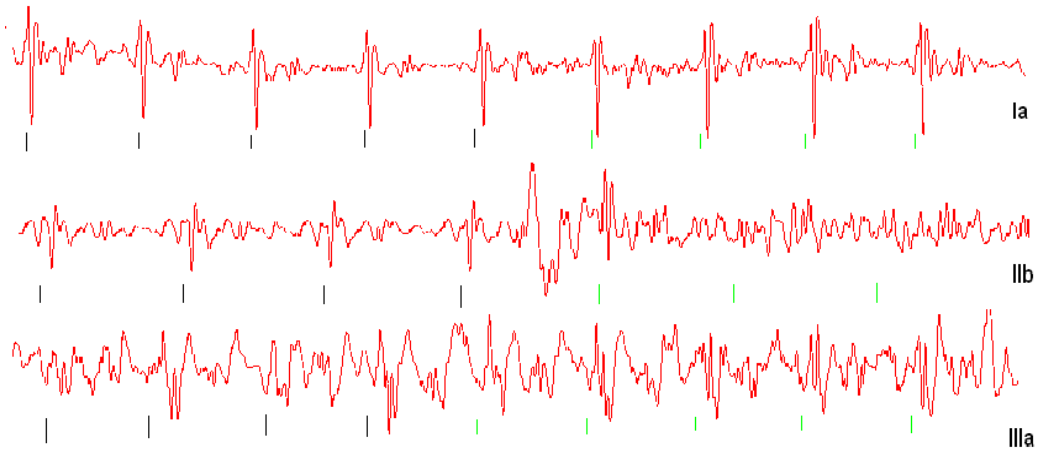

Figure 29. Three morphological classes based on the effect of respiration on SCG signal. The R waves of synchronous ECG signal have been indexed so that the BCG cycles can be differentiated from each other. The black indexes correspond to expiration and the green ones correspond to inspiration cycles. The top trace belongs to participant 37, pre-exercise, the second one is for participant 38, pre-exercise, the third trace belongs to participant 26, post-exercise. The subscript 'a' and 'b' are based on the amplitude classification. Notice that the traces are in different time scales.

5: GENESIS OF SCG WAVES

"These things, therefore, happen together or at the same instant: the tension of the heart, the pulse of its apex, which is felt externally by its striking against the chest, the thickening of its parietes, and the forcible expulsion of the blood it contains by the constriction of its ventricles" William Harvey 1628

This chapter includes subprojects that were conducted in order to improve the understanding of genesis of SCG waves and the physiological phenomenon behind them. Although, Salerno conducted some preliminary studies on this subject, the technologies used for those studies were quite old (Crow, et al. 1994). This chapter starts with the results obtained by echocardiography methods of M-mode and Doppler ultrasound, followed by the results of the comparison with impedance cardiogram (ICG) and ULF-BCG. The concluding section of this chapter details collaborative research with Johns Hopkins University in the development of a unique approach to SCG simulation that utilized a comprehensive 3D finite element model of the heart. Such an approach can provide a new tool for studying all precordial recordings.

The results, briefly reported in this chapter, on AO and AC point of SCG are the same results reported in the next chapter on measurement of PEP and

QS2 and are repeated here as they are required in better understanding of the proceeding materials.

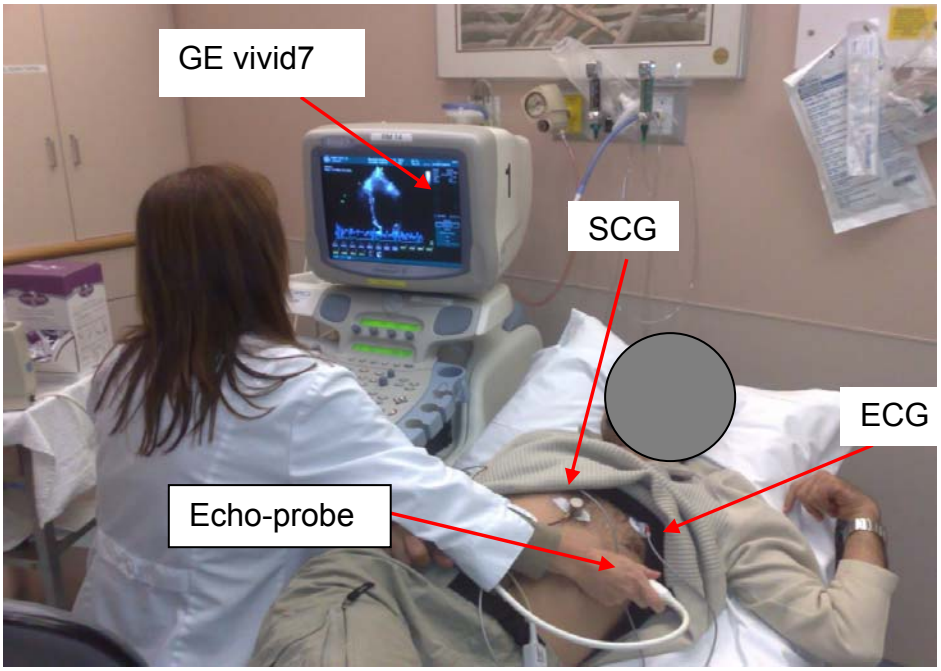

Figure 30. Simultaneous recording of SCG, ECG and M-mode echocardiogram at Burnaby General Hospital using the GE vivid 7 system.

5.1 Echocardiography

Echocardiography is a diagnostic technique that utilizes ultrasound to produce an image of the heart in real time. A piezoelectric transducer is used to emit short bursts of high frequency sounds through the chest to the heart, and then detect the reflected sounds as it returns from the heart. Since shape changes of several regions of the heart and their movement patterns correlate with mechanical cardiac function, echocardiography has become a frequently used methodology in non-invasive cardiology. In this research, two methods of M-mode and pulsed Doppler echocardiography were used, and a more detailed

explanation of different echocardiographic methods is presented by Webster (2006). The Doppler effect as used in echocardiography is the same effect as explained in Appendix 4 for radar and the concepts of the previous chapter.

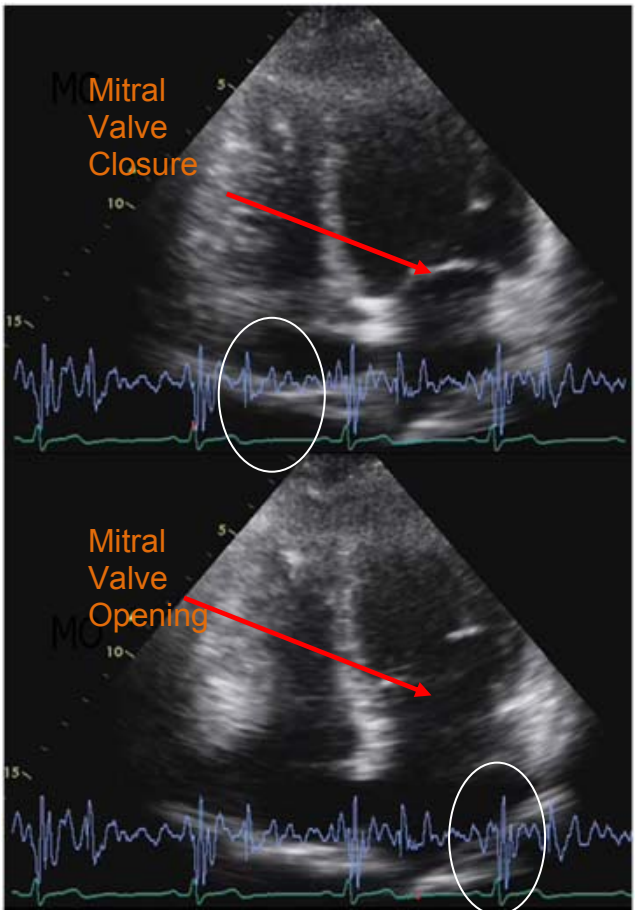

Figure 31. Simultaneous M-mode echocardiogram in four chamber view, SCG (blue) and ECG (green). The top snapshot shows the moments close to the closure of mitral valve and the bottom snapshot shows the moment close to its opening. On both snapshot the current frame is shown with a red dot on ECG trace and in order to better signify them they are encircled in while. The arrows point to the mitral valve.

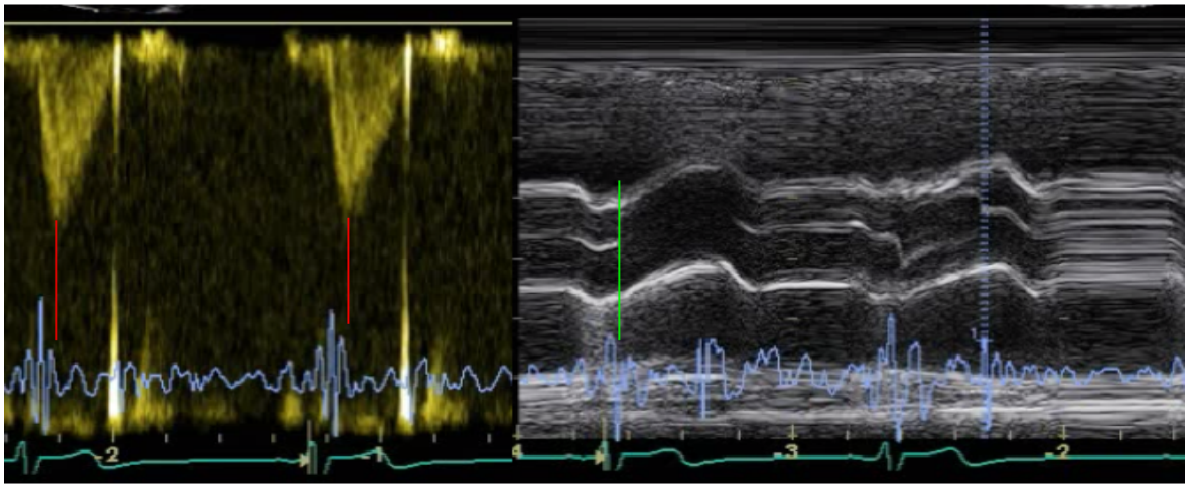

Figure 32. Left, Doppler echocardiogram for assignment of rapid systolic ejection point. Right, M-mode echocardiogram for assignment of aortic valve opening (AO)

5.1.1 M-Mode

M-mode echocardiography has been used in the past to analyze the genesis of SCG waves; the same experiments were repeated in this study to reproduce and confirm the findings of Crow, et al (1994), but with a newer echocardiogram. This study was conducted under an ethics approval with Fraser Health Authority in Burnaby General Hospital using a GE vivid7 echocardiogram; the recording setup is demonstrated in Figure 30. A sample snapshot from the 4 chamber view of the heart can be seen in Figure 31. In this view, the ventricles are on the top and atria on the bottom.

For the first year of this subproject, a protocol was established for recording echocardiogram, and recordings from a single participant were obtained. The analysis of this participant confirmed many of the findings of Crow, et al (1994). The protocol (listed in Appendix 4) was followed with the assistance

of the echocardiograph technician and the data were stored and later analyzed with the assistance of the cardiologist at Burnaby General Hospital. Figure 32 shows a sample of simultaneous recording of SCG and M-mode and Doppler echocardiograms. In summary, based on this protocol, a parasternal long axis M-mode for mitral valve and aortic valve opening and closure assessment were performed. An apical five chamber view was used for the assessment of the rapid systolic ejection point and left ventricular output tract (LVOT). An apical four chamber view was used for the detection of rapid systolic ejection and atrial systole.

Table 7. The difference between SCG temporal landmarks and echocardiogram points in ms. By Salerno in the table the purpose is the annotation originally proposed in this paper (Salerno and Zanetti 1990). The last column averages the differences of six heartbeats

Cycle	1	2	3	4	5	6	Average ±*std*
Mitral valve close (MC)	0	9	9	9	9	0	*6±4.6*
Mitral valve open - Salerno (MO)	17	26	9	60	43	-	*31±20.5*
Mitral valve open - Alternative (*MO*)	103	34	103	68	51	-	*71.8±31*
Aortic valve close (AC)	0	26	9	17	17	9	*13±8.9*
Aortic valve open (AO)	-	26	17	26	26	-	*23.7±4.5*
Rapid systolic ejection – Salerno (RE)	25	25	42	25	25	34	*29.3±7.2*
Rapid systolic ejection - Alternative (*RE*)	8	8	17	17	0	17	*11.2±7*
Rapid diastolic filling (RF)	59	51	17	34	25	8	*32.3±19.7*
Peak of atrial systole (AS)	51	59	25	25	17	-	*35.4±18.4*

For six different beats, nine different points on SCG were assigned by the author of this thesis (as in Figure 33), and the corresponding echo events were assigned by the cardiologist at Burnaby General Hospital. The differences in ms between the two assignments are listed in Table 7. For rapid systolic ejection

(RE) and mitral valve opening (MO) points, an alternative point, compared to annotation proposed by Salerno and Zanetti (1990), were also tried against the echocardiogram.

From the results in Table 7, the general observation was that for mitral valve and aortic valve closure times, the results from SCG and echocardiogram are close to each other (6 and 13 ms differences); while for the opening time, the differences are more than 20 ms. The alternative points we proposed yielded a better result in the case of the rapid systolic ejection, and reduced the difference between the SCG and echo from 29.3 to 11.2 ms. The alternative point we proposed for the MO gave a significantly worse result compared to the point proposed by Salerno and Zanetti (1990), as seen in the Table 7.

It should be noted that these measurements were made on one participant, and this part of the project was stopped at this point. During the development of the protocol, simultaneous echocardiogram and SCG were recorded on three other participants, but as the protocol was still not established, the stored results were erased by the echocardiograph technician. Nevertheless, the general observations on the other three participants were not significantly different than what is inferred from Table 7.

The echocardiograph system used at Burnaby General Hospital had the frame per second of 60 (fps)which means a time resolution of 16.6 ms. In other words, timings less than this period could not be detected. Thus, knowledge of

such a limitation was motivation to improve the resolution for the remainder of the research.

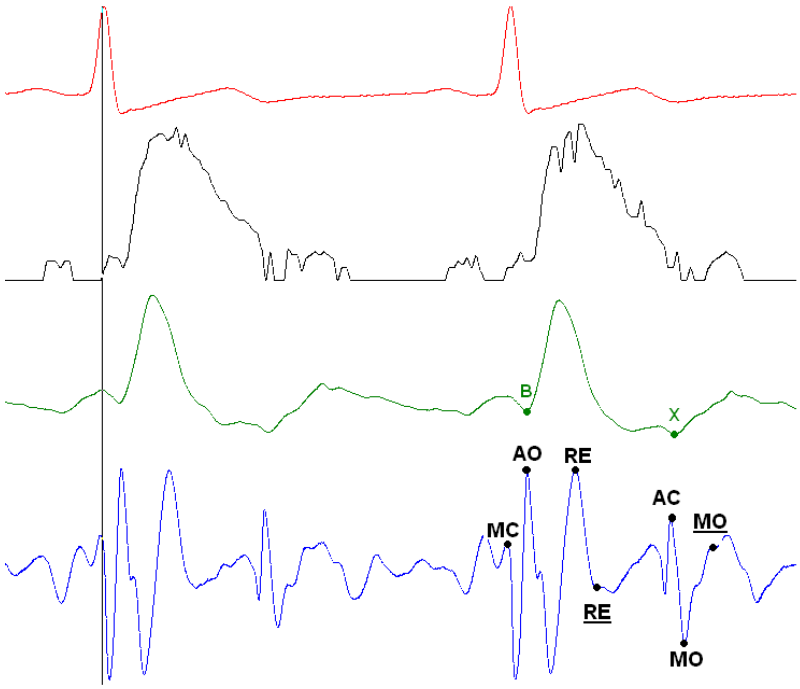

Figure 33. Simultaneous recording of (top to bottom) ECG, suprasternal Doppler of aorta, ICG (dz/dt) and SCG. The points detected on both SCG and echocardiogram are annotated here for this participant and the differences are listed in Table 7. The difference between SCG temporal landmarks and echocardiogram points in ms.AO, AC: aortic valve open and closure. MC, MO: Mitral valve close and open, RE: rapid systolic ejection.

5.1.2 Pulsed Doppler ultrasound

In this study, a Doppler ultrasound system with a resolution of 5 ms was used which was an improvement from our previous study with M-mode echocardiography. A 2MHz pulsed Doppler instrument (MultiFlow, DWL GmbH, Sipplingen, Germany) was used in the parasternal region to record velocity of

blood in the aorta; this velocity was differentiated to obtain the acceleration of blood in aorta.

The ultrasound measurements in the present study were made with an insonation depth of 6.5 to 7.5cm with the sample volume located 1.0 to 1.5cm above the aortic valve. The optimum position of the probe was the point which provided the maximum peak velocity with minimal spectral broadening, and a clearly identified upstroke on each beat. This was assessed from the spectrum analyzer display and through auditory confirmation of the audio-frequency Doppler signal. The velocity envelope of the Doppler signal was recorded simultaneously with SCG signal at 2.5kHz, using a National Instrument data acquisition system. The Doppler velocity was then differentiated in Matlab™ to provide the acceleration of the blood in the aorta. The impedance cardiogram was also recorded simultaneously.

The SCG signals were recorded by placing a piezoelectric accelerometer on the midline of the sternum with its lower edge at the xiphoid process. The sensor (model 393C, PCB Piezotronics, state/province, country) had a linear response between 0.3 and 800Hz, and sensitivity of 1.0V/g. Healthy, young adults (n=18) under the age of 33, and five individuals with a history of heart attack and low ejection fraction values (<35%) in the past two years took part in this study. The experimental setup can be seen in Figure 40 and a sample simultaneous recording is in Figure 33. A sample ensemble average of the signals is in Figure 34.

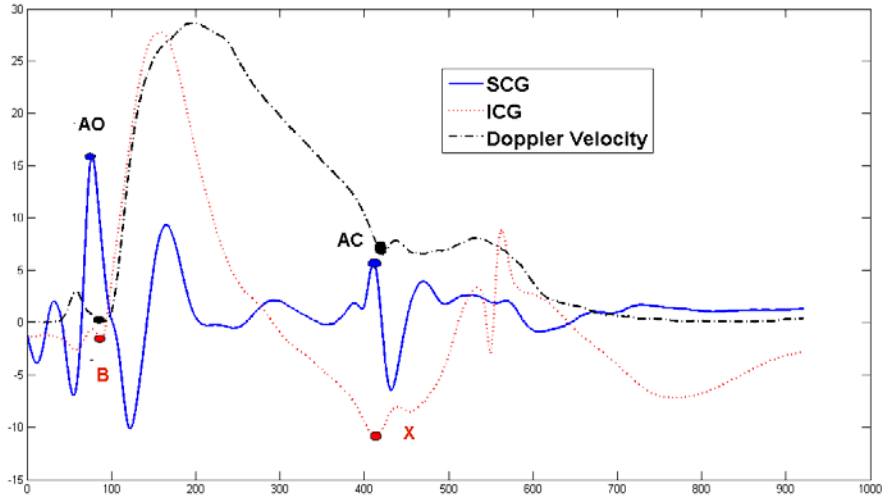

Figure 34. Ensemble average of SCG, ICG and Doppler ultrasound as used for the measurement of aortic valve opening and closure (AO, AC). The averaging was done with respect to Q wave of ECG. The vertical axis is calibrated in milli-g for SCG signal and the horizontal axis is in milli-seconds.

In a study of 23 participants the timing of the point of maximum acceleration in the aorta was determined from the ensemble average of the suprasternal Doppler signal and it was compared to the minimum point of the SCG signal, right after the start of the ejection of blood, for every individual beat For every individual heartbeat, the MA point was assigned by first, detection of the ECG Q wave and then assignment of the AO point (as the first peak of SCG after the Q wave on ECG). The MA is assigned accordingly as the minimum point after the AO point. Results for each participant is presented in Table 8 and is plotted in Figure 36. The beat by beat comparison of SCG and Ultrasound signal was not possible as the Doppler ultrasound signal is ragged in every individual beat because of sampling. Ensemble averaging, on the other hand, smoothes

the Doppler signal and reveals the time landmarks on it as seen in Figure 34 and Figure 35. Thus, for this study the beat to beat measurement of MA point on SCG is compared to the single value given for each individual subject from the Doppler ensemble averaging.

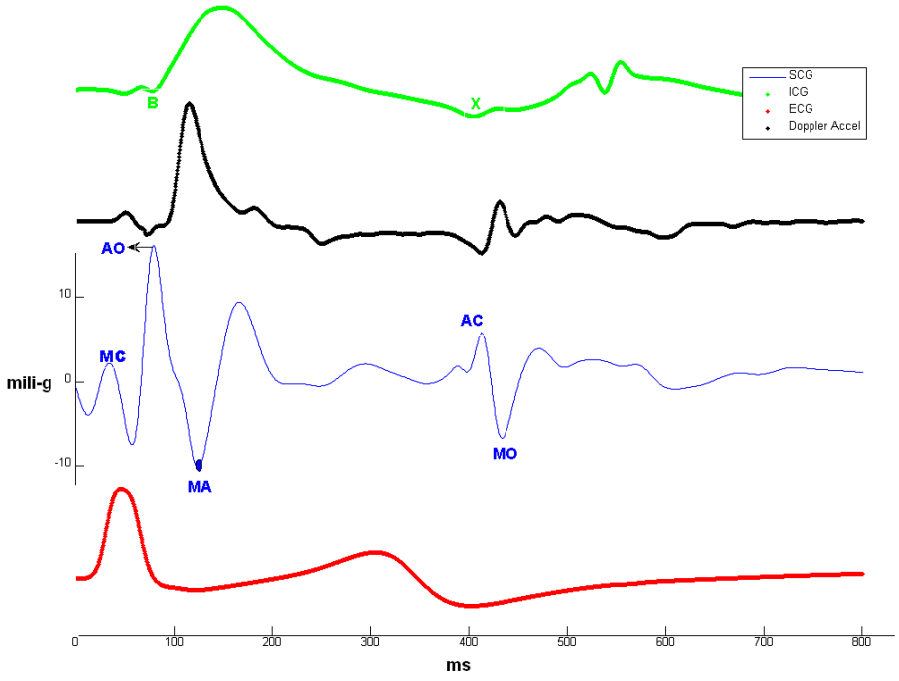

Figure 35. Ensemble averages of (top to bottom) impedance cardiogram (ICG), the acceleration of aortic blood derived from Doppler ultrasound, SCG (solid blue) and ECG. The global minimum of SCG (MA) follows the global maximum of the blood acceleration signal (black dot). The horizontal axes is time in milliseconds and the vertical axes is acceleration signal in milli-g for the SCG signal. The Doppler ultrasound measurements in this participant was made with an insonation depth of 5.4 cm with the sample volume located 0.5 cm above the aortic valve. The participant was a male participant (age: 27 years; weight: 75 kg; height: 167 cm. The averaging was done by aligning all beats with respect to the Q wave of the ECG signal.

Table 8. Measurement of point of maximum acceleration of blood in aorta and the MA points on SCG. The three right columns are derived from beat to beat annotation of SCG's MA point. The anthropometric data for the participants are also presented and the ejection fraction is given for the five patients.

Participant	Age	Weight (kg)	Height (cm)	Sex	EF%	Doppler acceleration maximum (ms)	Average of SCG MA points	High 95% CI (ms)	Low 95% CI (ms)
1	28	82	178	M	N	155.2	154.3	158.6	150.0
2	31	80	181	M	N	162.4	159.4	182.6	136.1
3	33	78	183	M	N	120	128.1	144.4	111.8
4	27	66	178	M	N	123.2	129.9	139.5	120.3
5	36	62	165	M	N	115.2	116.5	121.4	111.7
6	24	61	167	M	N	100.4	121.7	143.7	99.7
7	25	62	171	M	N	131.2	140.5	150.2	130.7
8	31	93	183	M	N	148.4	160.3	181.6	139.1
9	27	75	177	M	N	115.6	109.3	116.9	101.6
10	26	75	167	M	N	124.8	119.0	125.4	112.6
11	28	80	178	M	N	122.8	133.5	138.6	128.5
12	28	74	173	M	N	134.8	153.3	177.3	129.3
13	62	79	172	M	N	116.8	109.0	142.6	75.4
14	26	56	163	F	N	121.6	129.0	159.8	98.2
15	25	84	181	F	N	116	113.8	122.4	105.2
16	43	55	162	M	35	129.2	126.0	170.6	81.4
17	80	77	180	M	30	185.2	176.0	244.0	108.0
18	73	73	159	M	20	138	156.3	218.9	93.7
19	68	82	177	F	38	174	146.0	220.0	72.0
20	31	65	178	M	N	105.2	107.0	122.6	91.4
21	56	81	177	M	N	102.4	103.2	131.2	75.2
22	24	81	178	M	N	108.8	115.2	128.5	101.9
23	67	77	174	M	33	151.2	183.1	205.1	161.1
Averages ± std	**39± 18**	**74± 9.8**	**174± 7**		**-**	**130.6± 23ms**	**134.4 ±23ms**	**-**	**-**

There is a correlation coefficient of 0.85 between the results obtained from SCG and Doppler ultrasound as in Table 8. The Bland and Altman analysis (1986) yields the mean bias of 3.8 ms with the standard error of 2.6 ms (p-value=0.15) and the lower agreement interval of -1.55ms and higher agreement interval of 9.19 ms. This mean difference between the two methods is even less than the time resolution of the Doppler ultrasound system used in this study (5 ms).

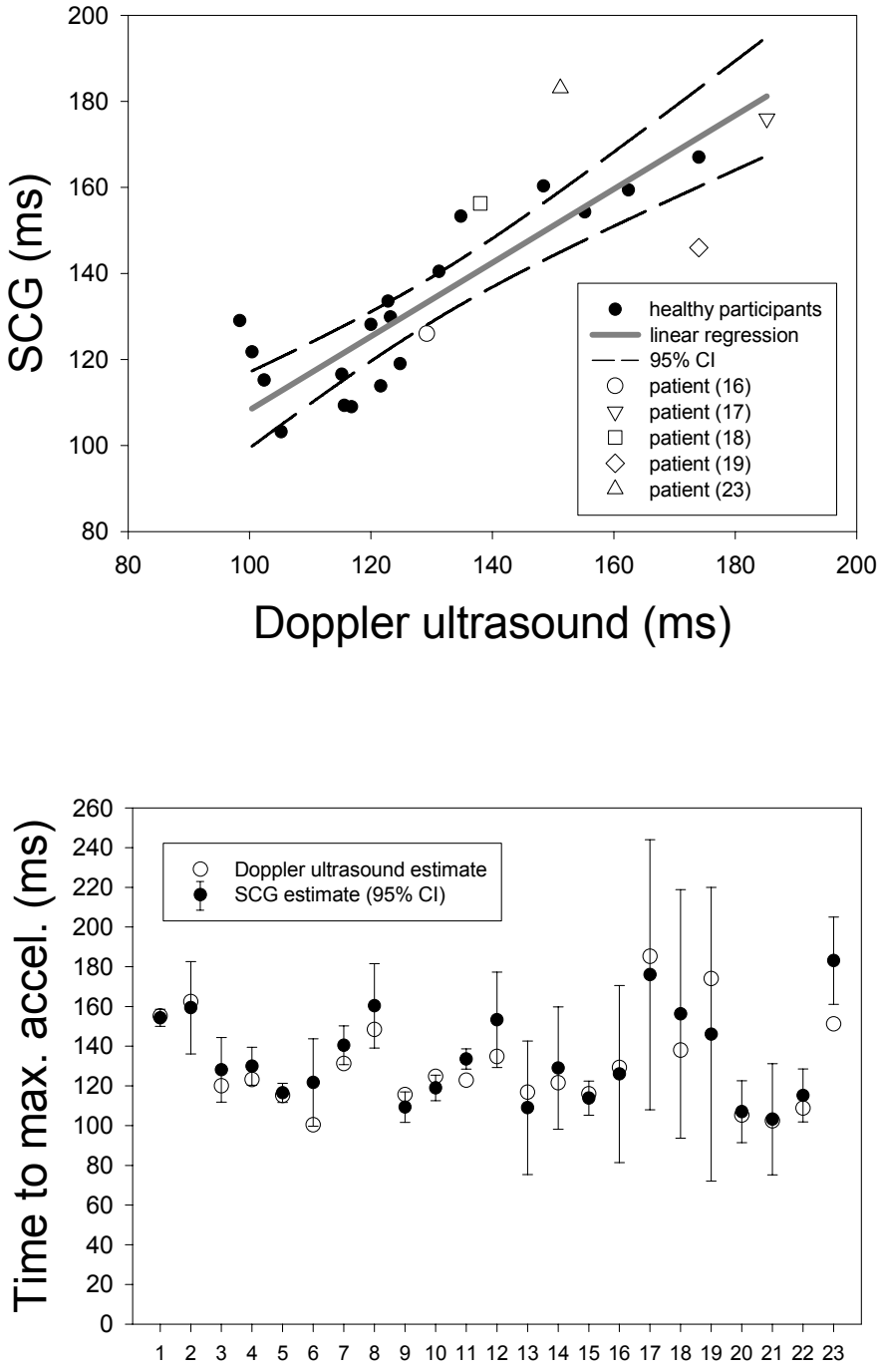

Figure 36. Top: maximum acceleration (MA) point estimated using SCG plotted against values given by the Doppler ultrasound (Linear equation: SCG = 22.6 ms + 0.87 * Doppler). The five patients are also indicated differently. Bottom: the plot of SCG measurement of MA point for every individual subject together the value given by the Doppler ultrasound.

The bottom part of Figure 36 indicates that the Doppler measurements falls in the 95% confidence interval of the SCG measurement in 21 participants out of the total 23 participants. The clear outlier in this is subject 23 who belongs to the group of five patients with low ejection fraction (less than 35%). The other exception is subject 11 where the ultrasound measurement falls slightly below the 95% interval.

The correspondence of MA point on SCG to maximum acceleration of blood in aorta is also in accordance with the experimental studies on the comparison of SCG and ultra low frequency ballistocardiogram as explained in next sections.

The ensemble average of the Doppler velocity signal, together with SCG and ICG, for one of the participants can be seen in Figure 34. On a dataset of twenty five participants (where twenty three of them are the same as the ones in Table 8) , the time of the aortic valve opening and closure were calculated from three different signals of SCG, impedance cardiography (ICG), and Doppler velocity and are listed in Table 11 under the PEP and QS2 columns, respectively. PEP is calculated from Q wave on ECG to the aortic valve opening point and QS2 is calculated by calculation of the interval from Q wave on ECG to aortic valve closure point.

A randomized, incomplete block design was used to test for the mean difference in response between the three devices (SCG, ICG and Doppler

ultrasound). The analysis provided no evidence to reject the null hypothesis (p-value=0.16 and 0.91 for aortic valve opening and aortic valve closure respectively). Thus, it was concluded there was no evidence to suggest a difference in mean response between the devices. The fact that the first positive peak after the R wave on the SCG signal was created by the opening of aorta was further confirmed by the findings of the model.

5.2 Impedance cardiography

Impedance cardiography (ICG) is considered to belong to the more general category of impedance plethysmography which refers to the estimation of volume changes in the body via measurements of changes in electrical impedance. ICG has been used in the past for the estimation of stroke volume and systolic time intervals (Sherwood, et al. 1990).

The temporal landmarks on ICG, which are of special interest to us, are points B and X (Figure 33). Based on the echocardiographic studies, point B corresponds to the start of systolic ejection or aortic valve opening, and point X corresponds to the end of systole or aortic valve closure. The use of point B in the detection of the aortic valve opening was demonstrated in the previous section, and its use in the detection of the aortic valve closure is shown in the next chapter with other methods that are used to prove the usability of SCG in detection of systolic time intervals. Thus, the quantitative comparison of SCG-ICG will not be repeated here again.

Figure 37. Simultaneous acquisition of ULF-BCG and SCG. The ULF bed was hanging, with wires 3 meters long, from the ceiling.

5.3 ULF ballistocardiography

Ballistocardiography and its role in non-invasive cardiology was explained in detail in chapter 2 and some results on its comparison with SCG was also presented. It was demonstrated that at the end of classical BCG research, ultra low frequency beds were the method of choice in BCG research. A lot of research was conducted in the past on the genesis of BCG wave, and the purpose of this subproject was to translate some of that knowledge to the understanding of SCG genesis. For this part of the research Dr. Abraham Noordergraaf from University of Pennsylvania was contacted who was a pioneer in ballistocardiogram research, and borrowed from him an old BCG bed used during the 1960s for BCG research (Starr and Noordergraaf 1967). The setup was reproduced as the original, and can be seen in Figure 37.

The BCG bed used in this experiment was an ultra-low frequency bed pendulum made of a piece of stretched canvas attached to the ends of a 207cm

by 78cm rectangular wooden frame that weighed approximately 8 kg. The frame was suspended at four points from the ceiling with 3 m long steel wire rope. A model 4381 piezoelectric accelerometer from Brüel & Kjær was fixed to the bed to measure the longitudinal acceleration such that headward movement was positive. The accelerometer had a charge sensitivity of 10.07 $pC/m/s^2$ and frequency response of 0.1 Hz to 4800 Hz. This was the same accelerometer used in the research presented in the previous chapter on respiration analysis.

The SCG signal was obtained as described by Salerno and Zanetti (1990) using the same piezoelectric accelerometer placed on the midline of the sternum with its lower edge at the xiphoid process. The sensor characteristics was explained in previous section. The three simultaneous signals of SCG, ULF-BCG, and ECG were recorded from five participants, and they were asked to lie supine on the suspended bed as in Figure 37. All five participants were healthy, male adults between 25-32 years old. For four of these participants, a sample of their recordings can be found in Figure 15. The R wave of the ECG wave has been marked by a vertical black line as a reference in Figure 15.

The H point on BCG corresponds to the start of blood flow in the aorta, and the I point corresponds to the peak of maximum acceleration of blood in the aorta as mentioned in chapter 2 (Smith 1974). The ensemble average for SCG and BCG for these participants were calculated (Figure 38) using Matlab software. It is clear that the H point of BCG aligns with the aortic valve opening (AO) on SCG, and the I point on BCG aligns with MA point.

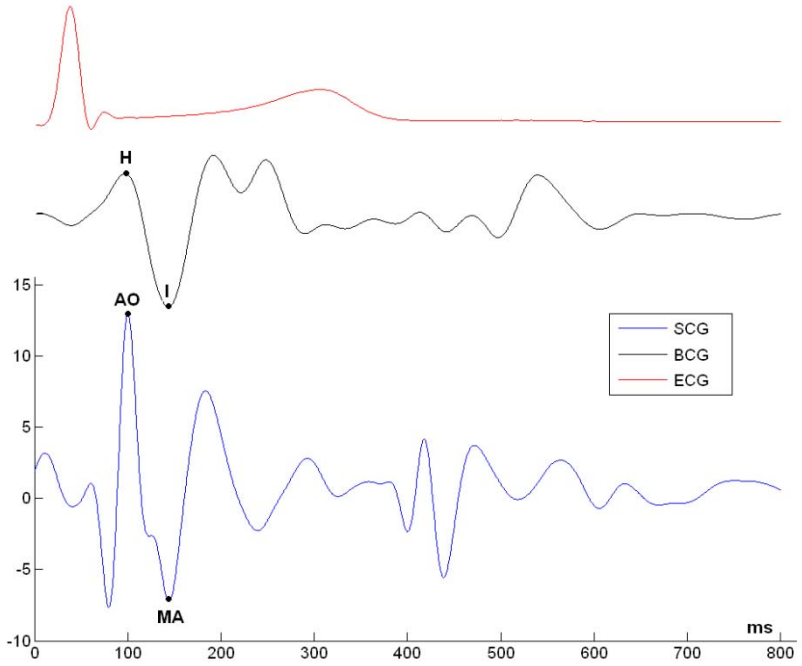

Figure 38. Ensemble average of SCG, ULF-BCG and ECG starting from the Q-wave on SCG

For all of the five participants, the aortic valve opening and maximum acceleration (MA) point on SCG and the H and I points on BCG were assigned manually as in Table 9. A paired t-test between the values of MA points on SCG and I points on BCG (p-value=0.95), and the values of AO and H (p-value=0.24) was used to confirm the intuitive interpretation from the ensemble averages (Figure 38).

The correlation of AO point on SCG and the H point on ULF-BCG is another proof for the accuracy of the AO point on SCG in assigning the aortic valve opening moment as will be explained in the next chapter on accuracy of

SCG in measurement of pre-ejection period (PEP). Considering the low number of participants in this study, the statistical power of the analysis is not high, however, the current analysis does not provide evidence against the intuitive observations from the experimental data as in Figure 15 and Figure 38, that show a correspondence between AO and MA points of SCG and H and I points of BCG.

Table 9. Results of comparison of two points of SCG (MA and AO) with two BCG points of H and I. The values are in ms and was calculated with reference to the ECG Q-wave

Participants	*MA*	I	*AO*	H
1	137.6	139.6	92.4	84.4
2	166.4	158.8	106	110.8
3	139.6	148	93.2	80.8
4	154	150.4	110.4	109.2
5	146	146	102.4	99.2
Averages	148.7±11.8	148.6±7	100.9±7.9	96.9±13.8

5.4 3D finite element cardiac model

In the 1950s, the introduction of mathematical models to simulate signal morphology ushered a new research avenue in ballistocardiography (Smith 1974). The mathematical models, derived from basic laws of Newtonian mechanics, assisted the understanding of the underlying physiological mechanisms of ballistocardiogram waves, and provided justification of the usefulness of ballistocardiogram in clinical studies (Starr and Noordergraaf 1967). The research presented in this section was inspired by such studies;

however, a model for the seismocardiogram proved to be a more complex task compared to the ballistocardiogram.

In the ballistocardiogram model, the whole heart was considered as a point source, which provided the pressure for the movement of blood in the body to move the centre of mass of the body, and the platform on which the body lies. In other words, the whole body was modelled with a network of Winkessle component, modelled as an electric component, each corresponding to a few centimetres of the body. The heart was modelled like a voltage source providing the required pressure for the blood to flow. The volume and mass of the heart could be neglected when compared to the size of the body and the platform. It was proven that the heart movement alone had a negligible effect on the ballistocardiogram morphology compared to the effect of blood circulation (Starr and Noordergraaf 1967)..

With SCG, and other precordial recordings, measurements are recorded from areas centimetres away from the heart, and heart movements dominate the morphology of the signal. Therefore, the point source model of the heart, as used in ballistocardiography, could not be used, and a more comprehensive model of the heart that included the volume of the heart itself was required. Thus, in the previous study from our group, SCG was simulated with an anatomically-accurate 3D electromechanical model of the heart ventricles (Akhbardeh, et al. 2009).

In the study detailed in this section, the 3D electromechanical model was improved to include a representation of the sternum and surrounding internal organs, and it was hypothesized that the movements recorded by SCG were stemmed from the pressure (compression and expansion) of the thoracic cavity between the heart and the chest wall. This hypothesis was fortified by both model results and experimental data, the latter of which included the direct measurement of the acceleration and velocity of aortic blood during ejection and also the ULF-BCG measurements as in previous sections.

5.4.1 The finite element model

5.4.1.1 Electromechanical model

The image-based, 3D, electromechanical model of canine ventricles (Figure 39A) has been described in detail by Gurev, et al (2010). Briefly, the geometry of the model was based on fiber and laminar sheet geometry determined from diffusion tensor MRI. The electromechanical activity of the heart was simulated by the combination of several models: monodomain model of electrical propagation; biophysical model of membrane kinetics; biophysical model of cardiac myofilaments; and continuous model of passive mechanics. The ventricular model was coupled with the circulatory model to simulate the different phases of cardiac cycle. Lastly, the surrounding anatomical structures such as the ribs and internal organs were incorporated, as described in the next subsection.

5.4.1.2 Representation of the sternum and internal organs

The ribs were represented as a solid cylinder of 10 mm radius that was placed next to the right ventricular apex, in accordance with the thoracic position of the heart observed from publically available cine-MRI videos (INRIA, Asclepios Research Project 2009). Since the displacement of the ribs due to contraction of the ventricles is much smaller than the movement of the ventricular walls and does not affect cardiac mechanics, the position of the cylinder was static, and changed only during respiration phases. Pressure of the cylinder on the ventricular surface, $\boldsymbol{P_C}$ (as well as pressure of the ventricles on the cylinder), was simulated using a penalty term which increased exponentially with the difference between the distance, ***d,*** of the point on the ventricular surface from the axis of the cylinder and the radius of the cylinder, ***r***:

$$P_c = \begin{cases} \alpha(e^{\beta \times (r-d)} - 1), & d < r \\ 0, otherwise \end{cases}, \qquad (1)$$

where α=1kPa and β=5mm^{-1}. Internal thoracic organs that surround the heart were simulated with a cylinder radius of 100m that was placed behind the posteriolateral wall of the left ventricle (LV). Since the orientation of the ribs changes during inspiration and expiration, simulations were performed with a control orientation (Figure 39B) and a rotated orientation in which the ribs were directed 15 degrees more in the longitudinal axis of the ventricles than in the control case.

5.4.1.3 SCG signal modelling

The SCG signal was represented as a function of pressure on the rib cylinder. Since mechanical properties of the sternum during contraction were unknown, two extreme cases were considered: 1) the elastic term was much greater than the viscous term (elastic case); and, 2) the viscous term was significantly larger than the elastic term (viscous case) of the Kelvin–Voigt model. Thus, the acceleration of the chest was proportional to either the first or second temporal derivative of the pressure on the rib cylinder for the viscous or elastic case, respectively.

The experimental SCG signals used for the validation of the model were the same ones used in the previous sections of this chapter.

5.4.2 Discussions on the simulation results

Normalized, simulated SGC signals for cases when the rib was considered elastic (top) and viscous (middle) is shown in Figure39C, along with the temporal changes in LV volume (bottom). Experimentally recorded SCG are also shown in Figure 39D for comparison.

Although the SCG in the elastic and viscous cases look similar, only the viscous case reproduced key features in the SCG signal. Consistent with previous publications and experimental results presented in section two of this chapter, the global positive peak occurred at the instant of aortic valve opening (the beginning of the ejection phase during which the LV volume decreases)

(Crow, et al. 1994). As noticed in Figure 39C during ejection, there was a rapid decrease followed by a slow increase in acceleration (2). The negative peak of acceleration coincided with the largest velocity of blood ejected from the ventricles, consistent with experimental observations from the Experimental Section below. Lastly, local negative and positive peaks occurred during the isovolumic relaxation (3) and ventricular filling (4) phases, respectively.

Unlike acceleration for the viscous case, the peaks of acceleration for the elastic component did not match the experimental findings. This would suggest that the forces due to elastic deformations were relatively small, and in the proceeding analysis, only acceleration for the viscous component will be discussed.

5.4.2.1 Longitudinal displacement velocity

Since the sternum is located near the right and left ventricular apex, SCG morphology is mostly affected by ventricular contraction in the longitudinal direction of the ventricles, which is reflected by the longitudinal displacement of the LV apex. The displacement velocity of the LV apex in the longitudinal direction is shown in Figure 39E. Indeed, the rapid increase of longitudinal velocity during isovolumic phase (1) results in a negative peak on SCG because the pressure on the rib cylinder decreases. The negative velocity peak, which follows this positive peak, is much smaller.

Nevertheless, the rising LV intracavitary pressure amplifies the force acting on the rib cylinder, which, in turn, results in a pronounced positive peak of the SCG signal at the end of the isovolumic contraction. The longitudinal displacement of the LV apex is further illustrated in the images of the anterior ventricular surface in Figure 39F. Indeed, at the end of isovolumic contraction, the longitudinal dimension of the ventricles decreases. The peaks during the other phases of the cardiac cycle can be explained in a similar manner.

5.4.2.2 Effect of rib orientation on SCG signal

Changes in the orientation of the rib resulted in different peak amplitudes in SCG, as well as different morphologies (Figure 39C). An additional positive peak appeared at the beginning of isovolumic contraction, and the amplitude of the negative peak was decreased. The magnitude of the SCG signal was different during ejection and isovolumic relaxation in the rotated case compared to the control case. Lastly, there was a local positive peak during ventricular filling in the rotated case that was absent in the control case. These findings suggest that the changes in SCG morphology can be attributed, to some extent, to the different orientation of the rib with respect to the ventricles.

5.4.3 Conclusions on the SCG finite element model

This study employed a novel image-based, anatomically accurate model of ventricular contraction to provide insight into the SCG morphology. The main findings of this study were

- the acceleration of the chest arises from the pressure of the heart applied to the chest and is primarily determined by the viscosity of the chest,
- the isovolumic peaks of the SCG signal arise due to the longitudinal contraction of the ventricles,
- changes in SCG morphology during respiration are, to some extent, explained by variations in the orientation of the ribs relative to the heart.

Some of these findings were fortified by the experimental findings as explained in the previous sections of this chapter. Statistical analysis on the accuracy of the assessment of aortic valve opening confirmed the validity of the model in assigning the first positive peak of SCG, appearing after the ECG R wave, to aortic valve opening (Figure 39). On the other hand, correspondence of the peak of the acceleration of blood in the aorta to the negative peak of SCG (as in Table 8) further confirmed the validity of the model in its claim that the SCG signal was the result of the pressure of the myocardium on the rib, rather than blood circulation.

The negative and positive peaks during the isovolumic phase of contraction are key features of SCG morphology during systole. Our results demonstrate that the negative peak arises due to a decrease in the longitudinal dimension of the ventricles. During isovolumic contraction, the LV apex moves rapidly towards the base, as noted by the increase in longitudinal velocity. Then, the longitudinal velocity is reduced at the end of isovolumic contraction. These

changes in longitudinal velocity are consistent with experimental recordings of longitudinal strain which show an initial, rapid decrease with subsequent, brief slowing (Edvardsen, et al. 2002).

In the framework of the model, contraction in the longitudinal direction is explained by the ventricular activation sequence and the fibre geometry of the heart. The electrical impulse travels through the Purkinje network to the endocardium, the inner most layer of the working myocardium. The endocardial myofibers are oriented mostly longitudinally due to the trabeculation. Activation of these myofibers results in the development of active stress in the longitudinal direction which, in turn, leads to longitudinal contraction of the ventricles. Then, electrical activation propagates transmurally from endocardium to epicardium (outer layer of the ventricles), resulting in activation of myofibers oriented more circumferentially.

As these layers contract, the short-axis diameter of the ventricles decreases, and since the ventricular volume is constant, the shortening of these circumferentially oriented myofibers impedes longitudinal contraction, leading to a positive peak in the SCG signal. Other factors that may determine the positive isovolumic peak in SCG signal include the asymmetry in contraction between the right and left ventricles, and the increasing intracavitary pressure.

Current results demonstrate that changes in amplitude and morphology of the SCG signal can be due to the orientation of the heart relative to the chest

during respiration. When the cylinder that represents the rib is oriented more in the longitudinal direction, there is an additional pressure on the rib from the right ventricular wall. However, other possible mechanisms may also be considered.

Specifically, the increased pulmonic pressure during inspiration elevates the afterload of the right ventricle and end-systolic right ventricular pressure, thus, increasing the pressure of the ventricles acting on the chest. In addition, respiration leads to changes in LV contraction. These alternative mechanisms will be tested further with the model. Further development of this novel electromechanical model will provide us with a platform where precordial pulsations, such as seismocardiogram, can be analyzed, and the effects of different abnormalities on the pulsations can be explained with greater insight.

5.4.4 Limitation of the current model

This study is the first step in the modeling of interaction between the heart and external objects. Particular configuration of the external objects affects SCG signal as well as overall cardiac contraction; thus, further studies with more detailed model of external organs and the chest are required. However, in the current paper we attempted to reproduce only general shape of SCG signal for which two-cylinder configuration seems to be sufficient.

In this study, we employed the canine ventricular model to simulate SCG, which was compared to human clinical data. Both human and canine ventricular walls have similar fiber geometry, in which the fibers rotate transmurally. As

explained in the Discussion, this is a key feature in the model that enables us to simulate the SCG signal. Because the durations of different cardiac cycle phases are different for canine and human, the absolute values of the timings of SCG peaks were not compared.

Figure 39. Electromechanical model of ventricular contraction and simulation of SCG signal. A. Diagram of electromechanical model coupled with the model of blood circulation in the body. B. Location of rib and thoracic organs in the model. C. Temporal traces of acceleration in the elastic case (top), acceleration in the viscous case (middle) and LV volume (bottom). Solid and dashed lines represent control and rotated rib orientation, respectively. Stars highlight changes in SCG morphology due to rotated rib. D. Clinically-recorded SCG signal during expiration and inspiration. E. Longitudinal displacement velocity of LV apex. F. Deformations of the ventricles during different phases of cardiac cycle (view from the anterior surface). Notations: (1) – isovolumic contraction, (2) – ejection phase, (3) – isovolumic relaxation, (4) – ventricular filling, LAD – left anterior descending coronary artery. MC – mitral valve closing, AO – aortic valve opening, RE – rapid ejection.

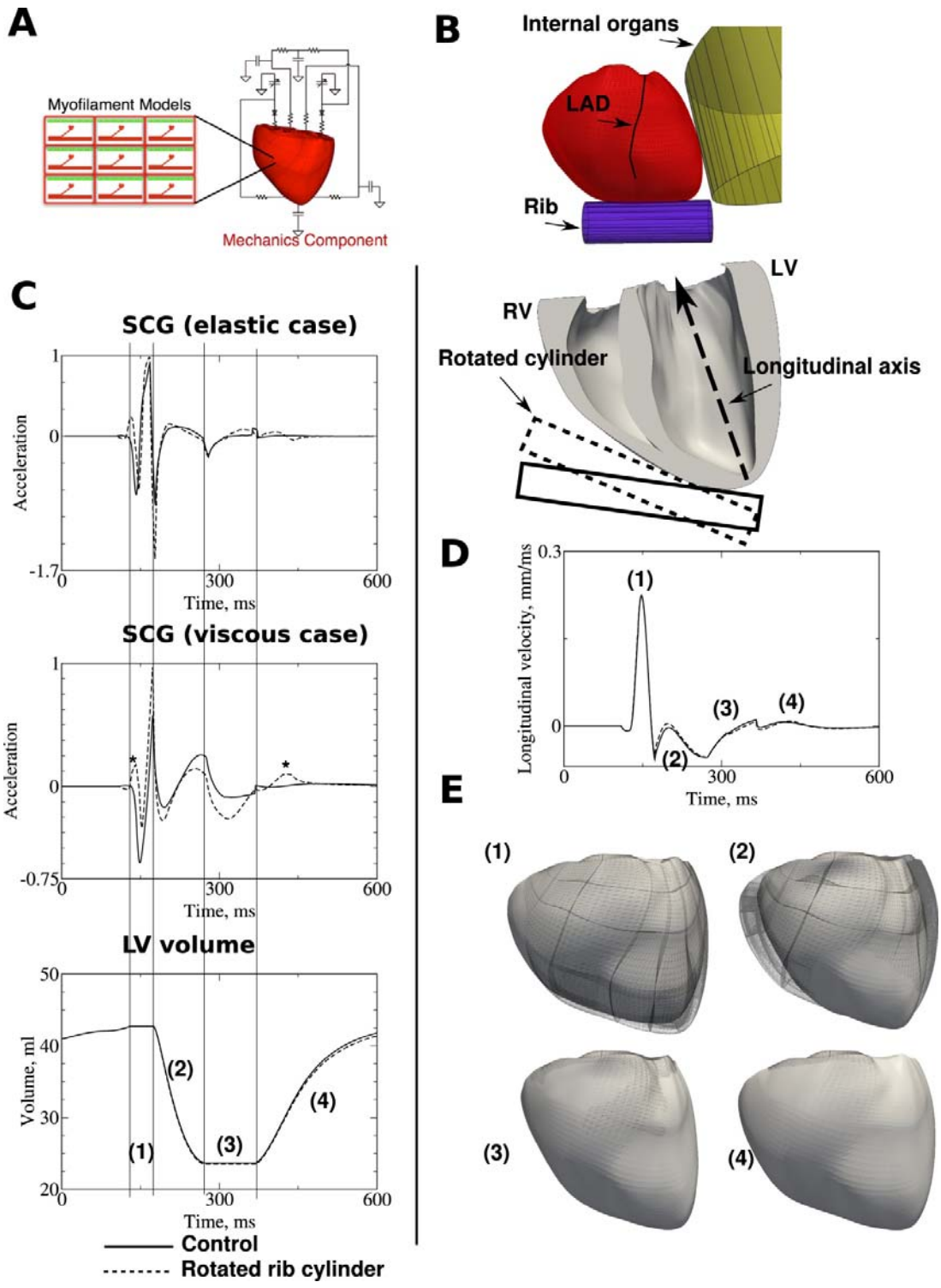
A
Myofilament Models
Mechanics Component
B
Internal organs
LAD
Rib
LV
RV
Rotated cylinder
Longitudinal axis
C
SCG (elastic case)
Acceleration
1
0
-1.7
0
300
600
Time, ms
SCG (viscous case)
Acceleration
1
0
-0.75
0
300
600
Time, ms
LV volume
Volume, ml
50
40
30
20
(1)
(2)
(3)
(4)
0
300
600
Time, ms
Control
Rotated rib cylinder
D
Longitudinal velocity, mm/ms
0.3
0
(1)
(2)
(3)
(4)
0
300
600
Time, ms
E
(1)
(2)
(3)
(4)

6: HEMODYNAMIC PARAMETER ESTIMATION

"Let us assume, either arbitrarily or from experiment, the quantity of blood which the left ventricle of the heart will contain when distended, to be, say, two ounces, three ounces, or one ounce and a half - in the dead body I have found it to hold upwards of two ounces. Let us assume further how much less the heart will hold in the contracted than in the dilated state; and how much blood it will project into the aorta upon each contraction"

William Harvey 1628

6.1 Hemodynamic parameters

Hemodynamic, literally means blood movement and is the study of blood flow or the circulation. The parameters that are extracted from the movement of blood, from the heart into the circulatory system, are of special attention to this thesis and conclude the goal of this research. This section describes these hemodynamic parameters, and the results of extraction of these parameters using SCG is explained in detail in the following sections.

6.1.1 Stroke volume, cardiac output and ejection fraction

Stroke volume (SV) is the quantity of blood ejected with every heartbeat and is approximately 70 mL for a 70 Kg healthy man. SV equals the difference of the end-diastolic volume (EDV) and end-systolic volumes (ESV) as in this

equation: SV=EDV-ESV. EDV is the maximum left ventricular volume and occurs right before the onset of systole and, ESV is the minimum of ventricular volume during the whole cardiac cycle (Guyton and Hall 2006).

Cardiac output (CO) is the amount of blood ejected out of left or right ventricle, and can be approximated by multiplication of stroke volume by heart rate; CO=SV x Heart Rate. The normal values of cardiac output are 5 L/min for men and 4.5 L/min for women,

Ejection fraction (EF) is the ratio of stroke volume to EDV and is generally expressed as a percent; EF=SV/EDV. In other words, SV is simply the percent of the EDV ejected out as the stroke volume. Normal EF values range between 55 and 75%, whereas ejection fraction in patients with heart failure can fall below 20% (Katz 1992).

Clinical conditions that result in abnormal stroke volumes can be simplified into four categories and some of them can coexist:

1) Filling volume changes, which result from either altered filling pressure, or altered diastolic compliance, such as: hypovolemic shock from bleeding; increased blood volume from chronic heart or kidney problem.

2) Altered effective length of contractile shortening, such as myocardial infarction and segmental hypokinesis where a segment of the myocardium does not contract.

3) Altered effective speed of contractile shortening such as decreased contractility as in generalized cardiomyopathy or increased contractility as in high adrenalin state in an acute anxiety attack.

4) Altered arterial impedance such as low impedance cases as in anaphylactic shock or septic shock or high impedance cases as in hypertension, atherosclerosis, or adrenergic physiologic response to low cardiac output of any cause.

Unfortunately, direct measurement of cardiac output in man is virtually impossible, (because of the heart being quite inaccessible) thus, many different methodologies have been proposed for indirect measurement of cardiac output of which the Fick method is the oldest. Fick method is based on the measurement of the amount of oxygen uptake by lungs that are an indicator of the amount of blood delivered to them (Rushmer 1965).

Indicator dilution was another method of cardiac output estimation where an indicator, such as a dye, was injected into a large systemic vein. The concentration of dye was measured later at one of the arteries and was an indicator of the cardiac output. This method was improved later to pulmonary artery thermodilution (PAT) where the dye was replaced by a heated or cooled solution and the changes in temperature was related to cardiac output (Guyton and Hall 2006). Of particular interest to this research are Doppler ultrasound and impedance cardiography methods that will be explained in more details in the

coming sections. Ballistocardiogram is also one of the old methods for non-invasive estimation of stroke volume (Starr and Noordergraaf 1967).

6.1.2 Cardiac cycle time intervals

The time intervals of the cardiac cycle are divided into systolic time intervals and diastolic time intervals. The correlation of the duration of systolic time intervals with other hemodynamic parameters is an old observation and goes back to a research in 1874 showing the inverse relation between left ventricular ejection and heart rate. A clear manifestation of this correlation was in Frank's work demonstrating the fact that increase in left ventricular filling will result in reduction of isovolumic contraction time and increase of ejection time, accompanied with an increase in stroke volume (Lewis, et al. 1974).

6.1.2.1 Systolic time indexes

The systolic time intervals were first defined by Wiggers as can also be seen in Figure 4 (Martin, et al. 1971). The advance of technology provided the tools for non-invasive measurement of the systolic time interval and this was one of the first methods in cardiology that the term non-invasive was applied to it (Weissler, Harris and Schoenfeld 1968). From infrasonic cardiac signals, apexcardiography was used in estimation of systolic time intervals (Lewis, et al. 1974).

Commonly used systolic time intervals are total electromechanical systole (QS2), the left ventricular ejection time (LVET), pre-ejection period (PEP),

isovolumic contraction time (IVCT) and electromechanical lag (EML). The definitions and the regression equations of their normal values are listed in Table 10 and are derived from analysis of 211 normal participants, 121 male and 90 females between 19-65 years old (Katz 1992). It should be noticed that the regression equation presented in the table have the standard deviation of more than 10 msec. These systolic time intervals were measured by simultaneous measurement of ECG, PCG and carotid arterial pulse tracing and all intervals were calculated from the mean of measurements made on 20 to 30 consecutive beats (Lewis, et al. 1974).

In these research, the QS2 was measured from the start of the QRS complex to the first high frequency vibrations of the aortic component of the S2. The LVET was measured from the beginning upstroke to the trough of the incisura of the carotid arterial pulse tracing. PEP was measured by subtracting LVET from QS2. EML was derived by subtraction of S1-S2 from QS2 and finally IVCT was calculated by subtraction of LVET from S1S2 (Weissler, Harris and Schoenfeld 1968).

The failing left ventricle was characterized, on 27 patients, by long PEP, shorter LVET and normal QS2 intervals. The prolongation of PEP included both the IVCT and the period before it. It was also demonstrated that the longer PEP and shorter LVET were well correlated with the reduced stroke volume and cardiac output (Weissler, Harris and Schoenfeld 1968).

There were studies on cases where the stroke volume and cardiac output were normal while but their PEP/LVET was clearly abnormal giving the idea that this index is more sensitive to ventricular dysfunction. These studies motivated further studies in correlating PEP/LVET index to ventricular function (Lewis, et al. 1974).

In a study on 68 patients, of different cardiac diseases, the systolic time intervals of PEP, LVET and the PEP/LVET ratio, each correlated significantly with angiographically determined ejection fraction (EF) and end diastolic volume and slight correlation to stroke volume was also observed. This study along with other studies provided additional evidence supporting the use of systolic time intervals as a non-invasive estimate of left ventricular performance in patients with cardiac disease (Garrard, Weissler and Dodge 1970).

There is a recent application for EML, systolic time interval that is the time between Q wave on ECG and the moment of mitral valve closure, and how this timing can be used in order to differentiate between supraventricular tachyarrhythmia and a ventricular tachyarrhythmia. If used in implantable devices, extraction of such a parameter can help in type of treatment delivered to the heart (Lincoln 2007).

Table 10. Systolic time intervals (Katz 1992)

Systolic interval	Definition	Physiological relation	Regression Equation	Standard Deviation
QS2	From beginning of Q to the high frequency vibration of S2	Total electromechanical systole	546-2.1*HR	14
LVET	From crotid upstroke to the dicrotic notch	Total ejection	413-1.7*HR	10
PEP	QS2-LVET	Pre-ejection period that equals EML+IVCT	131-0.4*HR	13
IVCT	From Mitral valve closure to Mitral valve opening	Isovolumic contraction time	38 (msec)	10
EML	From Q to start of S1	Electromechanical lag	90-0.4*HR	11

6.1.2.2 Diastolic time indexes

Recent extensive research has shown an increase in the prevalence of heart failure with preserved ejection fraction, previously known as diastolic heart failure, over time. The stability in the rates of death from this condition underscore the importance of developing diagnostic strategies against it by measuring diastolic performance (Owan, et al. 2006).

The time intervals between the precordial accelerogram's peaks are correlated with cardiac intervals such as isovolumic contraction and relaxation times and ventricular ejection time. Calculation of these three cardiac intervals

from SCG provided Marcus, et al (2007) with the possibility of non-invasive calculation of a combined myocardial performance index called Tei-index. This calculation was done by assumption of the equality of heart rate in the consecutive heartbeats and separate measurements of systolic and diastolic time intervals in different beats.

Tei index equals isovolumic contraction time plus isovolumic relaxation time divided by ejection time. Congestive heart failure is related to contraction and relaxation abnormalities of the ventricle. Isolated analysis of either mechanism may not be reflective of overall cardiac dysfunction. Tei-index has been described to be more effective for analysis of global cardiac dysfunction than systolic and diastolic measures alone. Tei-Index is evaluated against invasive examinations and proved a sensitive indicator of overall cardiac dysfunction in patients with mild-to-moderate congestive heart failure (Bruch, et al. 2000).

6.2 Estimation of systolic time intervals using SCG

Signals from 25 participants (3 female, 22 male) were used for the extraction of systolic time intervals. The average of age for these participants was 36±15.9, with an average weight of 73±10.4 kg and an average height was 173±7.7 cm. Five of the participants were chosen from a patient population in Burnaby General Hospital who had a history of heart attack and very low ejection fraction. The rest of the participants were healthy with no history of cardiac

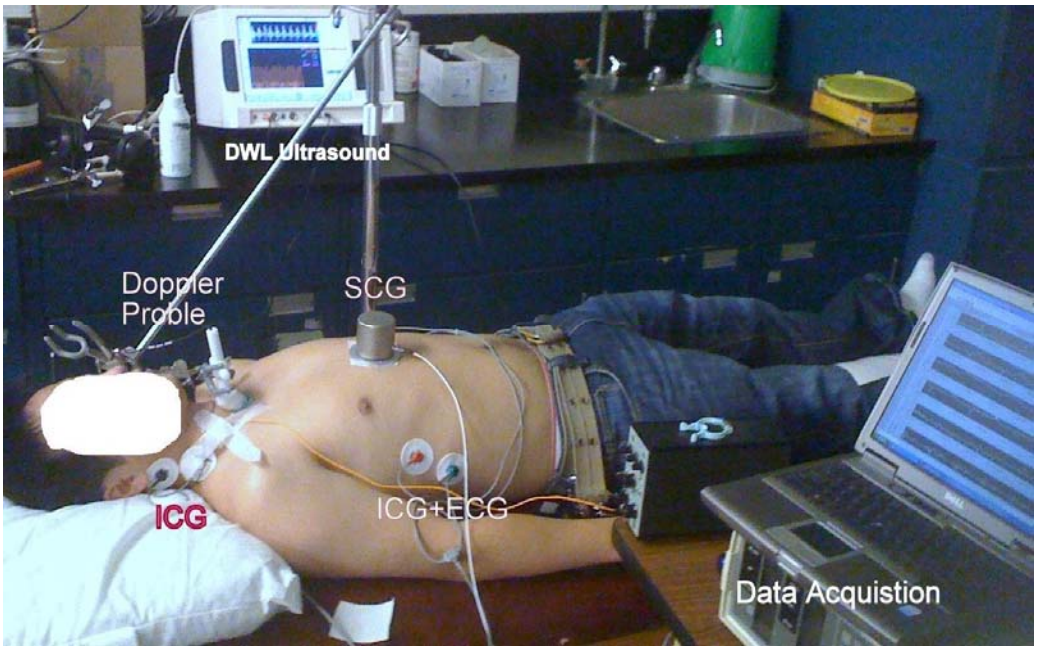

Figure 40. The data acquisition setup for simultaneous recording of SCG, ICG and parasternal Doppler ultrasound

problems. This is the same dataset that was used in the previous chapter for evaluation of MA point, except that two more participants are added to this recent study (participant number 24 and 25).

All the data were acquired with a National Instruments DAQ and GUI system at a sampling rate of 2.5 KHz. Suprasternal Doppler, SCG, ECG and Impedance cardiography were simultaneously recorded as shown in Figure 33. The SCG signal was recorded as described by Salerno and Zanetti (1991) with the same model piezoelectric accelerometer as explained in the previous chapter. The accelerometer was placed on the midline of the sternum with its lower edge at the xiphoid process and the data acquisition setup is as in Figure 40. A 2MHz pulsed Doppler instrument (MultiFlow, *DWL* GmbH, Sipplingen,

Germany) was used for this study. All the measurements in the present study were made with an insonation depth of 6.5 to 7.5 cm with the sample volume located 1.0 to 1.5 cm above the aortic valve. The optimum position of the probe was taken as that giving the maximum peak velocity, with minimal spectral broadening and a clearly identified upstroke on each beat. This was assessed from the spectrum analyzer display and by listening to the audiofrequency Doppler signal. The same experienced ultrasonographer obtained all signals.

The temporal landmarks on ICG, which are of special interest to this research are B and X points as explained in the previous chapter and seen in Figure 33. Based on the echocardiographic studies the B point on ICG corresponds to the start of systolic ejection (aortic valve opening) and the X point corresponds to the aortic valve closure. In this study the impedance cardiogram was measured using the BoMed NCCOM3 device.

The three systolic intervals of PEP, LVET and QS2 were measured in this study as defined in the previous section. The ensemble averages of signals were used for these measurements as in Figure 34. In order to derive these ensemble averages the Q wave of ECG was first calculated in order to separate different heartbeats and to also align the SCG , ICG and ultrasound signals for averaging

For SCG the two points AO and AC were detected and for ICG the two points of B and X were assigned as in Figure 33 and Figure 34. For the ensemble average of Doppler signal, the point from which the signal rises from

Table 11. Measurement results three systolic time intervals of systolic ejection time (LVET), pre-ejection period (PEP) and total electromechanical systole (QS2) for twenty four participants. Three different methods of SCG, Doppler ultrasound (Ult) and impedance cardiography ICG. Were used for these measurements. In two participants the Doppler measurement was not available and in one participant the ICG measurement was not available. The last row is the averages. All the values are in milli-seconds.

	LVET			PEP			QS2			PEP/LVET		
Subjects	SCG	Ult	ICG	SCG	Ult	ICG	SCG	Ult	ICG	SCG	Ult	ICG
1	327.2	318.4	328.4	105.2	116.8	106.8	432.4	435.2	435.2	0.32	0.36	0.32
2	319.6	309.2	334.8	121.6	110.4	107.2	441.2	419.6	442	0.38	0.36	0.32
3	320.8	329.6	321.6	86.8	88.8	81.6	407.6	418.4	403.2	0.27	0.27	0.25
4	297.2	302.4	296	84	88.8	88	381.2	391.2	384	0.28	0.29	0.30
5	321.2	323.6	314	74.4	82	82.8	395.6	405.6	396.8	0.23	0.25	0.26
6	288.4	293.2	288	88.4	84	86	376.8	377.2	374	0.31	0.28	0.30
7	318.8	306.8	306.4	89.2	106.8	100	408	413.6	406.4	0.28	0.35	0.32
8	309.2	319.6	317.2	104.4	97.2	102.8	413.6	416.8	420	0.34	0.30	0.32
9	339.6	336.8	324	73.2	83.2	85.6	412.8	420	409.6	0.21	0.24	0.26
10	323.6	318.4	324.4	78.4	89.6	88	402	408	412.4	0.24	0.28	0.27
11	308.8	310.4	312.4	96	98	86.4	404.8	408.4	398.8	0.31	0.31	0.27
12	291.2	298.8	287.2	84.4	86.8	84.8	375.6	385.6	372	0.29	0.29	0.29
13	278	288.8	318	96	84.4	84	374	373.2	402	0.34	0.29	0.26
14	316	328.4	330.8	112	106.8	108	428	435.2	438.8	0.35	0.32	0.32
15	319.6	291.2	314	82	98.8	82.8	401.6	390	396.8	0.25	0.34	0.26
16	338.8	322.4	335.2	90	98	94	428.8	420.4	429.2	0.26	0.30	0.28
17	280	256.4	278.8	160	160.6	147.2	440	422	426	0.57	0.62	0.52
18	331.2	331.2	306.8	112	108	109.6	443.2	439.2	416.4	0.33	0.33	0.36
19	304	297.6	300	120	120	120	424	417.6	420	0.39	0.40	0.40
20	334.4	336.4	329.6	73.6	80	78.4	408	416.4	408	0.22	0.23	0.24
21	262.4	-	260.4	60.8	60	67.6	323.2	-	328	0.23	-	0.26
22	266	252	252	109.6	108	108	375.6	360	360	0.41	0.43	0.43
23	312	310.4	-	112	115.2	-	424	425.6	-	0.36	0.37	-
24	317.2	-	312	66.8	-	80	384	-	392	0.21	-	0.26
25	285.2	-	284.8	116.4	-	115.2	401.6	-	400	0.40	-	0.40
Averages ±std	**308.4 ±21.9**	**308.3 ±22.6**	**307.4 ± 22.5**	**95.9± 21.8**	**98.8± 19.7**	**95.6± 17.4**	**404.3 ±27.4**	**409± 21.1**	**403± 26.2**	**0.31± 0.08**	**0.33± 0.08**	**0.31±0 .07**

zero and the dicrotic notch were identified for every one of the 25 participants. In one of the participants the dicrotic notch was faded over averaging thus, for this single participant only the PEP value was measured, from the three targeted systolic time intervals.

For two participants the Doppler was not available (number 24 and 25). For one of the participants the ICG was not measured as he had a pacemaker that could have been adversely affected by the current induced by the ICG measurement (number 23).

The detailed results of estimated systolic time interval for every individual is listed in Table 11 and using JMP7 software, a randomized incomplete block design was used to test for mean difference in response, on the four measured parameters of PEP, LVET,QS2 and PEP/LVET using the three methods of SCG, ICG and Doppler. The p-vales of 0.16, 0.93, 0.91 and 0.12 were obtained for the parameters of PEP, LVET,QS2 and PEP/LVET, respectively thus, the analysis provided no evidence to reject the null hypothesis. Thus, it is concluded there is no evidence to suggest there is a difference in mean response between treatments for the three systolic time intervals.

In Appendix 5 there are plots and tables derived from JMP 7 software that better clarifies the above findings. The values for PEP and QS2 in Table 11 were the same values used in the previous chapter, for validation of assessment of aortic valve opening and closure times, in the context of genesis of SCG waves.

The p-value of 0.16 for PEP, although not rejecting the null hypothesis, is clearly lower compared to the values obtained for LVET and QS2. The retrospective power analysis shows that there was 37% power for the PEP measurement using the three devices and that more than 39 participants are required to achieve statistically significant difference between the subjects. The prospective power analysis shows that about 63 participants are required to

achieve 80% power. In other words, the number of participants should be doubled or tripled to obtain enough statistical power for PEP.

Ideally, the ensemble averaged Doppler velocity ultrasound is supposed to take off from zero, as aorta opens, but this does not happen in most cases, because of the background noise. As mentioned previously, the aortic valve opening point is estimated from ensemble averaged Doppler velocity by determining the cross section of the up-going slope with zero. In other words the aortic valve opening point determination from Doppler was not an observation as the other points on SCG and ICG and even the aortic valve closure point on the same Doppler velocity signal. As the aortic closure point (AC) occurs in higher velocities, unlike aortic valve opening point (AO), it does not get affected by the background noise (Figure 34).

A paired t-test for aortic valve opening point (on the values of Table 11) between ICG and SCG yields a high p-value of 0.80 while the same test between ICG and Doppler ultrasound data yields the p-value of 0.054 (almost borders rejection). The same paired t-test between SCG and Doppler ultrasound gives the p-value of 0.14. This further confirms the assumption above that the inaccuracies in estimation of aortic valve opening point with Doppler ultrasound might have lead to the low p-value of 0.16 as explained before. The same reasoning is valid for PEP/LVET parameter.

On the other hand, such differences between the ultrasound method and SCG and ICG in estimation of PEP value have not affected the LVET estimation (which is derived from subtraction of PEP from QS2) as LVET is three times

more in value compared to the PEP and slight difference in PEP estimation has not affected the estimation of LVET (p-value=0.93).

6.3 Estimation of stroke volume using SCG

The same setup, as the previous section, was used for the extraction of stroke volume from SCG. In the preliminary study, phase 1, the capability of SCG in estimation of stroke volume was studied on signals recorded in one recording session while in phase 2 the capability of SCG in estimation of stroke volume on signals recorded on different days was assessed. For the second phase, the signal acquisition was conducted in two separate sessions at least a day apart and the signal from the first session was used for training and the second day for testing. In both phases eight healthy male participants, under the age of 32, were recruited for data acquisition.

Having limited number of participants, it was not feasible to develop a general estimator, independent of individual subjects, which could be used for estimation of stroke volume. On the other hand, in participants from whom the signals were collected, few of them had to be discarded in phase 2 as they did not have reproducible reference stroke volume between different days. The goal of phase 2 was to show that by recording mechanical vibrations from the chest, the stroke volume can be estimated in another day on the same subject.

After recording and proper pre-processing of the data, features were extracted from SCG signal based on current knowledge of the correspondence of SCG waves to cardiac events. This knowledge was obtained through a research as explained in previous chapter. The following features were extracted for this study: isovolumic contraction time (MC-AO) and its slope, systolic ejection time

Figure 41. Left ventricular output tract measurement for the fourth participant is 2.01 cm.

(AO-AC), isovolumic relaxation time (AC-MO), the area under curve during rapid systolic ejection (RE), the maximum of rapid ejection and the slope of its increase, the time between the ECG R wave and the opening of mitral valve.

For each beat, the Doppler stroke volume was determined by calculation of the area under the curve on the Doppler signal (stroke distance) and multiplication by the area of aortic ring. For the third and the fourth participants, as in Table 12, the diameter, identified as LVOT, was measured with a GE Vivid 7 echocardiograph machine. For participant number four the measurement is as in Figure 41, and the result of it is 2.01 cm

For the remaining participants the aortic ring diameters were not available and were assumed 2 cm (the average for men). The lack of exact values for aortic ring is not ideal but would not undermine the proposed estimation method since the stroke volumes are estimated as the multiplication of variable beat-to-beat stroke distances by a constant value (the area of the aortic ring). In other words, the aortic ring area simply scales up the values estimated from calculation of beat-to-beat area under the curve for the ultrasound or beat-to-beat stroke

distance. This scaling brings the values into the range of stroke volume and enables us to assess the accuracy of estimation in familiar millilitre values.

6.3.1 Single session estimation

In each regression or neural network session, one hundred vectors were selected for testing and one hundred for validation. The remaining vectors were used for neural network training and establishment of the linear multivariate regression. This was repeated, until every single vector was given an equal chance to be tested against the regressor or the neural network.

The beat-by-beat extracted features were input to a supervised neural network, which provided the preliminary SCG estimates of SV. A feed forward neural network trained by back propagation was used for this study. Twenty neurons in the hidden layer and one linear neuron at the output were considered. Each neural network was trained and tested 200 times, and the results of these simulations are shown in Table 12 and Figure 42.

The Bland and Altman (1986) method was used to test the results; over eight participants the average of the differences was 0.07 mL with higher and lower 95% confidence intervals of 7.4 mL and -7.6 mL respectively. The results for eight participants are as listed in Table 12. The distribution of correlation between the values estimated by the neural network and the values given by the reference Doppler method are shown as boxplots in Figure 42. The boxes have lines at the lower quartile, median, and upper quartile values. The whiskers are lines extending from each end of the boxes to show the extent of the rest of the data. Outliers are data with values beyond the ends of the whiskers.

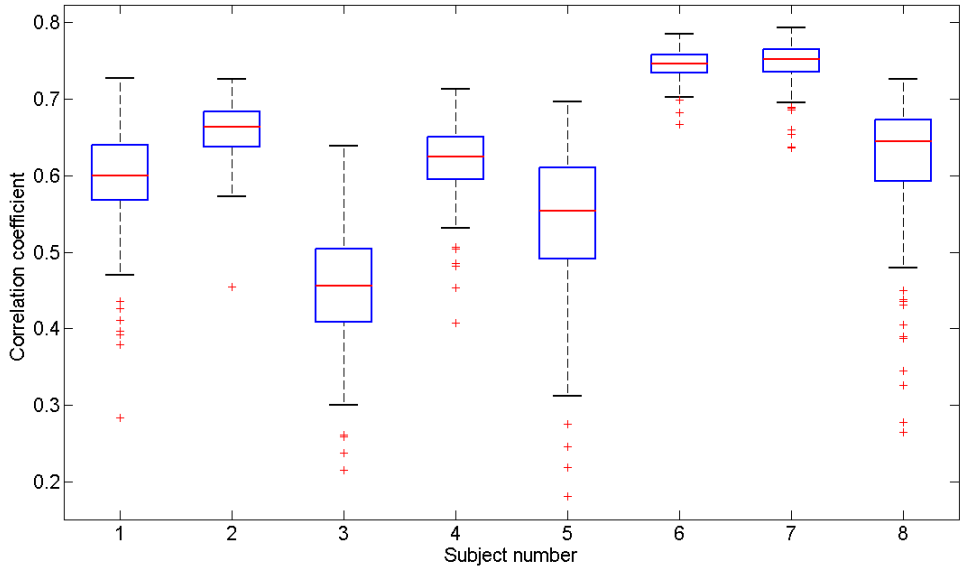

Figure 42. Boxplot and whisker plot of correlation coefficients estimated by the neural network for eight participants.

6.3.2 Double session estimation

As explained in previous section in phase 1, nonlinear methods such neural network and nonlinear regression were used for estimation of stroke volume and analysis showed that the linear regression gives close results to the neural network. In the previous study a cross validation method was used to divide the extracted feature vectors into training, testing and validation sets. This division was performed on the vectors of the same day data acquisition session.

In this study, it was decided to test the validity of the stroke volume assessment after few days, using SCG. The beat-by-beat extracted features from the first session were input into a multiple linear regression. The inputs contained 17 component vectors extracted from every individual heartbeat.

The extracted features included the features as in phase 1 and also added new features to it. These features included isovolumic contraction time (MC-AO) (also its slope and its peak to peak amplitude), systolic ejection time (AO-AC),

isovolumic relaxation time (AC-MO), the area under curve during rapid systolic ejection (RE), the maximum of rapid ejection and the slope of its increase, the time between the ECG R wave and the opening of mitral valve also the Tei and PEP/LVET indexes.

As explained before, the first session was used for training and the second session for testing. The results for the stroke volume estimation for the first participant, a 32 year old healthy male, can be seen in Figure 43 and the results for all participants are found in Table 13. As it is observed from the results the average of the differences over all participants was 2.56 mL. This is clearly worse than the results obtained previously on single session analysis (phase 1), which was close to zero. The confidence intervals are also not as narrow as our previous results of Table 12. The average correlation coefficient was 0.61.

Of the 4900 cycles analysed from all eight participants, 83 percent had an estimated value within a 10 mL range of the reference stroke volume as provided by the Doppler method. This 10 mL neighbourhood is also reported for every individual separately as in Table 13.

An important problem encountered during stroke volume measurement was the difficulty to reproduce the same reference Doppler estimation between days that could be changed by a slight change of angle or depth of measurement. Not having such problems, the results of Table 13 could have been improved.

Table 12. Comparison of Stroke Volume estimated by SCG and Doppler for Phase I for eight participants. The results of the last four columns are for linear regression and the rest for the neural network.

Participant	Mean Correlation coefficients	Mean differences	Upper 95% Confidence interval	Lower 95% Confidence Interval	Correlation coefficient Regression	Mean differences	Upper 95% Confidence interval	Lower 95% Confidence Interval
1	0.60	0.06	9.09	-8.96	0.35	0.68	20.15	-18.80
2	0.66	-0.08	8.84	-8.99	0.73	0.13	9.20	-9.03
3	0.45	-0.42	7.43	-8.28	0.64	0.32	8.12	-7.40
4	0.61	0.05	7.42	-7.32	0.62	0.67	15.10	-13.75
5	0.54	-0.36	6.08	-6.81	0.77	0	6.60	-6.6
6	0.74	0.04	6.43	-6.34	0.79	0.17	6.50	-6.15
7	0.75	0.30	7.42	-6.80	0.77	0.03	7.41	-7.36
8	0.62	-0.06	4.41	-4.54	0.65	-0.04	4.80	-5.70
Averages ± std	**0.62±0.1**	**-0.06±0.2**	**7.14±1.5**	**-7.25±1.5**	**0.66±0.14**	**0.24±0.3**	**9.7±5.2**	**-9.34±4.6**

Table 13. Comparison of Stroke Volume estimated by SCG and Doppler for Phase II

Participant	Correlation coefficient	Mean difference mL	Upper 95% confidence interval mL	Lower 95% confidence Interval mL	Percentage of 10 mL neighbours	Number of heart beats
1	0.83	5.92	12.49	-0.64	89.73	601
2	0.75	-6.6	1.12	-14.4	100	561
3	0.55	3.3	11.8	-5.2	97	685
4	0.62	7.7	23	-8.3	60.5	607
5	0.52	4	10	-0.6	96.3	513
6	0.6	2.5	10.3	-5.3	98.8	529
7	0.46	-1.5	3.7	-6.8	98	676
8	0.55	5.2	29	-19.1	40	728
Averages	**0.61±0.12**	**2.56±4.6**	**12.67±9.3**	**-7.54±6.41**	**85.1%±22.4**	**613±77.7**

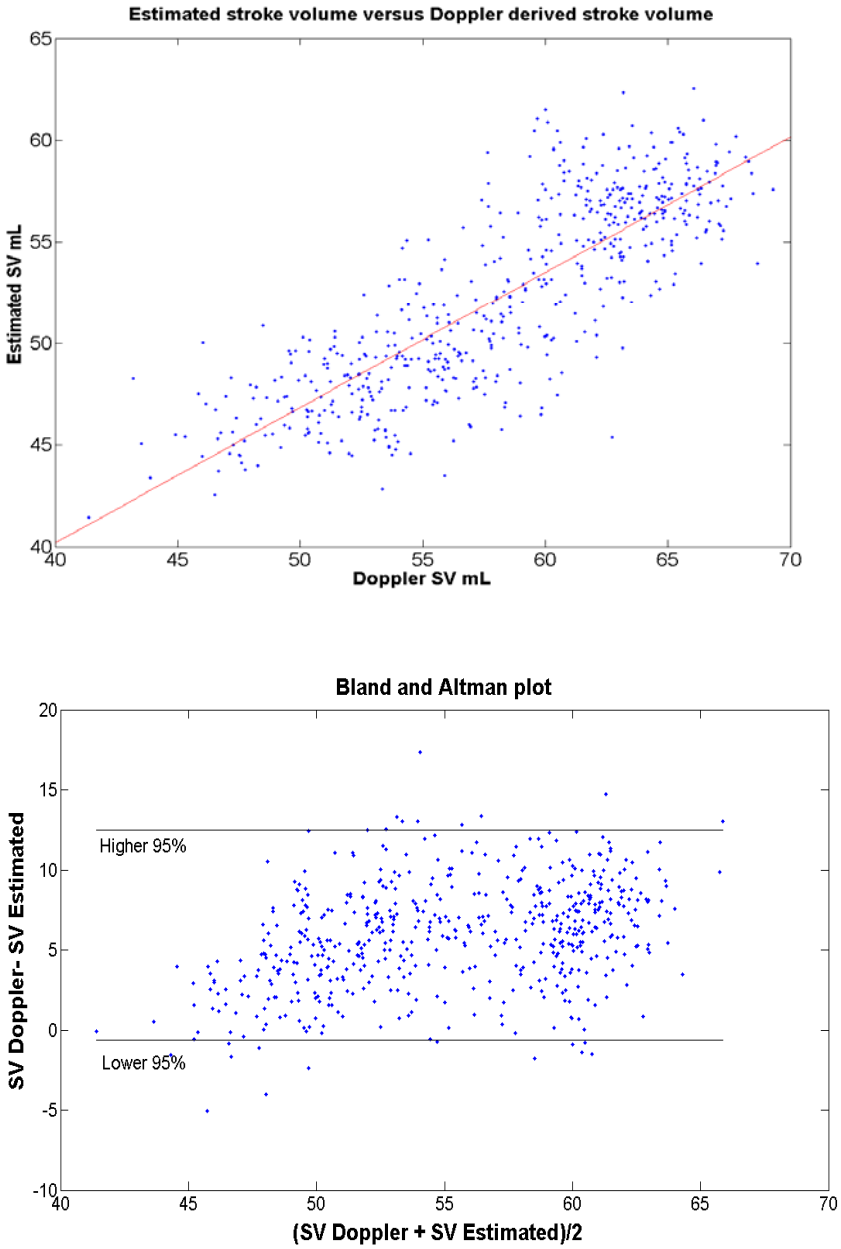

Figure 43. ***Top:*** **the estimated stroke volume versus Doppler ultrasound values in mL** ***Bottom:*** **Bland and Altman plot of the differences of the two methods versus their average together with the higher and lower 95% confidence intervals. 601 cardiac cycles were used from the first participant as in Table 13.**

7: CONCLUSION

Studies designed to determine the utility of any method often differ from those made to increase our understanding. This thesis was a mixture of both. This thesis covered the results of the analysis of SCG signals in order to extract hemodynamic parameters, and, conversely, presented the results of methodologies used to understand the genesis of SCG.

This thesis is the result of collaborative research at the Centre of Integrative Bio-Engineering Research (CiBER 2010) and Aerospace Physiology Lab at Simon Fraser University in Canada and the Institute for Computational Medicine at Johns Hopkins University in USA. In the first section of this chapter, the specific contributions of the author of the thesis are emphasized. In the second section, a summary of potential future work is presented.

7.1 Contributions

This thesis covered the results of two separate, but related, works on the estimation of stroke volume and systolic time intervals. With respect to systolic time intervals, using two other reference methods of ICG and Doppler ultrasound, it was proven that SCG can give accurate measurements for the three important intervals of PEP (p-value=0.16), LVET (p-value=0.93) and QS2(p-value=0.91). The obtained results proved that SCG estimation of systolic time intervals is comparable to the same parameters estimated using two reference methods of Doppler ultrasound and impedance cardiogram.

Stroke volume for 83% of the total (4900) cycles from eight participants was estimated within a 10 mL range of the value given by Doppler ultrasound. The obtained results were acquired from data recorded on two different days. The goal was to show that with a simple measurement of precordial acceleration from the chest, together with a reference methodology such as Doppler, one can estimate the stroke volume on the same participant days after the initial measurement. In other words, it was shown that that SCG could provide an estimation of stroke volume (results presented in chapter 6). The signal acquisition for this portion of the research was primarily performed at the Aerospace Physiology Lab and Burnaby General Hospital.

In this research, the effects of respiration on SCG was, for the first time, acknowledged and quantified. The statistical analysis showed a significant statistical difference (p-value<0.01) between the inspiration and expiration averages. Based on these observations, a new averaging method was proposed for SCG which is based on the separation of cycles dependent upon their place in the respiratory cycle. Also, from these results, it was proposed that if there is a single template representing an SCG recording, that template is best derived from expiration cycles rather than inspiration cycles. With this new proposed method of averaging SCG, one utilizes the respiration information to improve the averaging and interpretation of the SCG signal in the diagnosis of cardiac malfunctions before removing and filtering it out as an artefact. The data acquisition for this part of the project was performed at the Burnaby General Hospital.

The author of this thesis developed the algorithms that have proven the usability of novel techniques of acquisition of SCG, presented in chapter 3. In

particular, the algorithms presented in the mulisensor section that proved the usability of this sensor in the extraction of cardiac potentials and vibrations was developed by the author. On the radar system, the author was involved in data acquisition, and processed the recorded radar data in order to prove the capability of the microwave radar system in the extraction of SCG, and heart and respiration rates. The author used laser for the detection of SCG for the first time, and the preliminary results were presented at the end of the third chapter.

The results presented in chapter 5 include a set of four related projects that were conducted to gain a better understanding of temporal landmarks on SCG. One of the important findings of these projects was the assignment of a new meaning for a point on SCG that was identified by a previous research group to be isotonic contraction (IC) point, without a firm experimental foundation. The findings of Doppler ultrasound (n=23, r=0.85) and ULF-BCG (n=5, p-value=0.95) methods clarified that this point corresponds to maximum acceleration (MA) of blood in the aorta rather than the previous, unfounded, definition of isotonic contraction or “IC”.

Chapter five presented a novel approach to modelling SCG using a 3D, finite element model of the heart. The author’s involvement with this part of the project was on the experimental validation and interpretation of the obtained results from the model, and assisted the developer of the model in comprising ideas on applying new boundary conditions to the model that could yield more plausible results.

The main findings of this simulation study were that the acceleration of the chest arises from the pressure of the heart applied to the chest, and is mainly

determined by the viscosity of the chest. This finding was fortified with the findings of the Doppler ultrasound and ULF-BCG. In addition, changes in SCG morphology during respiration were, to some extent, explained by variations in the orientation of the ribs, relative to the heart.

Apart from the focused research on SCG, chapter two of this thesis provided a more thorough examination of the area of research to which SCG belongs. For the first time, a group of similar cardiac mechanical signals were studied in the same context of infrasonic cardiac signals, and few of them were actually recorded and compared to SCG in this research. The classification of these signals to two different categories, as in Figure 3, presents a new look to this whole research area, and can remove some of the ambiguities caused by imposing the ballistocardiogram terminology on precordial recordings such as SCG.

7.2 Future Work

Identification of early onset heart disease is difficult, requires specialized medical equipment, and highly trained analysis personnel. Current diagnoses rely on electrocardiograms (ECGs), stress tests, and imaging (such as angiography, radionuclide scan and echocardiography). While these tests are effective and used worldwide, they are expensive and have to be administered and interpreted by highly skilled medical practitioners. These tests do not lend themselves well to preventive monitoring and community-based healthcare, and as a result, the first indication of a cardiovascular problem may be a catastrophic event.

Often, ECG tests only show clear evidence of disease when patients are in an advanced pathological stage. For instance, the inability of the ECG to

detect early symptoms of heart disease was emphasized by the American Heart Association in a recent report which stated that 23% of seniors younger than 65 showed Non-ST-Segment Elevation Acute Coronary Syndrome (NSTEAS) in the absence of chest pain, but had an abnormally low cardiac output. In persons over 85 years of age, the number of NSTEAS cases with non-diagnostic ECGs rises to 43% (Alexander, et al. 2007). This is to be expected because the ECG records electrical activity, not the important mechanical dynamics of the pump-action (and blood flow) of the heart.

This thesis focused on the assessment of mechanical performance of the heart to complement information provided by ECG. Although this thesis provided information on the usability of SCG for the extraction of hemodynamic parameters, there are still challenges to overcome before such a system can be used in clinical settings. Some of these challenges and potential solutions are explained in this section.

7.2.1 Stroke volume and cardiac output

Diseases of the cardiovascular system are often associated with changes in cardiac output, particularly the pandemic diseases of hypertension and heart failure. CHF is associated with decreased cardiac output, as well. A cardiac output measurement, if accurate and non-invasive, would be adopted as part of every clinical examination from general observations to the intensive care ward, and would be as common as simple blood pressure measurements. This is the reason why cardiac output measurements are now an important research and clinical focus in cardiovascular medicine. Through the development of a simple, easy-to-use, inexpensive means of determining the mechanical performance of

the heart, we will be able to extract vital predictive information about the heart's condition, and many lives can be saved.

Although the absolute value of stroke volume is important to cardiologists, what may be an even more important benefit to patients clinically is the detection of sudden drops in stroke volume. Such an experimental condition was not studied in this thesis; however, in future studies, through the implementation of lower body negative pressure (LBNP), we will be able to change stroke volume in a short amount of time, and assess the capability of SCG to detect such a sudden drop.

7.2.2 Signal processing

SCG is very sensitive to motion artefacts and signal processing techniques; the removal of these artefacts can improve the accuracy of hemodynamic estimations. Adaptive linear and nonlinear filtering methods can be used to extract the respiration signal from signals recorded on the chest,. This extracted respiration signal can be used for the separation of inspiration and expiration cycles and to implement the averaging scheme which is based on such separation as proposed in chapter 4.

7.2.3 Multichannel SCG

As reviewed in chapter two of this thesis, different points on the torso produce different signal morphologies. The studies presented in this thesis were limited to recordings from the lower part of the sternum. It is clear that recordings from the other sites on the chest can give a more comprehensive view of the heart than a single locus recording. Development of small, affordable MEMS accelerometers can assist recording from multiple sites on the torso, and

combine the acquired information from all recording sites to produce a better assessment of the mechanical performance of the heart.

7.2.4 Physiological age versus chronological age

It is known that the hearts of certain persons are found to be much older physiologically than chronologically. Everybody knows what strength and weakness are. A strong man can lift weights that would be impossible for a weak man, or a strong man can support a burden for a long time and a weak man for a lesser time. The same reasoning is true when observing the mechanical vibration of the body created by heartbeats.

In a twenty-year longitudinal study, Starr monitored 211 healthy subjects and showed that there was a strong correlation between the age of the subjects and the amplitudes of their BCG, demonstrating the weakening of the heart over time (Starr and Wood 1961). While BCG amplitudes were reduced over time, those subjects who developed cardiac problems later had greater declines compared to those who were still healthy at the end of the study. After removing, the effect of age, the BCG of those who developed cardiac abnormalities was found to be 25% less, on average, compared to those who did not. This clarifies another capability of BCG to assess the physiological age of the heart versus its chronological age.

A longitudinal analysis of SCG might be able to provide similar information on one's physiological age, and would provide a less expensive technology with a simpler acquisition methodology compared to bulky BCG beds. This may serve as a tool to quantify the change of mechanical performance of the heart, after a change in life style or diet, using SCG measurements as a representation of

cardiac force. Such an approach requires a longitudinal dataset of SCG recorded from individuals of different ages and cardiovascular conditions.

7.2.5 Heart rate variability analysis

It is proposed that the same heart rate variability techniques applied to RR interval series to be applied to the corresponding AO to AO, or the estimated beat to beat stroke volumes, series derived from SCG. Such series can provide us with information on the inotropic effects of the myocardium versus chronotropic effect provided by the HRV which is based on ECG. The same time and frequency analysis tools applied to ECG can be used for SCG and the results can be compared.

REFERENCE LIST

Afonso, V X, W J Tompkins, T Q Nguyen, and S Luo. "ECG beat detection using filter banks." *IEEE Transactions on Biomedical Engineering*, 1999: 192-202.

Akhbardeh, A, et al. "Comparative analysis of three different modalities for characterization of the seismocardiogram." *31at IEEEE Engineering in Medinne and Biology Society conference.* Minneapolis : IEEE-EMBS, 2009. 2899-2903.

Akhbardeh, Alireza, Bozena Kaminska, and Kouhyar Tavakolian. "BSeg++: A modified Blind Segmentation Method for Ballistocardiograph Cycle Extraction." *29th IEEE Engineering in Medicine and Biology conference.* Lyon: IEEE-EMBS, 2007.

Alamestsa, J, J Viik, J Alakare, A Varri, and A Palomaki. "Ballistocardiography in sitting and horizontal positions." *Physiological Measurment* 29 (2008): 1071.

Alexander, K P, et al. "Acute coronary care in the elderly, part I: Non-ST-segment-elevation acute coronary syndromes: a scientific statement for healthcare professionals from the American Heart Association Council on Clinical Cardiology: in collaboration with the Society of Ger." *Circulation* 115 (2007): 2549-2569.

Alihanka, J, K Vaahtoranta, and I Saarikivi. "A new method for long-term monitoring of the ballistocardiogram, heart rate, and respiration." *Am J Physiol Regulatory Integrative Comp Physiol*, 1981: 384-392.

Aubert, A E, et al. "Laser method for recording displacement of the heart and chest wall." *Journal of Biomedical Engineering* 6 (1984): 134-144.

Baevski, R M, and A D Egerov. "The Method of Seismocardiography." *Kardiologiia* 18 (1964): 87-89.

Bancroft, W H, and E E Eddleman. "Methods and physical characteristics of the kinetocardiographic and apexcardiographic systems for recording low-frequency precordial motion." *American Heart Journal*, 1967: 756-764.

Basta, Lotfy L, Paul Wolfson, Dwain L Eckberg, and Francois M Abboud. "The value of left parasternal impulse recordings in the Assessment of Mitral Regurgitation." *Circulation* 48 (1973): 1055-1065.

Benchimol, A, and E G Dimond. "The apexcardiogram in ischemic heart disease." 24 (1962): 581.

Bershad, N J, and A J Rockmore. "On estimating signal to noise ratio using the sample correlation coefficient." *IEEE Transactions on Information Theory*, 1974: 112-113.

Biopac Systems Inc. www.biopac.com (accessed Nov 2010).

Biopac. *www.biopac.com.* 2006.

Bland, J M, and D G Altman. "Statistical methods for assessing agreement between two methods of clinical measurement." *Lancet*, 1986: 307-310.

Bozhenko, B S. "Seismocardiography- A New Method of the Functional Study of the Heart." *Terapevticheskii arkhiv* 33 (1961): 55-64.

Braunwald, Eugene, and Joseph K Perloff. "Physical Examination of the Heart and Circulation." In *Heart Disease*, by Eugene Braunwald, Douglas P Zipes and Peter Libby, 45-81. Philadelphia: Saunders, 2001.

Brown, H R, and V Delalla. *Clinical Ballistocardiography.* New York: Macmillan Company, 1952.

Brown, H R, V deLalla, and M A Epstien. *Clinical Ballistocardiography.* New York: Macmillan, 1952.

Bruch, C, et al. "Tei-Index in patients with mild-to-moderate congestive heart failure." *European Heart Journal* 21 (2000): 1888-1895.

Brüel & Kjær. 2006. www.bksv.com (accessed Nov 2010).

Canada, Heart and Stroke Foundation of. *Statistics.* 2005. http://www.heartandstroke.com/site/c.ikIQLcMWJtE/b.3483991/k.34A8/Statistics.htm#deaths (accessed June 23, 2010).

Castiglioni, P, A Faini, G Parati, and M Di Rienzo. "Wearable Seismocardiography." *IEEE EMBS.* Lyon, France, 2007. 3954-39667.

Centre of Integrative Bio-Engineering Research. www.ciber.ca (accessed Nov 2010).

Chen, K., D. Misra, H. Wang, and H. & Postow, E. Chuang. "An X-Band Microwave Life-Detection System. Biomedical Engineering." *IEEE Transactions on Biomedical Engineering*, 1986: 697-701.

Chuo, Y, and B Kaminska. "Sensor layer of a multiparameter single-point integrated system." *IEEE Transactions on Biomedical Circuits and Systems*, 2009: 229-240.

Chuo, Y, K Tavakolian, and B Kaminska. "Evaluation of a Novel Integrated Sensor System for Synchronous Measurement of Cardiac Vibrations and Cardiac Potentials." *Journal Medical Systems*, 2009.

CiBER. *www.ciber.ca.* 2010.

Crow, R S, P Hannan, D Jacobs, L Hadquist, and D M Salerno. "Relationship between Seismocardiogram and Echocardiogram for Events in Cardiac Cycle.,." *American Journal of Noninvasive Cardiology* 8 (1994): 39-46.

Dock, W, H Mandelbaum, and R Mandelbaum. *Ballistocardiography, the Application of the Direct Ballistocardiograph to Clinical Medicine.* USA: C.V. Mosby publishing company, 1953.

Dressler, W. "Pulsations of the chest wall." *Archives of INternal Medicine* 60 (1937): 225-239.

Droitcour, Amy Diane. *Non-Contact Measurment of Heart and Respiration Rates with a Single-Chip Microwave Doppler Radar.* PhD Dissertation, Stanford, California: Stanford University, 2006.

Dutta, P.K., and A.K.& Bibyk, S.B. Arora. "Towards radar-enabled sensor networks." *5th Int. Conf. on Information Processing in Sensor Networks (IPSN).* Nashville, Tennessee, USA, 2006.

Eddleman, E E. "Kinetocardiography." In *Noninvasive Cardiology*, by Arnold M Weissler, 227-273. New York: Grune & Stratton, 1974.

Edvardsen, T, B Gerber, J R Garot, D Bluemke, O Lima, and O Smiseth. "Quantitative assessment of intrinsic regional myocardial deformation by Doppler strain rate echocardiography in humans: validation against three-dimensional tagged magnetic resonance imaging." *Circulation* 106 (2002): 50-56.

Egorouchkina, K, M Braecklein, L Pang, I Tchoudovski, W Kellermann, and A Bolz. "Comparison of two different methods for coherent averaging in online ECG analysis." *Computers in Cardiology.* Lyon, 2005.

EMFiT Ltd. 2010. www.emfit.com (accessed Nov 2010).

FMS. 2007. www.finapress.com (accessed Nov 2010).

Fraser Health. 2006. www.fraserhealth.com (accessed Nov 2010).

Garrard, Clifford L, Arnold M Weissler, and Harold T Dodge. "The relationship of alterations in systolic time intervals to ejection fraction in patients with cardiac disease." *Circulation* 42 (1970): 455-462.

Gaziano, J Michael. "General Considerations of Cardiovascular Disease." In *Heart Disease*, by Eugene Braunwald, Douglas P Zipes and Peter Libby, 1-26. Philadelphia: Saunders, 2001.

Geisheimer, J L, and E F Greneker. "Applications of neural networks to the radarcardiogram (RCG)." *SPIE: Applications and Science of Computational Intelligence.* Florida, USA, 1999. 368-378.

Gillam, P M.S., A A Deliyannis, and J P.D. Mounsey. "The left parasternal impulse." *British Heart Journal* 26, no. 6 (1964): 726-736.

Giorgis L, Hernández A, Amblard A, Senhadji L, Cazeau S, Donal E, Jauvert G. "Analysis of Cardiac Micro-Acceleration Signals for the Estimation of Systolic and Diastolic Time Intervals in Cardiac Resynchronization Therapy." *Computers in Cardiology.* Bologna, Italy, 2008. 393-396.

Gordon, J W. "on Certain molar movements of the human body produced by the circulation of the blood." *Journal of Anatomical Physiology* 11 (1877): 533.

Greneker, E F. "Radar Sensing of Heartbeat and Respiration at a Distance with Applications of the Technology." *IEEE Conference on Radars.* UK, 1997. 150-154.

Gupta, L. Phegley, J. Molfese, D.L. "Parametric classification of multichannel averaged event-related potentials." *IEEE Transactions on Biomedical Engineering* 49 (2002): 905-911.

Gurev, V, J Constantino, J J Rice, and N A Trayanova. "Distribution of Electromechanical Delay in the Heart: Insights from a Three-Dimensional Electromechanical Model." *Biophysical Journal*, 2010: 745-754.

Gurev, V, T Lee, J Constantino, and N Trayanova. "Models of cardiac electromechanics based on individual hearts imaging data." *Biomechanics and Modeling in Mechanobiology* (Springer), 2010.

Guyton, Arthur C, and John E Hall. *Textbook of Medical Physiology.* 11. Philadelphia: Elsevier, 2006.

Harvey, William. *Exercitatio anatomica de motu cordis et sanguinis in animalibus.* London, 1628.

Henderson, Y. "The mass movements of the circulation as shown by a recoil curve." *American Journal of Physiology* 14 (1905): 287.

Inan, O T, M Etemadi, A Paloma, L Giovangrandi, and G T Kovacs. "A low-noise ac-bridge amplifier for ballistocardiogram measurement on an electronic weighing scale." *Physiological Measurment* 31 (2010): 51-59.

Inan, O T, M Etemadi, A Paloma, L Giovangrandi, and G T Kovacs. "Non-invasive cardiac output trending during exercise recovery on a bathroom-scale-based ballistocardiograph." *Physiological Measurment* 30 (2009): 261-274.

Inan, O T, M Etemadi, R M Wiard, L Giovangrandi, and G T Kovacs. "Robust ballistocardiogram acquisition for home monitoring." *Physiological Measurment* 30 (2009): 169-185.

Innes, J A, C J Mills, M I Noble, K Murphy, S Pugh, and A C Shore. "Validation of beat by beat pulsed Doppler measurment of ascending aortic blood velocity in man." *Cardiovascular Research* 21 (1987): 72-80.

INRIA, Asclepios Research Project. 2009. https://gforge.inria.fr/frs/?group_id=726 (accessed 2009).

Institute of Computational Medicine at JHU. http://www.icm.jhu.edu/ (accessed Nov 2010).

Jauchem, J.R., R.L. Seaman, H.M. Lehnert, S.P. Mathur, K.L. Ryan, and M.R. & Hurt, W.D. Frei. "Ultra-wideband electromagnetic pulses: lack of effects on heart-rate and blood pressure during two-minute exposures of rats." *Bio-electromagnetics*, 1998: 330-333.

Jensen, B H, B H Larsen, and K Shankar. "Monitoring of the Ballistocardiograph with the Static Charge Sensetive Bed." *IEEE transaction on Biomedical Engineering* 38 (1991).

JMP. 2010. www.jmp.com (accessed Nov 2010).

Junnila, S, A Akhbardeh, and A Varri. "An Electromechanical Film Sensor Based Wireless Ballistocardiographic Chair: Implementation and Performance." *Journal of Signal Processing Systems*, 2008: 305-320.

Junnila, Sakari, Alireza Akhbardeh, and Alpo Varri. "An Electromechanical Film Sensor Based Wireless Ballistocardiographic Chair: Implementation and Performance." *Journal of Signal Processing Systems* 57 (2009): 305-320.

Katz, Arnold M. *Physiology of the Heart.* New York: Raven Press, 1992.

Kim, J S, Y J Chee, J W Park, J W Choi, and K S Park. "A new approach for non-intrusive monitoring of blood pressure on a toilet seat." *Physiological Measurment* 27 (2006): 203-211.

Komarov, B D. "Dynaocardiographic Examination of Healthy Children Aged 8 to 15 years." *Bulletin of Experimental Biology and Medicine*, 1957: 903-908.

Lewis, R P, R F Leighton, W F Forester, and A M Weissler. "Systolic Time Intervals." In *Noninvasice Cardiology*, by Arnold M Weissler, 301-368. New York: Grune @ Stratton, 1974.

Li J. & Stoica, P. "Efficient mixed-spectrum estimation with applications to target feature extraction." *Signal Processing, IEEE Trans.* 44 (1996): 281-295.

Li, C, J Cummings, J Lam, E Graves, and W Wu. "Radar Remote Monitoring of Vital Signs. Microwave Magazine." *Microwave Magazine, IEEE* 10 (2009): 47-56.

Lim, Y G, Ki H Hong, Ko K Kim, Jae H Shin, and Kwang S Park. "Mechanocardiogram Measured at the Back of Subjects Sitting in a Chair as a Non-intrusive Pre-ejection Period Measurement." *1st International Conference om Pervasive Computing Technologies for Healthcare.* Innsbruck, Austria, 2006.

Lin, J C. "Non-invasive Microwave Measurement of Respiration." *Proceedings of IEEE* 63 (1975): 1530.

Lin, J C, J Kiernicki, M Kiernicki, and P B Wollschlaeger. "Microwave Apexcardiography." *IEEE Transaction on Microwave Theory and Techniques* 27 (1979): 618-621.

Lincoln, W C. Classifying tachyarrhythmia using time interval between ventricular depolarization and mitral valve closure. US Patent 7177685. Feb 13, 2007.

Lindqvist, A, K Pihlajamaki, J Jalonen, V Laaksonen, and J Alihanka. "Static-charge-sensetive bed ballistocardiography in cardiovascular monitoring." *Clinical Physiology*, 1996: 23-30.

Lohman, B, O Boric-Lubecke, V M Lubecke, P W Ong, and M M Sondhi. "A Digital Signal Processor for Doppler Radar Sensing of Vital Signs." *IEEE Engineering in Medicine and Biology.* 2002.

Lubecke, V, O Boric-Lubecke, and E Beck. "A compact low-cost add-on module for Doppler radar sensing of vital signs using a wireless communications terminal." *Microwave Symposium Digest.* IEEE MTT-S Int., 2002. 1767-1770.

Marcus, F I, et al. "Accelerometer-derived time intervals during various pacing modes in patients with biventricular pacemakers: comparison with normals." *Pace*, 2007: 1476-1481.

Martin, C Edwin, James A Shaver, Mark E Thompson, P Sudhakar Reddy, and James J Leonard. "Direct orrelation of external systolic time intervals with indices of left ventricular functin in man." *Circulation* 44 (1971): 419-431.

Mathworks. 2006. www.mathworks.com (accessed Nov 2010).

Mazlouman, S J, K Tavakolian, A Mahanfar, and B Kaminska. "Contact-less Assessment of Body Signals Using Microwave Doppler Radar." In *Biomedical Engineering*, 240-260. n-Tech, 2010.

McEwan, T E. Ultra-wideband radar motion sensor. US Patent 5361070. 1994.

Mckay, W P.S, Peter H Gregson, B W.S Mckay, and J Militzer. "Sternal acceleration ballistocardiography and arterial pressure wave analysis to determine stroke volume." *Clinical and investigative medicine* 22 (1999): 4-14.

Mckay, William P.S., Pter H Gregson, Benjamin W.S. Mckay, and Julio Militzer. "Sternal Acceleration Ballistocardiography and Arterial Pressure Wave Analysis to Determine Stroke Volume." *Clinical and Investigative Medicine* 22 (1999): 4-14.

Meyerhoff, N.J. "Intrusion Detection by Ultra-Wide Bandwidth Radar." *Technologies for Homeland Security, IEEE Conf.* 2007. 81-84.

Michahelles, F., and R. & Schiele, B. Wicki. "Less contact: Heart-rate Detection Without Even Touching the User." *Proceedings of Wearable Computers, 8th Int. Symp.* 2004. 4-7.

Morbiducci, U, L Scalise, M DE Melis, and M Grigioni. "Optical Vibrocardiography: A novel tool for the optical monitoring of cardiac activity." *Annals of Biomedical Engineering* 35 (2006): 45-58.

Morgan, D R, and M G Zierdt. "Novel Signal Processing Techniques for Doppler Radar Cardiopulmonary Sensing." *Signal Processing* 89 (2009): 45-66.

Mounsey, Patrick. "Praecordial Ballistocardiography." *British Heart Journal* 19 (1957): 259-271.

Ngai, B, K Tavakolian, A Akhbardeh, A P Blaber, B Kaminska, and A Noordergraaf. ""Comparative Analysis of Seismocardiogram Waves with the Ultra-Low Frequency Ballistocardiogram." *31th IEEE Engineering in Medicine and Biology conference.* Minneapolis: IEEE-EMBS, 2009. 2851-2854.

Noordergraaf, Abraham. *Circulatory system dynamics.* New York: Academic Press, 1978.

Norsworthy, S. R., and R., & Temes G. C. Schreier. *Delta-Sigma Data Conversions.* Wiley-IEEE Press.

Opie, H Lionel. *Normal and Abnormal Cardiac Function.* Vol. 1, in *Heart Disease*, by Eugene Braunwald, Douglas P Zipes and Peter Libby, 443-478. Philadelphia: Saunders, 2001.

Otis, A B, H Rahn, and M Mullins. "Ballistocardiographic Study of Changes in Cardiac Output Due to Respiration." *Journal of Clinical Investigation*, 1947.

Owan, Theophilus E, David O Hodge, Regina M Herges, Steven J Jacobsen, Veronique L Roger, and Margaret m Redfield. "Trends in Prevalence and Outcome of Heart Failure with Preserved Ejection Fraction." *The New England Journal of Medicine* 355, no. 3 (2006): 251-260.

Phibbs, B, C R Lowe, and R W Holmes. "The Ultra Low Frequency Force Ballistocardiograph in Acute Cardiomyopathy." *Circulation*, 1963: 92-100.

Pretorius, P J. *Experimental Investigation On Ultra-Low Frequency Acceleration Ballistocardiography.* PhD Thesis, Amsterdam, 1962.

Ronaszeki, A, A E Aubert, and H DE Geest. "Laser Apexcardiogram in healthy young men: A comparative study with conventional method." *Acta Cardiologica*, 1990: 203-210.

Rushmer, Robert F. *Cardiovascular Dynamics.* Philadelphia: Saunders, 1965.

Salerno, D M, and J M Zanetti. "Seismocardiograhy: A new technique for recording cardiac vibrations. Concepts, method, and initial observations." *Journal of Cardiovascular Technology* 92, no. 2 (1990): 111-118.

Salerno, D M, and J Zanetti. "Seismocardiography for monitoring changes in left ventricular function during ischemia." *Chest* 100, no. 4 (1991): 991-993.

Salerno, D M, J Zanetti, and R Crow. "Seismocardiography for detection of coronary artery disease." *American Journal of Noninvasive Cardiology* 6 (1992): 321-330.

Scarborough, William R, et al. "Proposals for Ballistocardiographic Nomenclature and Conventions: Revised and Extended: Report of Committee on Ballistocardiographic Terminology." *Circulation* 14 (1956): 435-450.

Schweizer, W, R V Bertrab, and PH Reist. "Kinetocardiography in Coronary Artery Disease." *British Heart Journal* 7 (1965): 263-269.

Shell, Jared B, Randall D Peters, and Michael J Russell. "Three-axis seismocardiography using a low-cost geophone accelerometer." *FASEB Journal* 21 (2007): 908-936.

Sherwood, A, M T Allen, J Fahrenberg, R M Kelsey, W R Lovallo, and Lorenz J.P Van Doornen. "Methodological Guidelines for Impedance Cardiography." *Psychophysiology*, 1990: 1-23.

Shin, J H, K M Lee, and K S Park. "Non-constrained monitoring of systolic blood pressure on a weighing scale." *Physiological Measurment* 30 (2009): 679-693.

Simon Fraser University. www.sfu.ca (accessed Nov 2010).

Skolnik, M I. *Radar Handbook.* New York: McGraw Hill, 2007.

Smith, N Ty. "Ballistocardiography." In *Noninvasive Cardiology*, by Arnold M Weissler, 39-139. New York: Grune & Stratton, 1974.

Staderini, E.M. "An UWB radar based stealthy ‘lie detector’." *Second Virtual Congress of HRV Scientific Material.* 2002.

Staderini, E.M. "UWB radars in medicine. Aerospace and Electronic Systems." *IEEE Aerospace and Electronic Systems Magazine*, 2002: 13-18.

Stapleton, J F, and B M Groves. "Precordial palpation." *American Heart Journal*, 1971: 409-428.

Starr, I, and A J Rawson. "The Vertical Ballistocardiograph; Experiments on the Changes in the Circulation on Arising; With a Further Study of Ballistic Theory." *American Journal of Physiology* 134 (1941): 403-425.

Starr, I, and A Schroeder. "Ballistocardiograph. ii. Normal Standards, Abnormalities Commonly Found in Diseases of the Heart and Circulation, and Their Significance." *Journal of Clinical Investigation* 19 (1940): 437.

Starr, I, and C Friedland. "On the Cause of the Respiratory Variation on the Ballistocardiograph, with a Note on Sinus Arrhythmia." 1945.

Starr, I, and E C Wood. "Twenty Years Studies with the Ballistocardiograph, the Relation Between the Amplitude of the First Record of 'Health' Adults and Eventual Mortality and Morbidity form Heart Disease." *Circulation* 23 (1961): 714-732.

Starr, Isaac, and Abraham Noordergraaf. *Ballistocardiography in Cardiovascular Research.* Philadelphia and Montreal: Lippincott, 1967.

Stork, M, and Z Trefny. "Quantitative Seismocardiography System With Separate QRS Detection." *Biosignal.* 2010. 61-68.

Such, O. "On-body sensors for personal healthcare." In *Advances in Health Care Technology: Shaping the Future of Medical Care*, by B. Spekowius and T. Wendler, 436-488. Springer, 2006.

Tavakolian, K, B Ngai, A Akhbardeh, A P Blaber, and B Kaminska. "Comparative Analysis of Infrasonic Cardiac Signals." *Computers in Cardiology.* 2009. 757-760.

Tavakolian, K., F.M. Zadeh, Y. Chuo, and A. & Kaminska, B. Vaseghi. "Development of a Novel Contactless Mechanocardiograph Device." *International Journal of Telemedicine Applications*, 2008.

Tavakolian, Kouhyar, Ali Vaseghi, and Bozena Kaminska. "Improvement of ballistocardiogram processing by inclusion of respiration information." *Journal of Physiological Measurement* (Institute of Physics) 29 (2008): 771-781.

Tavel, M E, R W Campbell, H Feigenbaum, and E F Steinmetz. "The apex cardiogram and its relationship to haemodynamic events within the left heart." *British Heart Journal* 27 (1965): 829-839.

Tavel, Morton E. *Clinical Phonocardiography and External Pulse Recording.* Chicago: Year Book Medical Publishers, Inc, 1967.

Thansandote, A., S.S. Stuchly, and Smith A.M. "Monitoring variations of biological impedances using microwave Doppler radar." *Physics in Medicine & Biology*, 1983.

Thijs, J A, J Muehlsteff, O Such, R Pinter, R Elfring, and C H Igney. "A Comparison of Continuous Wave Doppler Radar to Impedance Cardiography for Analysis of Mechanical Heart Activity." *IEEEEMBS 27th Annual International Conference.* 2005.

Vermarien, H, and E Van Vollenhoven. "The recording of heart vibrations: A problem of vibration measurment on soft tissue." *Medical and Biological Engineering and Computing* (Springer) 22 (1984): 168-178.

Webster, John G, ed. *Medical Device and Instrumentation.* Vol. 3. Hoboken, New Jersey: John Wiley & Sons, 2006.

Weissler, Arnold M, Willard S Harris, and Clyde D Schoenfeld. "Systolic Time INtervals in Heart Failure." *Circulation* 37 (1968): 149-159.

Yu, X, D J Gong, C Osborn, and D Dent. "A wavelet multireolution and neural network system for BCG signal analysis." *IEEE TECON-Digital Signal Process* 491-5.

APPENDICES

.

APPENDIX 1:
ULTRA-LOW FREQUENCY BCG EQUATIONS

Limiting ourselves to the head foot direction, as the a direction that most of the research on BCG's have been performed so far we have the differential equation 1 that relates the movement of the centre of mass of the body to the movement in the y-axis of a coordinate system fixed to the environment and can be measured using different recording systems. Equation 1 is the main equation that describes all different types of BCGs and in this equation m_s is the participant's mass m_b is the BCG's mass β is the coefficient of friction determined by the external damping and *D* is the coupling constant.

$$\left(F_{\text{int}}\right)_y - \beta\dot{y} - Dy = (m_s + m_b)\ddot{y} \xrightarrow{(F_{\text{int}})_y = m_s\ddot{y}_c} (m_s + m_b)\ddot{y} + \beta\dot{y} + Dy = m_s\ddot{y}_c \quad (1)$$

In case of a ULF-BCG the two terms in the left side of the equation are negligible thus, neglected and the equations are simplified to:

$$\left(m_s + m_b\right)\ddot{y} = m_s\ddot{y}_c \quad (2)$$

Or:
$$\ddot{y} = \frac{m_s}{\left(m_s + m_b\right)}\ddot{y}_c \quad (3)$$

So: $$\dot{y} = \frac{m_s}{(m_s + m_b)} \dot{y}_c + k_1 \tag{4}$$

and $$y = \frac{m_s}{(m_s + m_b)} y_c + k_1 t + k_2 \tag{5}$$

k1 and k2 can be close to zero in stationary cases and by having this in mind, it is noticed that that an external measurable body displacement, velocity and acceleration is proportional to the same quantities of the internal movement of centre of gravity of the body caused by internal forces. A good approximation of such a case exists in case of ULF-BCG where they are so weakly coupled to the environment that they are practically free to move. From equation 1 the same types of deduction as above can be done for HF-BCG where at the end the recorded external displacement is proportional to the acceleration of the internal movement of the centre of mass.

APPENDIX 2: MULTISENSOR ARCHITECTURE

The integrated sensor system consisted of multiple sensors (MEMS accelerometer and printed bioelectrodes), signal conditioning, processing, and radio communication. The system is was powered by rechargeable mini-batteries (i.e. hearing aid type or flexible film type). Depending on the mode of operation, the system was expected to consume anywhere from 1 mW (1 m range) to 10 mW (10 m range) during wireless data transmission. The wireless protocol and application mode would further dictate the period of autonomous operation ranging from several days to several hours. To maintain small device dimensions, the system was configured into multiple stackable thin layers. The system was further proposed to be encapsulated in flexible biomedical grade silicone such that it would be structurally reliable, mechanically flexible, and biocompatible.

A model of the multisensor layer containing a MEMS accelerometer and a printed bioelectrode was implemented. This model consisted of the sensors, analogue signal conditioning module, and test connector for characterizing the sensors placed on the layer.

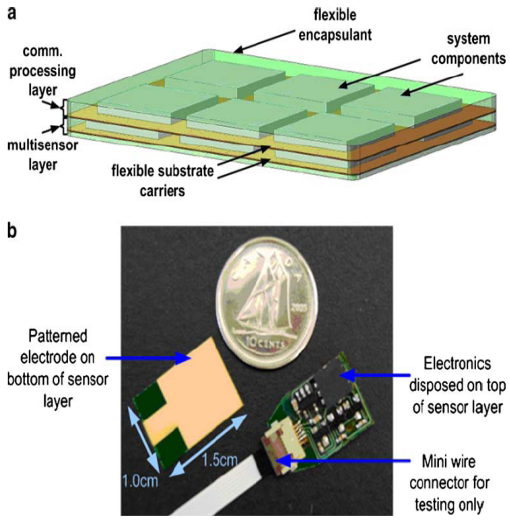

Figure 44. a) 3D-transparent view rotated to show layers from top side b) the multisensory layer of the multilayer integrated sensors systems measuring (Chuo, Tavakolian and Kaminska 2009). Reproduced with written permission from Springer.

Figure 44 shows the front and backside of the assembled sensor layer compared to a Canadian 10¢-coin. The device dimensions were approximately 1.1 by 1.5 cm, and weighed approximately 0.5-g. The MEMS accelerometer and signal conditioning module were populated on the front side of the circuit board, while the biopotential electrode was patterned on the reverse side.

APPENDIX 3: THE MICROWAVE DOPPLER RADAR-BASED SYSTEM BLOCK DIAGRAM

Radio detection and ranging (Radar) systems are used to identify the range, direction, or speed of both moving and fixed objects such as aircrafts, vehicles and terrain. These systems are usually comprised of an RF/microwave transceiver to transmit the electromagnetic signal to the object under testing and receive the reflected wave carrying the required data. Depending on the application, this data is further processed using basic or advanced signal processing techniques. Microwave Doppler radar-based systems are

A class of radars utilize the Doppler effect to measure the velocity of moving objects. This kind of approach has long been used to estimate the velocity of moving vehicles for speed control and other purposes. The Doppler principle has been used in different modalities including microwaves, laser and ultrasound. Doppler radars are commercially used in air defence, air traffic control, and sounding satellites,.

Microwave electromagnetic waves can propagate through the body, and are reflected at the interface between different tissue layers. By the Doppler effect for microwave radar, if a radio frequency wave is transmitted to a moving surface, the reflected wave undergoes a frequency shift proportional to the surface velocity. If the surface has periodic motion, like that of the heart and chest, this can also be seen as a phase shift proportional to the surface

displacement. If this displacement is small compared to the wavelength, a low-frequency component can be extracted from downconversion and filtering (removing the high-frequency component) the reflected wave that is directly proportional to the object displacement.

The Doppler Effect can be written as (Skolnik 2007):

$$\omega_r = \omega_0(1+\frac{v}{c}Cos\alpha) \tag{1}$$

where ω_r corresponds to the reflected wave frequency, ω_0 corresponds to the transmitted wave frequency, v corresponds to the relative speed, c corresponds to the prorogation speed of the wave (in this case, the Electromagnetic wave speed which is 3×10^8 *m/s*). and finally, α corresponds to the angle of the reflected wave versus the moving object. If the transmitter and the moving object are approaching each other, then the reflected wave frequency is higher than the transmitted wave frequency ($\omega_r > \omega_0$); if they are departing from each other, then the reflected wave is lower than the transmitted wave frequency ($\omega_r < \omega_0$). Assuming the transmitted wave and the object under investigation are moving in the same direct ($\alpha=0$), the Doppler Effect for a return wave can be re-written as:

$$\omega_r = \omega_0 + \omega_D = \omega_0(1+\frac{2v}{c}) \tag{2}$$

Therefore, the speed of the moving object can be calculated. The operation of the microwave radar based systems will be further analysed in Section 3.3.

As shown in Figure 21, on the transmit side, the RF stage includes a pulse generator (Gaussian pulse, in case of UWB system), a mixer (LO) to modulate the pulse, a power amplifier (PA) to radiate the modulated pulse, and finally a transmitting antenna. The transmitted signal can be a continuous wave monochrome (single frequency) non-modulated sinusoidal radar signal. In this case the system is simplified to the non-dashed blocks and only the signal generated at the LO is transmitted (no pulse generator or mixer stage required).

On the receive side, the reflected beams are captured by the receiving antenna, followed by a low-noise amplifier (LNA), a downconversion mixer, and a low-pass filter. The downconversion mixer multiplies the received signal by a replica (a delayed replica if time-gating is used) of the same signal as the one at the transmit side to demodulate it. The signal is then filtered to extract the low frequency component that includes the shift depending on the object motion data. Similar to the transmit side, if monochrome radar is used, no downconversion mixer stage is required.

The choice of a proper frequency is a compromise and depends on the test objectives, as a higher frequency enables a larger Doppler shift and therefore a higher resolution, but also results in a lower tissue penetration depth. In many reported works, the 2.45GHz frequency is chosen to exploit the commercially available components, e.g. (Lubecke et al., 2002). The frequency of the transmitted beam is adjusted by the mixer signal provided by the local oscillator (LO) block. The LO signal can be a voltage controlled oscillator (VCO) or simply a crystal oscillator. In the case of UWB radar systems, a short

Gaussian monopulse is generated with a pulse-width in the order of magnitude of a few nanoseconds. Several short pulse generators have been reported in the literature. For example, digital pulse generators have been suggested in (Wentzeloff & Chandrakasan, 2006), for on-chip or on-board implementation based on a short delay between two NAND gates.

The modulated signal is amplified by the PA and propagated by the transmitting antenna. In (Zito et al., 2008), a system-on-chip UWB sensor is implemented using a shaper block for the mixer and an integrator to sample and low-pass filter the received signal. In (Prak et al, 2007), quadrature mixers are used for the modulation/demodulation stages to increase accuracy and arctangent demodulation and dc-cancellation methods are used.

To reduce power, in particular where battery-operated wireless handheld devices are implemented, the same antenna and mixing stage can be time-gated between the transmitting and the receiving stage. For example, by assigning a 50% duty cycle to a generated square pulse, the system can transmit the illuminating monochrome signal for the first half of the pulse width and receive the reflected signal for the second half of the pulse width.

UWB short-pulse systems are usually implemented using this structure and pulses as short as a few nanoseconds are used. As shown in Figure 21, the pulse generator also activates a delay line block. This block controls proper sampling of the received signals from the object. The receiver only samples at short time intervals triggered by the delay line block. Proper timing of this triggering is essential to ensure sampling only when the received signals from a

certain distance are received, for example, only when echoes of the heart-wall are expected (Michahelles and Wicki 2004). Intuitively, this delay should be equal to the flight time of the pulse from the radar to the heart and then from the heart to the radar. Note that time gating and adjusting the sampling time increases the signal-to-noise-ratio at the receiver as less interference signals due to body movements and other moving objects are sampled. Therefore, the effect of the interferences is less pronounced.

Time-gating is specified by the pulse repetition frequency (PRF). The PRF is defined as the number of pulses transmitted per second. It should be noted that depending on the velocity of the object under test and the application, a minimum PRF should be met that depends on the radar range and the speed of the radar waves (in this case, *c*, for electromagnetic waves). To avoid ambiguity and increase the velocity measurement accuracy, sufficient observation time is required, which is possible by choosing proper PRF (Skolnik 2007).

For simplicity and without loss of generation, assume a monochrome continuous RF-modulated signal, *x(t)*, is chosen as the radar transmitting signal:

$$x(t)=A.Cos(\omega_0 t), \qquad 3)$$

The reflected signal captured at the receive side will include the transmitted signal provided by the signal generator, with a frequency shift, ω_d, that is proportional to the velocity of the blood flow. The received signal will therefore include a term:

$y(t)=A.\ Cos[(\omega_0+\omega_d)t],$

(4)

plus some noise terms, where,

$$\omega_d = \frac{2v\omega_0}{c} \tag{5}$$

where ω_0 is the mixer frequency, c is the speed of light, and v is the velocity of the moving object under test; for example blood-flow velocity in arteries and veins, or the heart wall.

The frequency displacement resulting from the motion of the object under test can also be modelled as a phase shift, $\Phi(t)$, that depends on the velocity: (Thijs, et al. 2005) (Thansandote, Stuchly and A.M. 1983) (Lohman, et al. 2002)

$$\Phi(t) = \frac{2\pi}{\lambda}\int_0^t v(\tau)d\tau = \frac{4\pi}{\lambda}s(t) \tag{6}$$

where λ is the wavelength and $s(t)$ is the movement amplitude. Therefore, the vital signals such as the movement of the Thorax can be sensed.

In the case of UWB radar, the transmitted signal would be the product of a narrow Gaussian pulse by the mixer signal:

$$x(t) = Cos(\omega_0 t).\sum_{n=0}^{\infty} \exp\left[-\frac{(t-\mu-nT_p)^2}{2\sigma^2} \right] \tag{7}$$

and the reflected, received signal will include the Doppler shifted component,

$$y(t) = Cos(\omega_0 + \omega_d)t.\sum_{n=0}^{\infty} \exp\left[-\frac{(t-\mu-nT_p)^2}{2\sigma^2} \right] \tag{8}$$

where ω_0 is angular frequency of UWB modulation signal, ω_d is the Doppler shift frequency, μ represents Gaussian envelope phase, σ represents the pulse width and T_p is the pulse repetition period (corresponding to the PRF). Here, the accompanying noise components not taken into account.

To extract the velocity of the object under test from the received signal, $y(t)$ is downconverted by $Cos(\omega_0 t)$, as (ignoring the mismatch errors)

$$y(t) = Cos((\omega_0 + \omega_d)t).Cos(\omega_0 t)\sum_{n=0}^{\infty} \exp\left[-\frac{(t-\mu-nT_p)^2}{2\sigma^2} \right] \tag{9}$$

That can be rewritten as:

$$y(t) = \left[Cos((2\omega_0 + \omega_d)t) + Cos(\omega_d t)\right] \cdot \sum_{n=0}^{\infty} \exp\left[-\frac{(t - \mu - nT_p)^2}{2\sigma^2} \right]$$

(10)

Therefore, the high frequency component can be filtered and the remaining baseband term that includes the shift data, i.e.,

$$y(t) = Cos(\omega_d t) . \sum_{n=0}^{\infty} \exp\left[-\frac{(t - \mu - nT_p)^2}{2\sigma^2} \right]$$

(11)

is transferred to the following baseband signal processing stage.

The baseband signal processing stage is the last stage in the Microwave Doppler radar-based system. In this stage, the frequency shift data and therefore the velocity/motion rate of the object under test is extracted from the signal received at the output of the lowpass filtering stage. Depending on the application, the received signal is processed through various digital signal processing (DSP) techniques. Usually, the received signal at the baseband stage is first amplified and converted into digital by an analog-to-digital converter stage (ADC) and then processed by further DSP techniques in the digital domain, where more flexible, simpler, and potentially lower cost implementations are possible. DSP techniques in the time-domain or frequency-domain such as fast Fourier transform (FFT), autocorrelation and noise cancellation methods, as well as several digital filtering stages can be used to increase coherency, attenuate

the noise terms (such as echo), cancel motion artefacts due to other movements in the body and surrounding objects, and extract the target data.

The DSP techniques can be implemented in hardware (board-level or integrated), or in software, using a PC (e.g. MatLab™ DSP toolbox), or both, depending on the application. The DSP blocks can be implemented in hardware, on an FPGA, or on a DSP module, depending on their complexity. Also, several DSP prototype development boards are available by Texas Instruments Inc., and Altera Co. that can accommodate various applications.

In order to select proper hardware for a specific application, requirements on the maximum measurement frequency and resolution should be decided. Body signal such as blood flow rate or heart rate are usually not high frequency and therefore the requirements are not tight. However, some applications may require better resolutions. The Nyquist-rate requirement for proper sampling by the ADC is specified as:

$$f_s \geq 2 f_{\max} \tag{12}$$

where f_{max} is the maximum measurement frequency and f_s is the sampling frequency of the ADC. Oversampling can help increase the signal-to-noise-ratio (SNR) and therefore the resolution of the digitized signal. Note that these two parameters are related as (Norsworthy and Schreier n.d.):

$$SNDR = 6.02n + 1.76dB$$

13)

where n is the effective number of bits (ENOB) of an ADC, known as the resolution of the ADC. As an example, in case of the heart signals measurements, a baseband signal of less than 30 Hz is expected at the output of the RF stage, therefore a sample rate of 80-100Hz for the ADC would be required.

APPENDIX 4: THE PROTOCOL FOR SCG AND ECHOCARDIOGRAM RECORDING

1. The participants will fill the forms and sign the consent form
2. The following recording will happen for few cycles and the echo cardiographer will cue the signal acquisition person in the start and stop of the recording thus we can find the corresponding cycles on Echo images and also the recorded BCG cycles later on for verification.
3. For Doppler cases aside from the short recording a 1 minute recording will happen too.

a) Mitral valve closure – parasternal long (or short) axis with m-mode (1-3)

b) Mitral valve opening – parasternal long (or short) axis with m-mode (15 second video)

c) Aortic valve opening – parasternal long (or short) axis with m-mode (4-6)

d) Aortic valve closure – parasternal long (or short) axis with m-mode (15 Second video)

e) LVOT diameter parasternal long axis (7)

\f) Peak of rapid systolic ejection - apical 5 chamber with aortic valve maximum velocity calculated using continuous wave Doppler (8-10) (RSE)

g) LVOT VTI apical pulse wave five chamber view (11) (LVOTVTI)

h) Peak of rapid diastolic filling – corresponds with the “e” wave which is found by determining the diastolic function of the left ventricle in the apical 4 chamber view (RDF/AS)

i) Peak of atrial systole – corresponds with the “a” wave which is found by determining the diastolic function of the left ventricle in the apical 4 chamber view (12-14) (RDF/AS)

j) Simpson’s LVEF assessment (End-diastolic and end-systolic volumes) (15-18) (Two videos)

Snapshots of different points assigned by the cardiologist and the simultaneous SCG signal can be seen in the following figures:

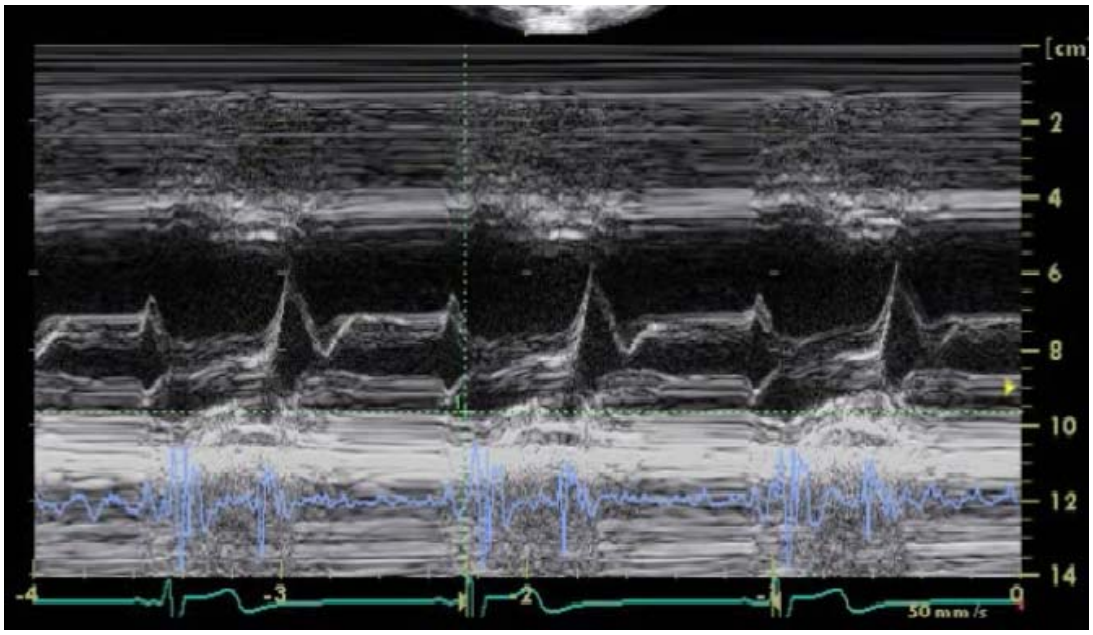

Figure 45. Simultaneous M-mode echocardiogram, SCG (blue) and ECG (green) and the moment of mitral valve closure (MC)

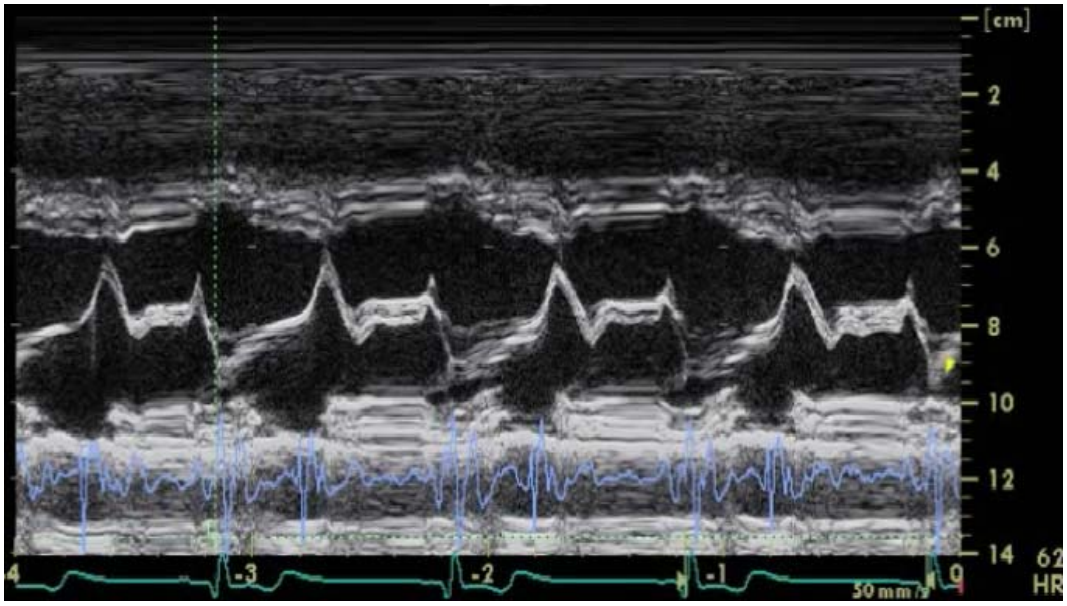

Figure 46 Simultaneous M-mode echocardiogram, SCG (blue) and ECG (green) and the moment of aortic valve opening (AO)

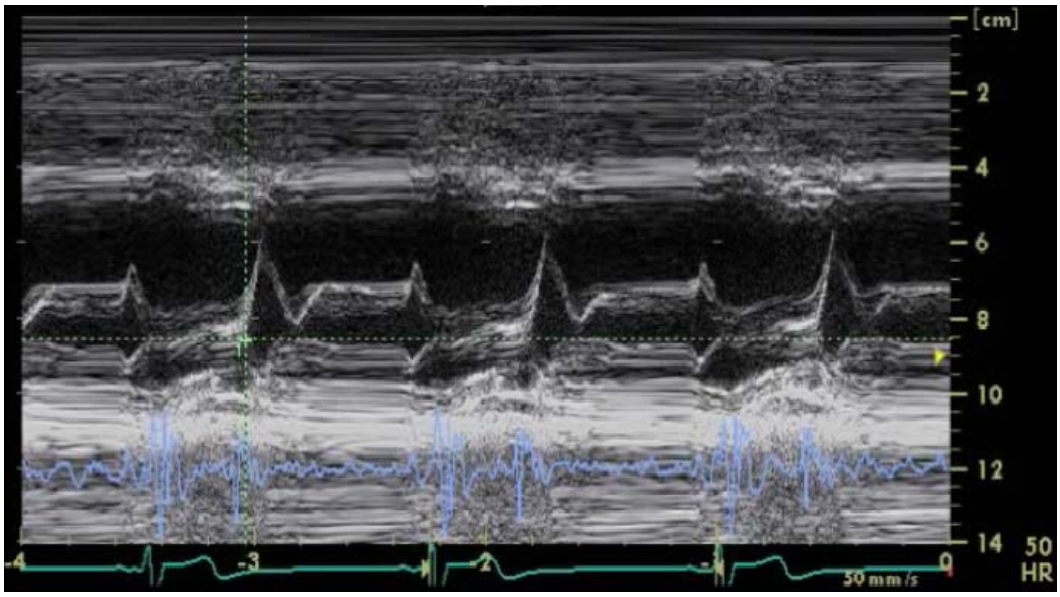

Figure 47. Simultaneous M-mode echocardiogram, SCG (blue) and ECG (green) and the moment of mitral valve opening (MO)

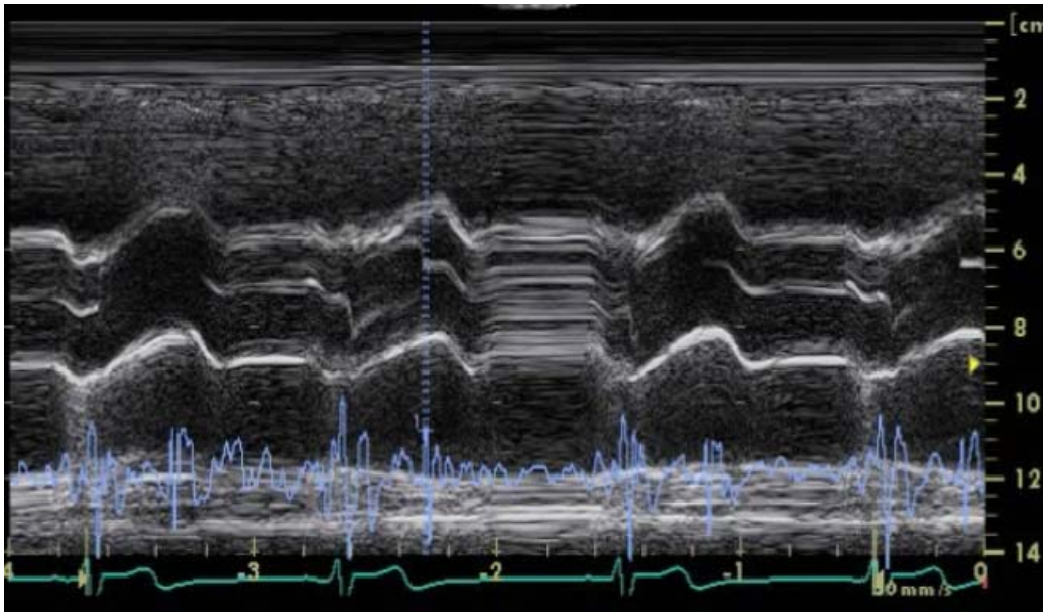

Figure 48. Simultaneous M-mode echocardiogram, SCG (blue) and ECG (green) and the moment of aortic valve closure (AC)

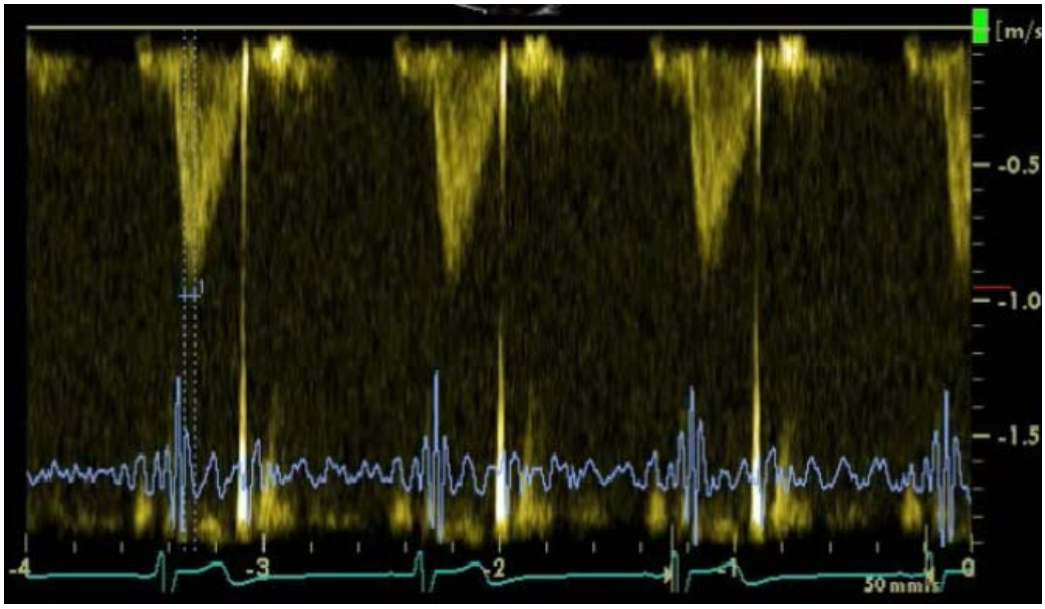

Figure 49. Simultaneous Doppler echocardiogram, SCG (blue) and ECG (green) and the moment of rapid systolic ejection.

Figure 50. Simultaneous Doppler echocardiogram, SCG (blue) and ECG (green) and the moment of atrial systole.

APPENDIX 5: FURTHER STATISTICAL RESULTS

Least Squares Means Table for LVET

Level	Least Sq Mean	Std Error
ICG	307.48805	4.4319946
SCG	308.41600	4.4042326
ULT	307.39096	4.4619747

LS Means Plot

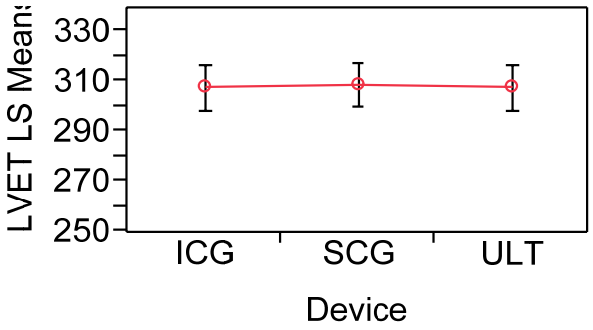

****

Least Squares Means Table for PEP

Level	Least Sq Mean	Std Error
ICG	96.272679	3.9640204
SCG	95.888000	3.9556396
ULT	98.667139	3.9731099

LS Means Plot

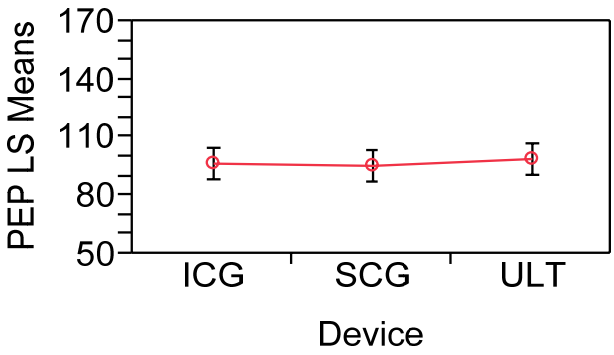

Least Squares Means Table for QS2

Level	Least Sq Mean	Std Error
ICG	403.79176	5.2941305
SCG	404.30400	5.2810141
ULT	404.79751	5.3238204

LS Means Plot

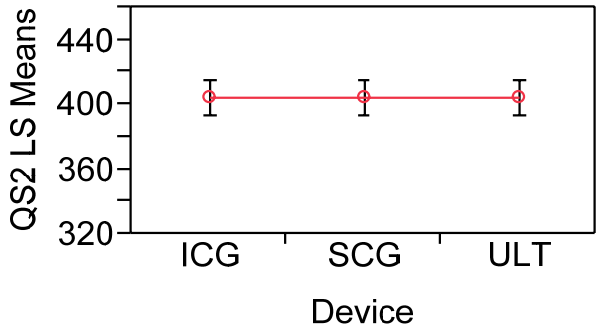

****

Least Squares Means Table for PEP/LVET

Level	Least Sq Mean	Std Error
ICG	0.31309779	0.01550083
SCG	0.31120000	0.01545417
ULT	0.32529356	0.01560636

LS Means Plot

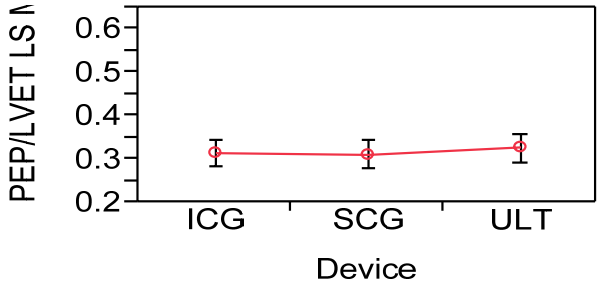

APPENDIX 6: PUBLICATIONS

Book Chapter:

[1] S. Jalali Mazlouman, K. Tavakolian, A. Mahanfar, and B. Kaminska, “Contact-less Assessment of Body Signals Using Microwave Doppler Radar,” Biomedical Engineering, In-Tech, pp. 240-260, March 2010.

Journal Papers:

[2] Viatcheslav Gurev, Kouhyar Tavakolian, Jason Constantino, Bozena Kaminska, Andrew P. Blaber, Natalia A. Trayanova "Seismocardiogram Records Pressure of the Heart Ventricles on the Ribs" submitted to Journal of Medical and Biological Engineering Sept 2010.

[3] Yindar Chuo, Marcin Marzencki, Benny Hung, Camille Jaggernauth, Kouhyar Tavakolian, Philip Lin, and Bozena Kaminska, "Mechanically Flexible Wireless Multisensor Platform for Human Physical Activity and Vitals Monitoring" IEEE Transactions on Biomedical Circuits and Systems, Oct 2010, pp 281-294.

[4] Marcin Marzencki, Kouhyar Tavakolian, Yindar Chuo, Benny Hung, Philip Lin, and Bozena Kaminska, "Miniature Wearable Wireless Real-time Health and Activity Monitoring System with Optimized Power Consumption" Journal of Medical and Biological Engineering, 30(4): 227-235, May 2010.

[5] Yindar Chuo, Kouhyar Tavakolian, and Bozena Kaminska "Evaluation of a novel integrated sensor system for synchronous measurement of cardiac vibrations and cardiac potentials" Journal of Medical Systems, Springer, Oct 2009.

[6] Kouhyar Tavakolian, Ali Vaseghi, Bozena Kaminska, "Improvement of ballistocardiogram processing by inclusion of respiration information" Journal of Physiological Measurement, Institute of Physics, 29 (2008) 771-781.

[7] Kouhyar Tavakolian, Faranak M.Zadeh, Yindar Chuo, Ali Vaseghi, Bozena Kaminska, “Development of a Novel Contactless Mechanocardiograph Device” International Journal of Telemedicine and Applications, vol. 2008, Article ID 436870, 5 pages, 2008. doi:10.1155/2008/436870.

[8] Siamak Rezaei, Kouhyar Tavakolian, A.M.Nasrabadi, S.K.Setarehdan, “Different classification techniques considering brain computer interface applications” Institute of Physics(IOP), Journal of Neural Engineering 3 (2006) 139-144.

[9] Kouhyar Tavakolian, Siamak Rezaei, A.M.Nasrabadi “Classification of Different Mental Tasks Using Neural Network” WSEAS Transactions on Electronics pages: 343-347, Issue2, Volume1, April 2004.

Refereed Conference Publications:

[10] Kouhyar Tavakolian, Andrew Blaber, Brandon Ngai, Bozena Kaminska, “ Estimation of hemodynamic parameters from Seismocardiogram", Accepted at Computing in Cardiology 2010, Belfast, Irland.

[11] Kouhyar Tavakolian, Andrew P Blaber, Alireza Akhbardeh, Brandon Ngai, Bozena Kaminska "Estimating Cardiac Stroke Volume from the Seismocardiogram Signal” Canadian Medical and Biological Engineering Society Conference, June 2010 Vancouver.

[12] Viatcheslav Gurev, Kouhyar Tavakolian, Jason Constantino, Bozena Kaminska, Natalia A. Trayanova “Seismocardiogram records pressure of the heart ventricles on the ribs” Canadian Medical and Biological Engineering Society Conference, June 2010 Vancouver.

[13] Kouhyar Tavakolian, Brandon Ngai, Alireza Akhbardeh, Andrew P. Blaber and Bozena Kaminska "Comparative Analysis of Infrasonic Cardiac Signals" Computers in Cardiology, vol. 36, pp. 757−760, 2009.

[14] Alireza Akhbardeh, Kouhyar Tavakolian, Viatcheslav Gurev, Ted Lee, William New, Bozena Kaminska, Natalia Trayanova "Comparative Analysis of Three Different Modalities for Characterization of the Seismocardiogram" 31th IEEE Engineering in Medicine and Biology conference, pp. 2899:2903.

[15] Brandon Ngai, Kouhyar Tavakolian, Alireza Akhbardeh, Andrew P. Blaber, Bozena Kaminska and Abraham Noordergraaf "Comparative Analysis of Seismocardiogram Waves with the Ultra-Low Frequency Ballistocardiogram" 31th IEEE Engineering in Medicine and Biology conference, pp. 2851:2854, Minneapolis Sept 2009.

[16] Kouhyar Tavakolian, Alireza Akhbardeh, Bozena Kaminska, "An Objective Approach towards Assessment of the Physiological Age of Heart" Association for the Advancement of Artificial Intelligence Symposium on AI in Eldercare, pp 131-133, November 2008, Washington, DC.

[17] Kouhyar Tavakolian, Ali Vaseghi, Bozena Kaminska, Holly Kennedy-Symonds, "Respiration Analysis of the Sternal Ballistocardiograph Signal" Computers in Cardiology 2008;35:401−404.

[18] Kouhyar Tavakolian, Faranak M.Zadeh, Ali Vaseghi, Yindar Chuo, Bozena Kaminska, "Radar Mechanocardiography: a Novel Analysis of the Mechanical Behavior of the Heart" 30th IEEE Engineering in Medicine and Biology conference, Pages 4863-4866 Vancouver, Canada, August 2008.

[19] Alireza Akhbardeh, Kouhyar Tavakolian, Bozena Kaminska, "Recognition of Aging Effect from Cardiomechanical Signals Using Novel SF-ART Neural Network" 30th IEEE Engineering in Medicine and Biology conference, pages 5246-5249 Vancouver, Canada, August 2008.

[20] Alireza Akhbardeh, Bozena Kaminska, Kouhyar Tavakolian, "BSeg++: A modified Blind Segmentation Method for Ballistocardiogram Cycle Extraction" 29th IEEE Engineering in Medicine and Biology conference, Pages: 1896-1899, Lyon, France, August 2007.

[21] Kouhyar Tavakolian, Bozena Kaminska, Teimour Maleki Jafarabadi "Novel Micromachined Valved Glaucoma Drainage Devices" Proceedings of 28th IEEE Engineering in Medicine and Biology conference, USA, New York, Sept 2006

[22] Siamak Rezaei, Kouhyar Tavakolian, Kiarash Naziripour, "Comparison of Five Different Classifiers for Classification of Mental Tasks" Proc. of IEEE Engineering in Medicine and Biology conference. Shanghai, China. Sept 2005.

[23] Mohammad Fathi, Hamid Taheri, Kouhyar Tavakolian "A Comparison between One-Pass and Three-Pass JPEG-LS Image Compression" IASTED Visualization, Imaging and Image Processing Conference, VIIP 2006, Spain, Aug 2006.

[24] Kouhyar Tavakolian, Siamak Rezaei "Classification of Mental Tasks Using Gaussian Mixture Bayesian Network Classifiers" IEEE international workshop on biomedical circuits and systems. Dec 2004 Singapore.

[25] Kouhyar Tavakolian, Siamak Rezaei, A.M.Nasrabadi "Selecting Better EEG Channels for Classification of Mental Tasks" IEEE International Symposium On Circuits and Systems ISCAS2004. Volume III pages 537-540. 23-26 May 2004. Vancouver, Canada.

[26] Saeedeh Parsaeian, Kouhyar Tavakolian, M.B.shamsolahi "Classification of Knee Joint Vibroarthrographic Signals Using Feedforward Neural Network" IASTED International Conference on Biomedical Engineering. Pages 343-345. Feb 2004. Innsbruck Austria.

[27] Kouhyar Tavakolian, Siamak Rezaei "Mental Task Classification for Brain Computer Interface Applications" CSCBS 2006, Kingston, Canada, May 17th 2006.

[28] Kouhyar Tavakolian, Siamak Rezaei , S.K.Starehdan “Choosing Optimal Mental Tasks for Classification in Brain Computer Interfaces” International Conference on Artificial Intelligence and Applications. Pages 396-399. 16-18 Feb 2004. Innsbruck Austria.

[29] Kouhyar Tavakolian, S.K Setarehdan, A.M.Nasrabadi ,M.Hashemi Golpayegani, Caro Lucas, M.A Khalilzadeh “Using Genetic Algorithm to Reduce Channels and Features in EEG Mental Tasks Classification” Proceedings of IASTED International Conference on Artificial Intelligence and Soft computing (ASC2003), July 2003 Banff, Canada, pages 795-800

[30] Kouhyar Tavakolian, Siamak Rezaei “Genetic Algorithm for Feature Reduction in Brain Computer Interfaces” IASTED International Conference on Biomedical Engineering. Pages 289-292. Feb 2004. Innsbruck Austria.

[31] Kouhyar Tavakolian, A.M.NasrAbadi, S.K Setarehdan , M.A Khalilzadeh “Effects of Different Feature Vectors and Neural Network Topology on EEG Mental Task Classification” Proceedings of IASTED International Conference on Biomedical Engineering, Biomed2003, Salzburg, Austria, June 2003, pages 39-43.

Non-refereed Conferences and Abstracts

[32] Kouhyar Tavakolian, Viatcheslav Gurev, Alireza Akhbardeh, Bozena Kaminska, Natalia Trayanova "Investigation of the Seismocardiogram Morphology Using an Integrated Platform for Dynamic Cardiac Simulation" submitted to Biomedical Engineering Society Annual Meeting, Pittsburgh 2009.

[33] Bozena Kaminska, Yindar Chuo, Marcin Marzencki, Kouhyar Tavakolian, Benny Hung, Camille Jaggernauth, Philip Lin" Complete Platform for Remote Health Management" The 3rd international Symposium on Bio- and Medical Informatics, Orlando July 2009.

[34] Bozena Kaminska, Kouhyar Tavakolian, Brandon Ngai, Yindar Chuo, Ali Vaseghi and Brent Carmichael “Prevention and Risk Reduction in Heart Health” Nanotech 2007, Vol. 2, page 838, Santa Clara, USA, May 2007.

[35] Brent Carmichael, Brandon Ngai, Teena Love, Yindar Chuo, Kouhyar Tavakolian, Bozena Kaminska, Gloria Gutman “Integrated Environment and Wearable Monitoring Technology for Medical Applications” Festival of International Conferences on Caregiving, Disability, Aging and Technology (FICCDAT), June 2007, Toronto, Canada.

[36] Siamak Rezaei, Kouhyar Tavakolian “Planning for BioMedical Computing” The Western Canadian Conference on Computing Education, May 2005, Prince George, Canada.

[37] Kouhyar Tavakolian and A.M Nasrabadi , M. Hashemi Golpayegani, M.A Khalilzadeh, A.Sharifi, S.K Setarehdan "Comparison between Linear and Nonlinear EEG Signal Processing During Different Mental Activities" SCI 2003 Conference proc. July 2003, Orlando, U.S.A.

[38] A.M. NasrAbadi, Kouhyar Tavakolian, M. Hashemi Golpayegani, Caro Lucas, S.K Setarehdan, M.A Khalilzadeh, A. Sharifi "Genetic Algorithm as the Selection Criteria of Superior EEG Channels in Classification of Mental Tasks" SCI2003 conference proceedings. July 2003, Orlando, USA.

[39] Kouhyar Tavakolian, M Nasrabadi, S.K Setarehdan, M.A Khalilzadeh "A Novel Hybrid Linear & Nonlinear Feature Vector for Discriminating Five Different Mental Tasks from Spontaneous EEG Signals" SCI2003 conference. July 2003, Orlando, USA.